UNIVERSITÀ DEGLI STUDI DELL'INSUBRIA

Department of medicine and surgery

PhD in Experimental and Translational Medicine

Cycle XXXIII

INVESTIGATING NOVEL TARGETS FOR NEXT GENERATION CHRONIC PAIN THERAPIES.

Ricerca di nuovi target terapeutici per la terapia del dolore cronico

PhD Thesis of

Fozzato Stefania

701185

Supervisors: *Prof. Surace Michele Francesco*

Prof.ssa Bossi Elena

Academic Year 2019/2020

Index

Abstract

Chronic low back pain (CLBP) is a painful condition arising from spinal structures and due to traumatic, degenerative, or inflammatory diseases, whose etiopathogenetic mechanisms are not completely known. Although several ion channels are implicated in nociception, among them transient receptor potential (TRP) channels, a superfamily of trans-membrane Ca^{2+}-permeable channels, are one of the most studied group. Indeed, TRP channels act as sensor of various exogenous and endogenous stimuli, regulating pain sensation.

In the first phase of this research, morphological, ultrastructural, histochemical, immunohistochemical and gene expression analyses were performed on sample tissues collected during the necessary surgery in patients affected by CLBP. An increase in TRP channel mRNAs and proteins was observed in pathological tissues compared with tissues retrieved from the non-symptomatic areas, in almost all patients. The most expressed channels were TRPV4 and TRPM8, associated with a greater infiltration of nervous fibers in pathological tissues.

In a second phase using tissue samples collected from coxofemoral joint during hip replacement surgery of a patient affected by hip osteoarthritis, we assessed whether the same morphological changes and the same TRPV4 and TRPM8 expression pattern were maintained. By performing morphological and immunohistochemical analyses, the presence of numerous nerve fibres in the pathological tissues and a higher expression of TRPV4 and TRPM8 in samples from the capsule compared to the labrum were highlighted.

Finally, using *Xenopus laevis* oocytes as a heterologous expression system, electrophysiological analyses were performed to better characterized the TRPV4 and TRPM8 functionalities. The response to different substances of *X. laevis* oocytes was first evaluated after TRPV4 and/or TRPM8 cRNA microinjection and then after the injection of membranes obtained from pathological coxofemoral tissues, in order to observe any possible difference. Immunofluorescence analyses were also performed to confirm the presence of these channels on oocyte membranes. The currents recorded in membranes-injected oocytes were different from those injected with cRNAs, suggesting a functional alteration of the channels considered.

Our data, although preliminary, offer a model for studying TRP channels and their possible interactions by replicating a situation similar to that occurring *in vivo*. This model study would allow to identify and characterize specific modulators of TRP channels for the treatment of chronic pain.

Introduction

Chronic Low Back Pain (CLBP) is a painful condition arising from spinal structures such as bones, joints, muscles, tendons, ligaments and intervertebral discs due to traumatic, degenerative or inflammatory diseases. CLBP is a highly prevalent condition associated with disability, work absenteeism, and huge health care costs (Surace et al., 2012). Its onset and regulatory mechanisms are not properly understood, due to the multiple factors concurring in its pathogenesis, such as the neuroinflammatory peripheral pathways (Albrecht et al., 2018) as well as mechanical and osmotic stress(Kameda et al., 2019; Sadowska et al., 2019). The inflammatory response prompts the release of an array of molecules that acts altering the expression and modulating the function of various ion channels as the transient receptor potential (TRP) ion channels, inducing sensitization in nociceptors, pain hypersensitivity or hyperalgesia (Eitner et al., 2017; Surace et al., 2009). Under pathophysiological conditions TRP channels are sensitized, their activation threshold reduced and, consequently, perception of painful (hyperalgesia) and non-painful (allodynia) stimuli enhanced (Levine & Alessandri-Haber, 2007; McEntagart, 2012; Lippoldt et al., 2013). The peripheral sensitization in primary sensory neurons together with central one induces neuronal plasticity in pain-coding pathways. Plasticity is commonly considered a participant in chronic pain onset (Basbaum et al., 2009; Ji et al., 2018).

To understand the players involved in peripheral pain hypersensitivity, the altered expression of selected membrane receptors was investigated in specimens from patients of different age and gender, with a confirmed diagnosis of CLBP. TRPV1-4, TRPA1 and TRPM8 were selected because of their expression in peripheral sensory neurons as molecular nociceptors, actively transducing thermal, chemical and mechanical stimuli (Marwaha et al., 2016; Kameda et al., 2019) thus being involved in CLBP. For example, TRPV4 acts as a sensor of mechanical or osmotic signals and it is present not only in the nervous system but also in several musculoskeletal tissues, including cartilage, bone, and synovium. This protein was shown to have altered expression in pathological conditions and to have a role in pain perception in CLBP (McNulty et al., 2015). Also TRPV1 is known to be stimulated by several inflammatory neuropeptides and signalling molecules (Kelly et al., 2015) and overexpressed in osteoarthritis (Valdes et al., 2011; Nilius & Voets, 2013); thus, it is reasonable to expect a similar pattern of expression in specimens retrieved from patients affected by CLBP. Moreover, in inflammatory tissue, it is often co-expressed with TRPA1 (Dai, 2016) that can be equally stimulated by an array of molecules present in inflammation and in acute mechanical hypersensitivity (Asgar et al., 2015; Sheng Wang et al., 2018; Kameda et al., 2019). Finally, many papers reported that alsoTRPM8 is expressed on both Aδ and C fibers and overexpressed in pain conditions, where it plays a

role in amplifying pain sensation after injury, particularly in models of neuropathic pain. To date, the role of TRPM8 is not completely understood: some data show that TRPM8 is active in reducing pain, others suggest that TRPM8 increases pain after injury (Caspani et al., 2009; Marwaha et al., 2016; Jankowski et al., 2017; Weyer & Lehto, 2017).

Nociception

Nociception is the process of transmission of painful signals by nociceptors in the primary afferent nerve fibers. The noxious stimuli are detected by nociceptors and converted into electrical signals, which are then transmitted to the spinal cord, thalamus, and the cerebral cortex, where pain is finally sensed (Dai, 2016).
Among different channels implicated in nociception, the TRP channels family represent candidates as peripheral sensors of pain signals. Indeed, TRP channels act as sensor of various exogenous and endogenous stimuli. Endogenous agonists, induced or upregulated following pathological conditions such as inflammation or nerve injury, determine the activation or sensitization of TRP channels and contribute to generation and development of pain perception (Dai, 2016). For example, inflammatory mediators, such as arachidonic acid (AA) derivate and oxidative stress products, can act directly as TRP channels activators or can induced a rapid translocation of TRPs from the cytoplasm to the plasma membrane, increasing the channel function.

TRP channels

Transient receptor potential (TRP) channels are a super family of trans-membrane ion channels involved in transduction of chemical and physical stimuli and located in the plasma membrane and in the membrane of intracellular organelles (Dai, 2016).
TRP channels are cation permeable channels and are expressed in almost every tissue and cell types, with a role in different homeostatic functions (Everaerts et al., 2010). They are also regulators of cellular responses to a diverse array of physical and chemical signals, including mechanical loading, osmolarity, heat, cold, and a variety of other physical and chemical stimuli, necessary for the normal cellular function in the body (Fig. 1)(Nilius & Voets, 2013; McNulty et al., 2015).
In mammals, the TRP super family has been divided in 6 subfamilies based on sequence homology: ankyrin (TRPA), vanilloid from 1 to 6 (TRPV), melastatin from 1 to 8 (TRPM), canonical from 1 to 7 (TRPC), polycystin 2, 3 and 5 (TRPP) and mucolipin from 1 to 3 (TRPML) (Pedersen et al., 2005).
TRP channels, composed of four subunits with six trans-membrane helices (TM1–TM6) each, can homo- or heterotetramerize to create a pore for cation permeation (Muller et al., 2019). The N- and C-terminal segments are located in the cytosol and vary in the number of amino acids and the functional motifs among the different subfamilies. The N-terminus can contain between 4 and 30 tandem copies of ankyrin repeat domains (ARD), involved in protein-protein interaction (Latorre et al., 2009), while the TRPM subfamily has not ankyrin repeats. Furthermore, the N and/or C-terminal segments contain domains, which have a role in the assembly of homomeric and heteromeric complexes

(Lepage& Boulay, 2007; Schindl& Romanin, 2007). TRPV1 and TRPM8 also contain a conserved TRP box, a short hydrophobic region located just C-terminal of the putative last transmembrane segment (Nilius et al., 2006).

The TRP channels show complex gating behaviour that can integrate a number of different physical and chemical stimuli (McNulty et al., 2015). In pathological conditions, TRP channels are sensitized and their activation threshold is reduced, so perception of painful (hyperalgesia) and non-painful (allodynia) stimuli is increased (Levine & Alessandri-Haber, 2007; Dai, 2016).

Among different TRP channels TRPA1, TRPV1-4 and TRPM8 have progressively gained attention because were shown to be expressed on peripheral sensory neurons with role of nociceptors, actively transducing thermal, chemical and mechanical stimuli (Marwaha et al., 2016).

After peripheral nerve injury, TRP channel expression changes dynamically in sensory neurons.

The expression of TRPV1, TRPA1, TRPV3 and TRPM8 decreases in the injured neurons, due to the loss of trophic support after injury. Instead, TRPV1 and TRPA1 are upregulated in nearby spared neurons and are essential for the development of hyperalgesia and allodynia. The release of growth factors and neurotransmitters by damaged neurons causes an increased excitability of the surrounding neurons, explaining the clinical manifestations of the neuropathic pain, such as numbness, hyperalgesia, allodynia, paresthesia or hypoesthesia (Dai, 2016). In case of nerve injury, TRPV4 contributes to the development of increased sensitivity to mechanical or osmotic stimuli that are normally not or only mildly painful, inducing neuropathic pain. Both $\alpha 2\beta 1$ integrin and Src tyrosine kinase are required for the development of neuropathic hyperalgesia, suggesting that these proteins form a signalling complex with TRPV4.

TRPM8, instead, might contribute to neuropathic hypersensitivity to cold stimuli and tactile allodynia (Sałat & Filipek, 2015; Dai, 2016).

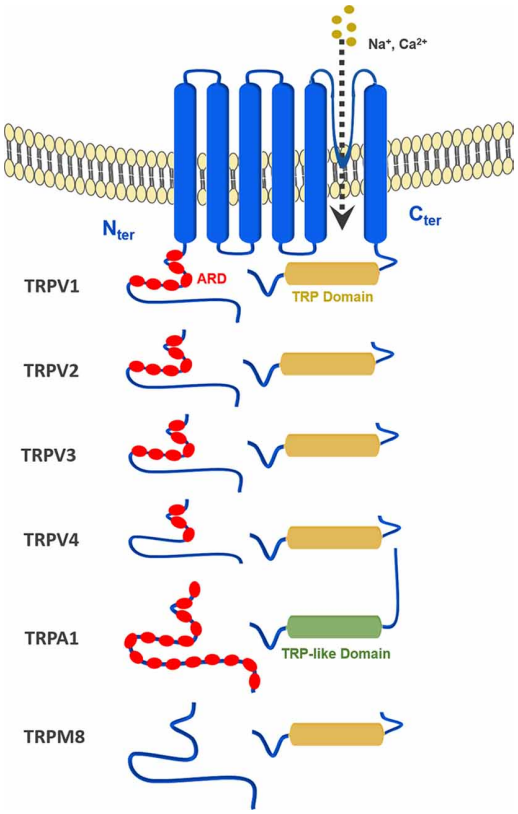

Figure1. Different TRP channels (Muller et al., 2019) .

TRPA1

TRPA1 functions as a polymodal receptor, that can be activated by multiple stimuli such as chemical, thermal (<18° C), mechanical and osmotic stimuli. It is critically involved in nociception.

Pungent compounds found in mustard, garlic, and onions activate TRPA1 (Muller et al., 2019). Moreover, TRPA1 is activated by allyl-isothiocyanate, cinnamaldehyde, farnesyl thiosalicylic acid, formalin, hydrogen peroxide, 4-hydroxynonenal, acrolein, tear gases and non-reactive compounds such as nicotine or PF-4840154 (Talavera et al., 2009; Ryckmans et al., 2011). Most exogenous compounds activate TRPA1 channels by covalent modification of cysteines and lysines in the N-terminus (Hinman et al., 2006; Macpherson et al., 2007; Nilius & Owsianik, 2011).

The structure of TRPA1 (Fig. 2) shows the features of the TRP family and consists of six membrane-spanning domains and a pore-forming region between the fifth and sixth transmembrane domains. A characteristic feature of TRPA1 is the presence of a very long N-terminus, which contains at least 16 ankyrin repeat domains (Story et al., 2003; Paulsen et al., 2015). It is the only mammalian TRP channel with such high number of ankyrin repeats, which might provide the protein a certain degree of elasticity, as well as, the

ability to interact with other proteins, especially those of the cytoskeleton (Corey et al., 2004). The channel assembles as a homotetramer and possesses numerous structural features that hint at its complex regulation by irritants, cytoplasmic second messengers (e.g., calcium), cellular co-factors (e.g., inorganic anions like polyphosphates), and lipids (e.g., PIP2).

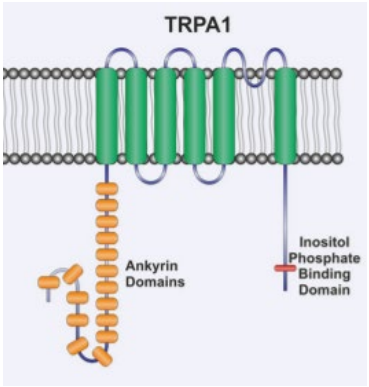

Figure2. Schematic representation of a single TRPA1 subunit (Jardín et al., 2017).

In the sensory nervous system, TRPA1 is expressed in the dorsal root ganglion (DRG), trigeminal ganglion (TG), nodose ganglion (NG), geniculate ganglion (GG) and superior cervical ganglion (SCG).

TRPA1 is co-expressed with TRPV1 on nociceptive primary afferent C-fibers, a subset of peripheral sensory neurons in humans. These fibers are important sensors of nociception, so TRPA1 may be considered as an attractive pain target (Muller et al., 2019).

TRPA1 channels have also been shown to mediate mechanical and bradykinin- evoked hyperalgesia, playing an important role in neuropathic and inflammatory pain (Yekkirala, 2013) and it has been reported to be associated to noxious cold sensation (Patapoutian et al., 2003).

TRPV1

TRPV1is a non-selective cation channel with high Ca^{2+}permeability. TRPV1 is expressed by all major classes of nociceptive neurons and is important for the detection of noxious stimuli (Vay et al., 2012; Michael J. Caterina, 2014; Muller et al., 2019). It is expressed by the peripheral and central terminals of nociceptors in DRG, TG, NG, GG and jugular ganglion (JG). About 30% of TRPV1-expressing sensory neurons also exhibit TRPA1 expression (M. J. Caterina & Julius, 2001; Story et al., 2003).

The structure of TRPV1 (Fig.3) follows the pattern of the TRP channels, with six transmembrane spanning domains, six ankyrin repeats in the N-terminus and a large C-terminal region (Cao et al., 2013).

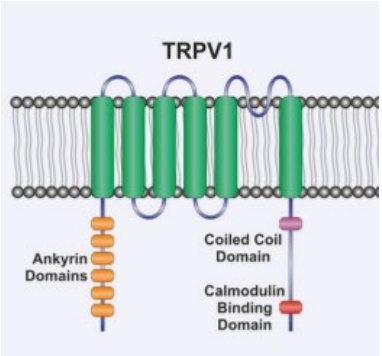

Figure 3.Schematic representation of a single TRPV1 subunit (Jardín et al., 2017).

TRPV1 functions as polymodal receptor, and it can be activated by a number of endogenous and exogenous stimuli including capsaicin, resiniferatoxin (RTX),noxious heat (>43°C), low pH<5.9 (protons),N-acyl amides, arachidonic acid (AA) derivates, TNF-α, vanilloids and cannabinoids (Muller et al., 2019). TRPV1 is widely recognized as a heat sensor(Dai, 2016). Two agonists, Capsaicin and RTX, potently activate TRPV1 and evoke strong burning sensations. Upon activation, Ca^{2+} enters the cell and stimulates a series of calcium-dependent processes that ultimately lead to desensitization of the channel. Upon desensitization, the channel enters a refractory period in which it can no longer respond to further stimulation, leading to the paradoxical analgesic effect of the same compounds (Iannotti et al., 2014). These agonists can cause ablation of the nociceptive terminals, which can cause a loss of the ability to identify potential tissue-damaging stimuli in the future (Muller et al., 2019). TRPV1 antagonists have been shown to be efficient attenuating thermal hyperalgesia induced under inflammatory conditions and increasing the noxious heat threshold (Tékus et al., 2010)

TRPV2

TRPV2 is widely expressed in a subpopulation of medium and large diameter sensory neurons (Vay et al., 2012; Michael J. Caterina, 2014) that do not express TRPV1. TRPV2 is activated by high temperature (>52°C), and seems to act as a high-threshold temperature sensor in Aδ nociceptors. TRPV2 is insensitive to protons and capsaicin but can be activated by high temperatures and inflammation. Similar to TRPV1, the activation and desensitization of TRPV2 is deeply involved in inflammatory and chronic pain (Muller et al., 2019).

TRPV3

TRPV3 is expressed in neurons in DRG, TG, SCG, spinal cords, certain brain regions. TRPV3 is also expressed in skin keratinocytes testis and tongue, and might participate in sensing physical stimuli by means of signal relay to sensory nerve endings through chemical mediators such as ATP and prostaglandin E2. It is also activated by warm temperature

(>34°C) and has a role in thermos-sensation. TRPV3 has been shown to exhibit sensitization in response to repetitive heat stimuli (Chung et al., 2004).

TRPV4

TRPV4 is a Ca^{2+}-permeable cation channel, first identified as a channel activated by hypotonicity. However, TRPV4 is a polymodal receptor activated by warm temperature (>24-27°C), extracellular osmolarity, inflammatory or mechanical and chemical signals. A wide range of tissues including neurons in central nervous system (CNS), DRG, TG and NG, expresses TRPV4. TRPV4 has an essential role in the normal detection of pressure and as a receptor of high-threshold mechanosensory complex (Dai, 2016).

TRPV4 is able to integrate different stimuli and confers many distinct cellular functions in various cell type throughout the body (Everaerts et al., 2010). In fact, it was found to be widely expressed also in the epithelium, kidney, lungs, vascular endothelium, bladder and bone-related cell types (chondrocytes, osteoblasts and osteoclasts). TRPV4 plays an important role in inflammatory and neuropathic mechanical hyperalgesia in rodent models. However, it appeared to be specifically activated under pathological conditions while not contributing to baseline mechanical nociceptive thresholds (Vincent et al., 2009).

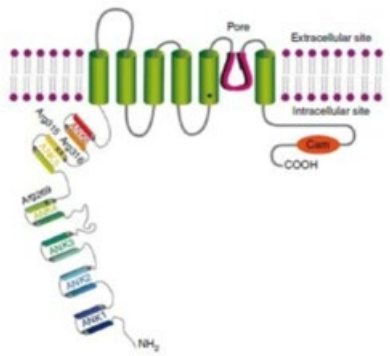

Figure4. Schematic representation of a single TRPV4 subunit (Auer-Grumbach et al., 2010).

TheTRPV4 protein has six transmembrane (TM) segments with a putative ion pore region between TM5 and TM6, an intracellular N-terminal domain containing six ankyrin repeats (ARD), and a C-terminal intracellular domain (Fig. 4). TRPV4forms a homotetramer within the endoplasmic reticulum (ER) and then is trafficked to cell surface. Intermolecular disulfide bonds may contribute to TRPV4 tetramer assembly and stabilization (Lamandé et al., 2011).

The ankyrin motifs are likely critical mediators of protein-protein interactions that regulate TRP channel localization and activity (Landouré et al., 2010).

In the close proximity to the first ankyrin repeat, TRPV4 contains a proline-rich-domain (PRD) involved in mechanosensitive properties of the channel. The central proline residues in PRD, constitute an interaction site with PACSIN3, a cytoskeleton protein involved in synaptic vesicular membrane trafficking, endocytosis and cytoskeleton reorganization. Mechano-sensitivity of TRPV4 is dramatically impaired by a deletion of the N-terminal ARD. This domain is responsible for a correct trafficking of TRPV4 to the plasma membrane and might anchor the channel to cytoskeleton or constitute a mechanical link for gating (Everaerts et al., 2010).

The C- terminus of TRPV4 comprises several putative Calmodulin (CaM) binding sites, and a binding site for cytoskeletal proteins such as MAP7, actin and tubulin. The best characterized CAM domain is involved in Ca^{2+} dependent activation of TRPV4 (Everaerts et al., 2010; Nilius & Voets, 2013).

TRPV4 channel is present in the intervertebral disk and is the highest expressed TRP channel observed. In the IVD and cartilage, TRPV4 regulates the metabolic response to loading through changes in the local osmotic environment, function as mechano- and osmo-sensor, which can influence pro- inflammatory cytokine expression (O'Conor et al., 2014; Walter et al., 2016). During IVD degeneration, TRPV4 expression increases with decreasing IVD osmolarity and its expression was qualitatively elevated in regions of aggrecan depletion in degenerated human IVDs (Walter et al., 2016; Sadowska et al., 2019). However, there is a threshold effect where further reductions in osmolarity did not continue to increase TRPV4 expression (Walter et al., 2016).

TRPV4 in cartilage

Cartilage is an avascular connective tissue that provides a low-friction surface that supports and distributes joint loads. The extracellular matrix (ECM) is inherently charged due to the concentration of negatively charged proteoglycans, predominantly aggrecan. This fixed charge attracts free cations (e.g., Na^+, K^+, Ca^{2+}), resulting in an increase in interstitial osmotic pressure that causes the tissue to retain water. With joint loading, water is extruded from the tissue and is reabsorbed when the tissue is no longer compressed. Chondrocytes experience acute and/or diurnal osmotic fluctuations due to normal joint loading, mechanical stimuli, cell deformation, fluid flow and fluid pressure. These cells respond to the osmotic fluctuations with intracellular signalling cascades and acute volume change followed by active volume regulation, which involves cytoskeletal F-actin and solute transport. In particular, osmotic stimulation elicits extracellular Ca^{2+} influx, which is amplified by release from intracellular stores. The increase of intracellular Ca^{2+} concentration may play a role in cell volume regulation, cell metabolism, and gene expression.

The molecular mechanisms by which chondrocytes sense external osmotic changes are not fully understood. A potential candidate could be TRPV4, which is highly expressed in articular cartilage, and is playing a role in the Ca^{2+} response of chondrocytes to compression-induced changes. TRPV4 is necessary for Ca^{2+} to enter chondrocytes in response to hypotonicity(Clark et al., 2010). During normal joint loading, TRPV4 expression levels may be altered *in vivo*(McNulty et al., 2015).
In the absence of TRPV4, chondrocytes were osmotically incompetent and unable in maintaining tissue homeostasis leading to the loss of joint health and normal skeletal structure, which determines a progressive, sex-dependent increase in bone density and progressive osteoarthritic degenerative changes in a murine model (Clark et al., 2010). These findings suggest a critical role for TRPV4-mediated Ca^{2+}signalling in the cartilage.

TRPV4 in chondrogenic differentiation

TRPV4 has been implicated as a regulator of chondrogenic differentiation.TRPV4 expression and activation increase SOX9 activity in mesenchymal stem cells, via a Ca^{2+} calmodulin dependent mechanism (Everaerts et al., 2010). SOX9 is a chondrocytes transcription factor critical for the expression of cartilage extracellular matrix proteins, chondrogenic differentiation and bone formation(Everaerts et al., 2010; McNulty et al., 2015). Therefore, mutated TRPV4 channel activity might lead to defects of the SOX9-dependent initiation of bone formation in the growth plate, which might determine skeletal dysplasias (Nilius & Voets, 2013).

TRPV4 in bone

TRPV4 is expressed in both osteoblasts and osteoclasts, and has a role also as a bone mechanosensor, controlling bone remodelling and resorption (Clark et al., 2010; Everaerts et al., 2010). The loss of TRPV4 results in the uncoupling of osteoblast and osteoclast activity (McNulty et al., 2015) and suppresses unloading-induced reduction in the levels of mineral apposition and bone formation rate (Clark et al., 2010). In osteoblastic cells, the activation of TRPV4 induces Ca^{2+} influx, and has critical role in mediating the osteoblastic response to fluid flow mechanical stimulation(Suzuki et al., 2013). TRPV4 has also a role in osteoclast function, differentiation and maturation (Masuyama et al., 2008; Everaerts et al., 2010). The activation of TRPV4 associated to acidosis caused by inflammation and injury, promotes the last phase of preosteoclast differentiation and a large osteoclast formation (Kato & Morita, 2011). Instead, the loss of TRPV4 is associated to increased bone mass and trabecular bone volume due to impaired bone resorption and decreased osteoclastic activity in murine model (Masuyama et al., 2008).

TRPV4 in synovium

TRPV4 is expressed by primary human synovial cells that were isolated from patients with inflammatory arthropathies, rheumatoid arthritis, and control patients (Itoh et al., 2009; Kochukov et al., 2009).

TRPV4 and pathologies.

Although TRPV4 is expressed in a variety of tissues, the effects of TRPV4 mutations are seen primarily in the skeletal and nervous systems, causing several disabling or even lethal diseases. TRPV4 is also involved in a surplus of acquired diseases (Nilius & Voets, 2013). To date nearly 70 different single amino acid substitutions have been identified in TRPV4 causing diseases (McEntagart, 2012).Mutations are found throughout the TRPV4 protein, with no apparent link between mutation location and functional consequences(Nilius & Voets, 2013). In the case of TRPV4-dependent diseases, the same mutation can lead to variable degrees of disease manifestation. The disease manifestation depends not only on the specific mutation in the TRPV4 gene, but also on other genetic and environmental factors.

TRPV4 mutations can be associated to different diseases: skeletal dysplasia, neuropathies and arthropathy (Nilius & Voets, 2013).

Possible mechanisms by which TRPV4 might induce this large variety of pathological phenotypes are defects in Ca^{2+}homeostasis, dysfunctional gene expression, defective channel trafficking and dysregulation of protein–protein interactions. Many mutations associated to skeletal dysplasia or neuropathies are gain-of-function mutations, where the mutation increases channel permeability, as indicated by higher basal or stimulated calcium levels, or larger basal and stimulated whole-cell currents (Rock et al., 2008; Krakow et al., 2009;Camacho et al., 2010). Increased basal Ca^{2+} influx cause cellular toxicity and increased cell death. Another pathogenetic mechanism could be an altered gene expression downstream from TRPV4 function, for example, dysregulation of SOX9 activity from mutated TRPV4 channel might lead to defects of SOX9-dependentbone formation in the growth plate, causing skeletal dysplasias. About dysregulation of protein–protein interactions, TRPV4 activity is regulated by binding of ATP and calmodulin to the ARD. Therefore, mutations in the ARD affect thermal stability and ATP binding, which might contribute to altered channel function in disease. It has been suggested that mutations in the convex surface of the ARD are associated with neuropathies, whereas those in the concave surface cause bone dysplasia. This might suggest that the opposite surfaces of the ARD have distinct and cell-type-specific interacting partners responses to TRPV4 gating (Nilius & Voets, 2013). Instead, the arthropathy mutations cause a decrease in channel function by preventing normal trafficking of TRPV4 to the membrane (Lamandé et al., 2011). Such alterations can affect the spatial distribution of TRPV4 at the

plasma membrane. They also cause accumulation of TRPV4 in intracellular organelles, all of which have important effects on cellular responses to TRPV4 gating (Nilius & Voets, 2013). The most important diseases caused by mutations in TRPV4 channel are:

- *Brachyolmia*, a skeletal deformation with short stature, short trunk, scoliosis, platyspondyly, vertebral and long bone abnormalities, caused by R616Q and V620I gain-of-function mutations which increase basal and stimulated channel activity(Clark et al., 2010; Landouré et al., 2010). These mutations are localized in the TM5 domain of TRPV4(Everaerts et al., 2010).

- *Spondylometaphyseal dysplasia Kozlowski type,* where D333G and R594H mutations have been identified in the 5th ankyrin repeat, resulting in increased basal activity of the channel *in vitro* (Landouré et al.,2010).This disorder is characterized by short stature, scoliosis, platyspondyly, progressive kyphoscoliosis, metaphyseal abnormalities in the pelvis and premature degenerative joint disease(Everaerts et al., 2010; Nilius & Voets, 2013).

- *Metatropic dysplasia* is a spondylometaphyseal dysplasia with high variable clinical and radiological severity and different inheritance patterns, determined by two de novo missense mutation in TRPV4: I331F and P799L. The non-lethal dominant form is characterized by progressive kyphoscoliosis, metaphyseal enlargements and shortening of the appendicular skeleton and dense wafer like vertebral bodies(Everaerts et al., 2010; Krakow et al., 2009).

- *Familial digital arthropathy-brachydactyly (FDAB)* is a dominantly inherited condition characterized by aggressive osteoarthropathy of the fingers and toes and consequent shortening of the middle and distal phalanges. During the first decade of life, patients develop progressive deformations of the interphalangeal, metacarpophalangeal and metatarsophalangeal joints and adults have deforming and painful osteoarthritis. Other parts of skeleton are unaffected (Nilius & Voets, 2013). FDAB is caused by mutation encoding p. Gly270Val, p. Arg271Pro and p. Phe273Leu substitutions in the intracellular ankyrin-repeat domain in TRPV4. The mutant channel is more active than wild type but has poor cell-surface localization and did not respond to hypotonic stress. It is likely that the primary pathology occurs in articular chondrocytes, which are not able to respond appropriately to articular cartilage loading due to mutation in TRPV4 (Nilius & Voets, 2013).

- *Charcot-Marie-Tooth disease type 2C (CMT2C)*, an autosomal dominant neuropathy characterized by limb, diaphragm, and laryngeal muscle weakness. Progressive axonal degeneration and cell death result in disabling muscle weakness, sensory loss, bladder urgency, and respiratory symptoms and shorten life expectancy (Landouré et al., 2010; Nilius & Voets, 2013). The mutations involved in CMT occurs in the ankyrin repeats region of the TRPV4, and consists of the substitutions at the same amino acid (R269C, R269H), which is conserved across multiple vertebrate species. The substitutions are unlikely to disrupt the protein folding, but could alter protein-protein interactions that may be critical to TRPV4 function. In CMT2C TRPV4 presents an aberrant activity that lead to an increased intracellular calcium levels and marked cellular toxicity causing an increased cell death in DRG neurons (Landouré et al., 2010). The altered activity can be blocked by the TRP channel antagonists and by the TRPV4 pore-inactivating mutation M680K.

- *Scapuloperoneal spinal muscular atrophy (SPSMA)* is characterized initially by scapuloperoneal atrophy, weakness and scapular winging, which progresses to distal muscle wasting in the lower limbs and is often associated with vocal cord paralysis and respiratory stridor. It is characterized by an autosomal dominant inheritance pattern and heterogeneous expression and progression. Patients often have clear but mild sensory defects, for example, a reduced detection of weak mechanical stimuli such as vibration. TRPV4 mutations have been identified in the N-terminus or the transmembrane region (Nilius & Voets, 2013).

The latter two belong toTRPV4-axonal neuropathies, a group of disorders that can presents as a predominantly motor axonal peripheral neuropathy that can be associated with distinct sensory disturbances (Nilius & Voets, 2013).

TRPM8

The transient receptor potential melastatin 8 (TRPM8) is a Ca^{2+}-permeable cation channel and was the first cold-activated ion channel to be identified (Sherkheli et al., 2010). TRPM8 is a polymodal receptor, activated by cold temperatures (<25°C), membrane depolarizing voltages and by compounds such as menthol, icilin, eucalyptol and PIP2.

Structurally, the TRPM8 channel is formed by four identical subunits. Each subunit shows six transmembrane domains (TM1-TM6) that surround the central pore, with TM5 and TM6 forming the pore and selective filter. The TM4 segment and the TM4−TM5 linker are responsible for voltage sensing, TM6 is involved in the selectivity for cations and the TM2−TM3 linker seems to be implicated in the interaction with icilin. Residues in TM2 and TM4 segments are important for menthol-induced channel opening and voltage and temperature activation (Pérez De Vega et al., 2016). The N- and C-terminal domains are in the cytoplasmic side (Peier et al., 2002; Latorre et al., 2011). The ankyrin repeats domain, often present in other TRP channels, is missing from the N-terminus that instead contains melastatin homology regions (Fig. 5). The C-terminus contains a predicted coiled coil and its domain is essential for the maturation, oligomerization and trafficking of the channel to the plasma membrane (Erler et al., 2006). The "TRP box", located in C-terminal tail, is a binding site for phosphatidylinositol-4, 5-bisphosphate (PIP2). The presence of the C-terminal domain as well as the region between amino acids 40 to 86 of the N- terminal coil is essential to obtain functional TRPM8 channels (Phelps & Gaudet, 2007).

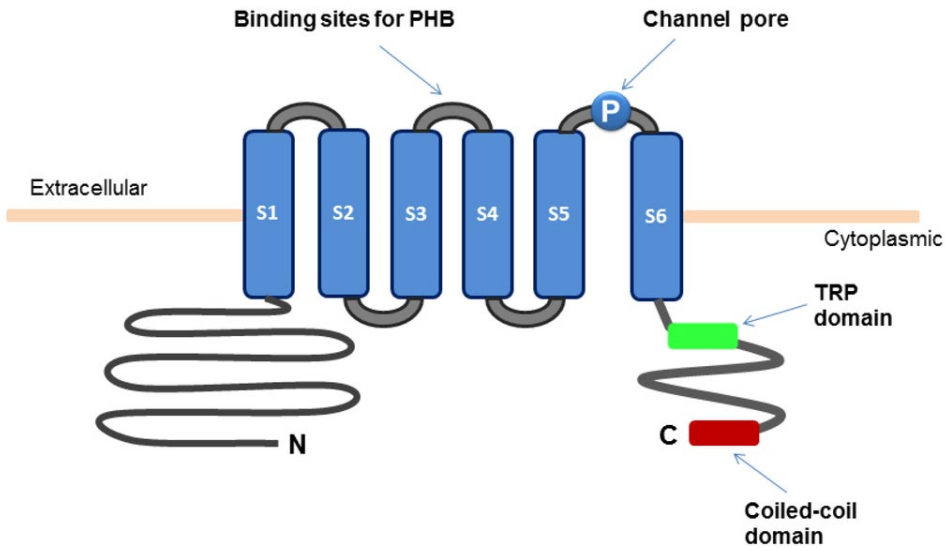

Figure5. Schematic representation of a single TRPM8 subunit (Yee, 2015).

TRPM8 is expressed mainly in a subpopulation of primary afferent neurons of DRG, TG, ND and GG in the peripheral nervous system (Latorre et al., 2011). TRPM8 transcripts are

in both Aδ- and C-fibers. In TG and DRG, TRPM8 is expressed in <15% of small-diameter (~20µm) sensory neurons that do not express TRPV1, consistent with the proportion of neurons that have been shown to be cold- and menthol-sensitive in neuronal cultures.
Although TRPM8 is undoubtedly critical for transduction of thermal stimuli in the peripheral nervous system, it is expressed in other tissues, such as in prostate and male urogenital tract, bladder, sperm, vascular smooth muscle, liver, lung epithelium cells, artery myocites and odontoblasts (Latorre et al., 2011; Pérez De Vega et al., 2016). It is also over expressed in a variety of cancers including prostate, breast, lung, colon and skin melanomas, suggesting it has other biological roles in addition to neuronal thermal sensing (Sherkheli et al., 2010).
The role of TRPM8 in pain sensation is debated; some studies supported a role for TRPM8 in reducing or limiting pain sensation under injury conditions, but an equal number of publications propose that TRPM8 actually exaggerates pain after injury (Weyer & Lehto, 2017).
The enhanced sensitivity to innocuous cold (allodynia) and to mildly noxious stimuli (hyperalgesia), occurring after nerve injury or inflammation, have been correlated with an augmented expression of TRPM8 in sensory neurons making the channel a potential molecular target for pain relief (Caspani et al., 2009; Belmonte et al., 2009; Brederson et al., 2013; Pérez De Vega et al., 2016). Some experiments showed that activation of TRPM8 channels, mediated by agonist such as menthol and icilin, resulted in attenuating pain in inflammatory and acute pain states, paradoxically TRPM8 antagonism may provide relief from some forms of pain (Pérez De Vega et al., 2016).
After injury, activation of TRPM8 seems to consistently cause cold pain, while simultaneously reducing mechanical and heat pain. Therefore, individuals with a primary complaint of mechanical hyperalgesia may respond better to TRPM8 agonists, while those with cold hyperalgesia may respond best to TRPM8 antagonists (Weyer & Lehto, 2017). This does not mean that TRPM8 is sensitive to both mechanical and cold stimuli, indeed, the pharmacological blockade of TRPM8 has no effect on basal mechanical responsiveness. Rather, the effects of TRPM8 agonism/antagonism seems related to the actions at the spinal level, with TRPM8-expressing afferents able to directly or indirectly inhibit mechano-nociceptive afferents (Weyer & Lehto, 2017).

TRPM8 and pathologies

TRPM8 channels are overexpressed in a number of malignant cancers, especially solid ones, and are involved in different stages of cancer development, proliferation, migration, and invasion. In the past decade, the number of cancers in which up-regulation of TRPM8 has been detected has increased. TRPM8 has been identified in prostate, lungs, skin, breast, bladder, brain, liver, thymus, melanoma and colon cancer, neuroblastoma, osteosarcoma, urothelial carcinoma, and pancreatic adenocarcinoma (Pérez De Vega et

al., 2016; Liu et al., 2020). A TRPM8 gene variant (2q37.1, rs10166942) is associated with increased susceptibility to common migraine. The exact role of this variant is unknown, however, it has been supposed that it may have a role in general pain sensitivity mechanisms such as the cutaneous allodynia present in the majority of patients (Pérez De Vega et al., 2016). TRPM8 is also associated to respiratory disorders, bladder sensation, obesity, ocular disorders and vasodilatation-related processes. However, TRM8 functions and distribution are still not well characterized.

TRP channels and cannabinoids

Recent studies have shown that cannabinoids can target, not only canonical cannabinoid receptors (CB1 and CB2), but also some TRP channels (TRPV1–4, TRPA1 and TRPM8) providing a promising multitarget approach to pain treatment (Muller et al., 2019).

Cannabinoids, a family of over 70 olivetol-derived compounds found in the flowers of *Cannabis sativa*, are emerging as some of the most interesting natural products that can interact with TRPV1-TRPV4, TRPA1 and TRPM8, also called ionotropic cannabinoid receptors (de Petrocellis et al., 2012; Muller et al., 2019).

The most famous cannabinoid, Δ^9-tetrahydrocannabinol (THC), responsible for the psychotropic effects of cannabis preparations, was found to activate TRPA1 and antagonize TRPM8 channels, but possess lower activity on TRPV1 or TRPV2. Instead compounds, such as cannabidiol (CBD) and cannabichromene (CBC), have been reported to activate TRPV1 or TRPV2 and TRPA1 channels respectively, or in the case of the former, to antagonize TRPM8 channels (de Petrocellis et al., 2012).

Although some TRP channels can be activated by a variety of endogenous, phytogenic and synthetic cannabinoids, current knowledge is still scarce. The relationship between the channels and their activation in response to cannabinoids should be further explored for various therapeutic uses, including chronic pain and inflammation.

Heterologous expression system with *X.laevis* oocytes

To study the structure and function of human membrane proteins, neurotransmitter receptors and ionic channels the *X.laevis* oocytes, which allow the expression of exogenous proteins, are used (Miledi et al., 2002).

X.laevis is an African aquatic frog of 12-13 cm in size, belonging to the family of the Pipidae, order of the Anuri. These animals are kept in enclosures inside tanks, equipped with a water recycling system that must be chlorine-free and with controlled salinity and hardness. The water temperature must be maintained between 18-20°C.

The oocytes of *X.laevis,* germ cells produced during the female gametogenesis process blocked in the prophase of meiosis I, are used to obtain expression of heterologous proteins at the membrane level.

The main characteristics of the oocytes are large dimensions (diameter 0.5-1 mm), the production in high quantities and in a short time, the easy handling, and not having to supply nutrients from the outside.

It is possible to distinguish two hemispheres in the oocytes: the animal and the vegetative pole. The first one contains the nucleus and is characterized by a brown colour, due to high concentrations of melanin. The second one is yellow coloured and is composed of reserve materials. Externally they are surrounded by the vitelline membrane, formed by glycoproteins, which gives structural rigidity and allow to maintain the spherical shape. During maturation, the vitelline membrane is surrounded by a follicle to protect and nourish the oocyte.

To create a heterologous expression system, once the oocytes have been obtained, heterologous cRNA is injected into the oocyte. The oocyte, through its efficient biosynthetic apparatus, translate the heterologous cRNA, process the products, and incorporate them into their plasma membrane, expressing heterologous functional proteins, with their correct targeting and functionality correlated to post-translational modification (Wagner et al., 2000). The co-expression of many proteins is possible with co-injections of the corresponding cRNAs. It is easy to distinguish exogenous and endogenous proteins because the endogenous ones have low expression levels and have been studied extensively.

However, *X.laevis* oocytes have some disadvantages, such as the expression of exogenous proteins is just transient in oocytes and their genetic pool might affect the expression of exogenous proteins. Moreover, the ideal temperature for maintain *X.laevis* oocytes is about 18°C and it is significantly lower than the one needed for many exogenous proteins, so the folding process can suffer from this difference. Finally, the foreign proteins are inserted into a membrane that already contains other native proteins coupled to various signalling cascades, and that the proteins in their native cells may have a different cohort of associated proteins and lipids that could confer to the receptors

properties different from those seen in the oocytes injected (Wagner et al., 2000; Miledi et al., 2002). To solve this problem, a different method has been developed, which allows incorporating into the oocyte membrane foreign receptors and channels, already assembled in membrane vesicles. This approach will help to elucidate the properties of ion channels in the human tissues, because they are incorporated into the host oocyte membrane while still in their native cell membrane. Using membrane transplantation technique, these receptors should retain their original subunit stoichiometry, structural features, and complement of associated proteins and lipids.
The oocytes allow studying the functionality of TRP channels using electrophysiology techniques such as "Two Electrode Voltage Clamp (TEVC)" technique. TEVC allows recording ionic currents generated after the activation or inhibition of ion channels present on the oocytes membrane after cRNA injection or membrane transplant.

Functional studies on TRP channels in *X. laevis* oocytes using TEVC

To understand the function of TRPV4 and TRPM8 channels and their possible interactions, various agonist or antagonist substances were tested in the heterologous expression system on *X. laevis* oocytes.

Agonists and Antagonist of TRPV4

TRPV4 can be activated by endogenous molecules, such as arachidonic acid metabolite 5, 6-epoxyeicosatrienoic acid (5, 6-EET), semi-synthetic ones, as phorbol ester 4α-PDD, and fully synthetic ones like GSK1016790A. TRPV4 can also be activated by natural compounds isolated from Andrographis paniculata, such as bisandrographolide A (BAA)(Everaerts et al., 2010).
The part between TM3 and TM4 seem to constitute an agonist-binding pocket, in particular for phorbol compounds, and might contribute to channel gating (Nilius & Voets, 2013).

Heat
TRPV4 is activated by moderate heat, this implies an increased basal activity at normal body temperature. However, repeated application of heat gradually diminishes TRPV4 activation. Temperature appears to be a critical modulator of TRPV4 channel gating, leading to activation of the channel by a diverse range of micro-environmental chemical and physical signals. At body temperature, TRPV4 is rapidly activated by all stimuli (Vriens et al., 2004).

4α- Phorbol 12, 13-didecanoate (4α-PDD) and its derivates.

The most specific semi-synthetic agonist of TRPV4 is 4α- phorbol 12, 13-didecanoate (4α-PDD) (Fig.6). Phorbol esters directly bind to TRPV4 at a binding pocket formed by residues in TM3 and TM4. New 4α-PDD-like agonists have been designed such as the 4α-phorbol-12, 13-dihexanoate (4α-PDH), which shows a very high efficacy of TRPV4 activation, being 5 times more potent than 4α-PDD. In addition, lumi-4α-PDD, prepared from 4α-PDD by intramolecular photocycloaddition, is a much faster and more robust TRPV4 activator than unmodified 4α-PDD(Everaerts et al., 2010).TRPV4 activation with 4α-PDD decreases production of the proinflammatory mediator nitric oxide (Hu et al., 2013; McNulty et al., 2015).

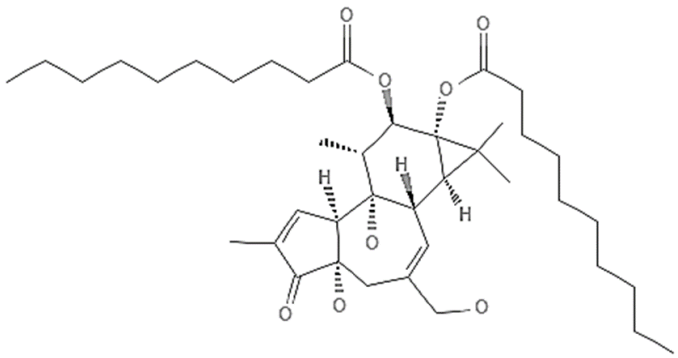

Figure6.Chemical structure of4α-PDD ($C_{40}H_{64}O_8$) PubChem Substance ID24898900 (Kim et al., 2021)

GSK1016790A

GSK1016790A is a potent and selective agonist for the TRPV4 channel (Fig. 7), which has been shown to be a more specific and potent activator compared to the traditional 4α-PDD. GSK1016790A stimulates TRPV4 in multiple cell types including endothelial cells, urinary smooth muscle cells, and urothelial cells. However, the signalling pathway of GSK1016790A is not still well understood (Jin et al., 2011).

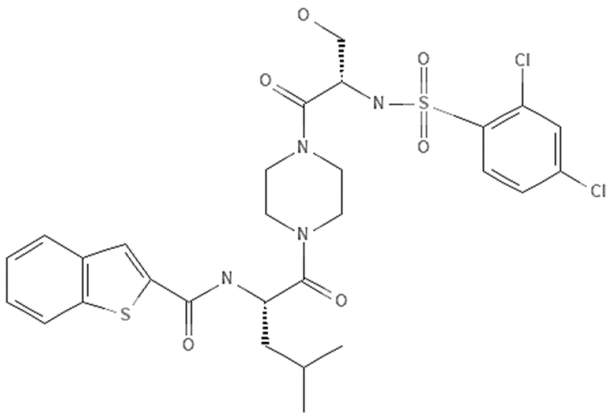

Figure7. Chemical structure ofGSK1016790A ($C_{28}H_{32}Cl_2N_4O_6S_2$) PubChem Substance ID329799716 (Kim et al., 2021)

Ruthenium Red (RR)

Between TRPV4 antagonists, there is a metal-derived Ruthenium Red, which is known to act as a pore blocker of this and other ion channels. RR inhibits inward but not outward TRPV4 current, showing similar actions on other TRPV channels. A lack of selectivity is the most important issue afflicting the use of this antagonist as a research probe for TRPV4 as this can complicate the interpretation of biological data obtained with this compound.
TRPV4 inhibition with ruthenium red upregulates production of nitric oxide (Hu et al., 2013; McNulty et al., 2015).

HC-067047

HC-067047is a potent and selective antagonist for TRPV4 channel (Fig. 8). It does not inhibit other TRPV isoforms at concentrations up to 5µM. However, HC-067047 inhibits the menthol receptor TRPM8 with IC50 values of 780nM.It has been used to investigate the role of TRPV4 receptors in a number of areas, such as regulation of blood pressure, bladder function and some forms of pain, as well as neurological functions (Everaerts et al., 2010).

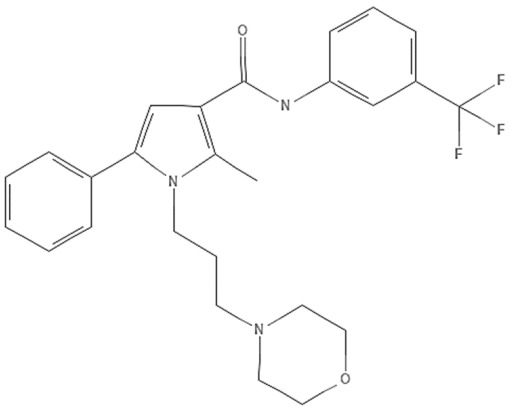

Figure8.Chemical structure ofHC-067047($C_{26}H_{28}F_3N_3O_2$) PubChem Substance ID 329825191(Kim et al., 2021).

Agonists and Antagonist of TRPM8

Menthol

TRPM8 is activated by a wide range of natural cooling agents first of all menthol, a cyclic terpene alcohol found in mint leaves (Fig.9). Menthol acts on TRPM8 as a gating modifier by shifting the voltage dependence of activation towards physiological voltages, in a similar way to cold. Furthermore, the effects of cold and menthol are additive.

Topical menthol has been used as an analgesic to treat chemotherapy induced peripheral neuropathy and post-mastectomy pain syndrome (Liu et al., 2020). At high doses, menthol can be noxious, causing burning, irritation, and pain.

However, menthol is not selective for TRPM8 channels, as it modulates both TRPV3 and TRPA1 channels (Macpherson et al., 2007; Sherkheli et al., 2010). In animal studies, menthol blocked the mechanical and heat hyperalgesia caused by injection of inflammatory compounds such as Complete Freund's adjuvant (CFA) or capsaicin (Frederick et al., 2007; Eitner et al., 2017).

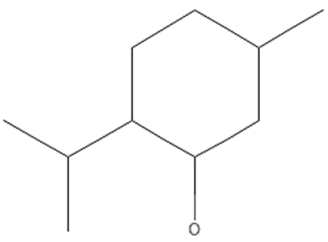

Figure 9.Chemical structure of Menthol ($C_{10}H_{20}O$) PubChem Substance ID 57651951(Kim et al., 2021)

Icilin

Icilin or AG-3-5 is more potent and effective than menthol in activating TRPM8channel (Fig.10). The mechanism whereby AG-3-5 activates TRPM8 is different from that of menthol or cold. AG-3-5 requires a coincident rise in cytoplasmic Ca^{2+}, either through the channel or by release from intracellular stores, in order to evoke TRPM8 currents. This requirement is not necessary for cold- or menthol-induced channel activity, suggesting that the channel can be activated by multiple mechanisms. Additionally, a critical amino acid, located between the TM2-TM3 domains, was identified, which when mutated, renders AG-3-5 unable to active TRPM8 channel. Icilin inhibits menthol activation of TRPM8, so menthol is only a partial agonist and when a partial agonist is mixed with full agonist, the partial agonist acts as antagonist. Icilin activates also TRPA1 (Sherkheli et al., 2010).

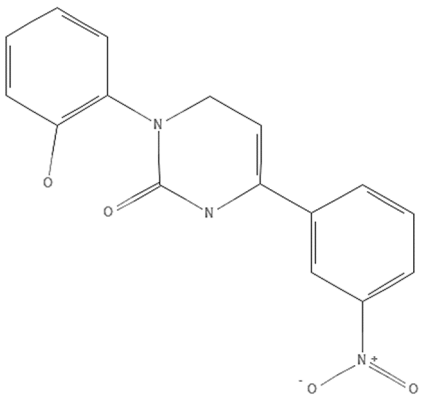

Figure 10.Chemical structure of Icilin ($C_{16}H_{13}N_3O_4$) PubChem Substance ID 24898900(Kim et al., 2021)

Other agonists

TRPM8 is also activated, at higher concentrations, by products with a menthol-like effect such as eucalyptol, geraniol, linalool, and a large number of cooling agents, including Cool-actP, Cooling Agent 10, FrescolatMGA, FrescolatML, hydroxycitronellal, PMD38, WS-3, and WS-23 (Pérez De Vega et al., 2016).

Antagonists

A number of TRPM8 antagonists have been identified, including BCTC, thio-BCTC, CTPC, and capsazepine. It also has been shown that inflammatory components that develop after an injury can inhibit TRPM8. Some of these compounds also antagonize the heat-gated channel TRPV1. Thus, there is significant pharmacological overlap between the two channels. It has been reported that low pH inactivates TRPM8, making it less responsive to the TRPM8 agonist icilin and cold temperatures (but interestingly not menthol). Similarly, bradykinin, an inflammatory component, reduces TRPM8 activity through the action of PKC in both periphery and central synapse in the dorsal horn (Weyer & Lehto, 2017).

Aim

In order to shed light on the role played by different TRP channels in detection and processing of painful stimuli, and possibly to identify novel therapeutic targets, we investigated their expression in samples of connective tissues retrieved from patients undergoing surgery for CLBP. The surgical technique for the placement of bilateral pedicle screws implies their positioning in the adjacent vertebrae. Therefore, there is the opportunity to collect pathological tissue samples from the symptomatic site but also from some non-symptomatic contralateral or adjacent level, these tissues that were used as controls from the same patient. Harvested samples were evaluated for morphological, ultrastructural, histochemical and immunohistochemical alterations. The expression of several members of the TRP family ion channels was evaluated for immunohistochemical and gene expression analyses.

In a second phase, tissue samples were harvested from the coxofemoral joint of a patient suffering from primary osteoarthritis undergoing to hip replacement surgery. These samples, as the connective tissues samples harvested from the spine, were immediately fixed in paraformaldehyde or immersed in liquid nitrogen, then dissected and processed for morphological, histochemical and immunohistochemical analyses.The results were compared to the ones obtained from spinal tissue samples, to evaluate the possible maintenance of TRPV4 and TRPM8 expression pattern in pathologies characterized by chronic pain.

Finally, we propose a model based on *X.laevis* oocytes as a heterologous expression system. *X. laevis*oocytes were microinjected withTRPV4 and/or TRPM8 cRNA or with membranes from coxofemoral tissues, containing the TRP channels of interest. This model allows studying the possible mechanisms of function and interaction between TRPV4 and TRPM8, the most expressed TRP channels in pathological tissues. Furthermore, it could serve as a study model for testing therapeutic agents for the treatment of chronic pain.

Material and Methods

Samples collection

All the procedures with human tissue were performed with the informed consent of the patient and were approved by the Ethics Committee of the Circolo Hospital – Macchi Foundation (n°139/2019) in association with the University of Study of Insubria (Varese). Indeed, patients were adequately informed of the study and signed an informed consent to donate samples for the present research.

Connective tissue samples collection from patients affected by CLBP

Samples of connective tissues were retrieved from six patients affected by CLBP, caused by degenerative disk disease, segmental instability, interapophyseal arthritis, and degenerative lumbar pathology. The interapophyseal joints are synovial joints. Each joint is composed of the upper articular process of the lower vertebra that articulates with the lower articular process of the vertebra above it. A layer of articular cartilage covers the surfaces of each facet, resting on a thickened layer of subchondral bone. There is also a synovial membrane connecting the edges of the cartilaginous portions of the joint, surrounded by a fibrous connective capsule (Gellhorn et al., 2013). During the necessary surgical decompression, fragments of periarticular fibrous capsular tissue were collected from interapophyseal joints (Fig. 11).

The surgical technique for the placement of bilateral pedicle screws required “reshaping” the adjacent interapophyseal joints, contralateral or cranial level, in order to free the access to pedicles.

Tissue samples collected from the pathological capsule are characterized by a greater extent of fibrosis and vascularization. Proliferation of fibrocartilage occurs throughout the hypertrophic posterior capsule and is particularly pronounced at the capsular attachment. The formation of osteophytes and the remodeling of the subchondral bone are the most evident pathological phenomena. When present, osteophytes are mainly found at the lateral margins of the joint at the capsular insertion site (Gellhorn et al., 2013). All these characteristics allow to distinguish the symptomatic sites from the non-symptomatic ones. Therefore, it was possible to collect pathological tissue samples from the symptomatic sites but also from the non-symptomatic ones. The samples harvested from the latter were used as controls, without any damage for the patient. The samples available were dependent on the amount of material removed during the surgical procedure without any damage for the patient. The dissected joint tissues were processed for histological, ultrastructural, immunohistochemical and gene expression analyses. The samples obtained from patients 1 and 3 were insufficient for a complete

analysis, and only immunohistochemical and gene expression analysis were respectively performed in these cases.

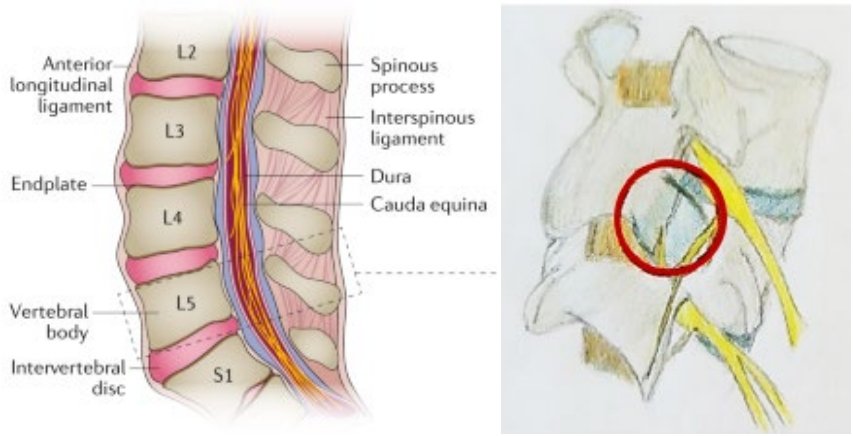

Figure11. Harvested site for tissue samples in patients affected by CLBP (Vlaeyen et al., 2018).

Anamnesis and clinical data of patients included in the study.

Patient 1:

A 22-year-old man suffering from CLBP radiated in the posterior side of right thigh for 3 years. Instrumental investigations showed intraforaminal and paramedian hernia at L5-S1 level. The patient was previously treated with corticosteroid therapies without benefits. In May 2016 herniectomy and discectomy of L5-S1 disc, associated to right selective hemilaminectomy were performed with improvement of symptoms. Specimens were obtained from the affected L5-S1 right joint, whereas a sample from the unaffected right L4-L5 level joint was used as control tissue.

Patient 2:

A 33-year-old woman suffering from degenerative intervertebral disc disease at L4-L5 level. The patient was previously operated to remove herniated left paramedian disc at the same level. Then, in February 2016, she was surgically treated with postero-lateral intervertebral fusion with pedicular screws and rods. During the latter surgery, samples from the articular capsule, bone and muscle of L4-L5 inter-apophyseal joints bilaterally were obtained. Moreover, during pedicular screws insertion procedure, tissues from unaffected, pain-free L3-L4 level joint was collected and used as control.

Patient 3:

63-year-old man with lower back pain radiated in the posterior side of thighs, with worse symptoms on the right side, associated with intermittent neurological claudication. In

2000, the patient was already treated with L4-L5 laminectomy. The instrumental investigations showed a spinal stenosis accompanied by discs protrusions in the L3-L5 levels. In October 2016, the patient underwent L3-S1 decompression surgery and stabilization with pedicular screws and rods and autologous postero-lateral bone grafting. Specimens were obtained from the affected L4-L5 and L5-S1 bilateral joints, whereas samples from L3-L4 level joints were collected as control tissue.

Patient 4:
60-year-old man affected by lumbar spinal stenosis in the L4-L5 tract, with radicular compression of both femoral and sciatic nerves related to an intermittent neurological claudication. Symptoms were worse on the right side. Instrumental investigations showed spondyloarthritis, L4-L5 anterior spondylolisthesis associated with multiple paramedian and intraforaminal hernias in the L3-L5 tract. In October 2016, both a bilateral L4-L5 decompression and foraminotomy were performed, followed by posterolateral intervertebral fusion with pedicular screws and rods and autologous bone grafting. Specimens were collected from the affected L4-L5 and L5-S1 bilateral joints, while tissues samples from L3-L4 level joints were used as control.

Patient 5:
54-year-old woman with L4-S1 lumbar spinal stenosis with bilateral radicular compression of sciatic nerve. Symptoms were worse on the right side. In December 2016, the patient was treated with L4-S1 right-selective hemilaminectomy and flavectomy, L5-S1 foraminotomy and posterolateral intervertebral fusion with pedicular screws and rods associated to autologous bone grafting on L4-S1 intervertebral spaces. Specimens were collected from affected L4-L5 and L5-S1 bilateral joints, whereas samples from L3-L4 level joints were used as control tissue.

Patient 6:
41-year-old woman with lumbar spinal stenosis L4-S1 and radicular deficit on right sciatic nerve. In 2007, L4-L5 and L5-S1 herniectomy, implantation of interspinous device (DIAM) at the L4-L5 level and left L5-S1 decompression were realized. However, due to persistent symptoms, in January 2017 the patient was subjected to hemilaminectomy, flavectomy, L4-S1 right foraminotomy, removal of interspinous device and L4-S1 posterolateral intervertebral fusion with pedicular screws and rods associated to autologous bone grafting. Specimens were obtained from affected L4-L5 and L5-S1 bilateral joints, whereas samples from L3-L4 level joints were used as control tissue.

Connective tissue samples collection from patient affected by hip osteoarthritis

In a second phase, tissue samples were harvested from the coxofemoral joint of a patient suffering from primary osteoarthritis during the hip replacement surgery. Tissue samples were harvested from the capsule and the labrum. The samples available were dependent on the amount of material removed during the necessary surgical procedure without any damage for the patient. The dissected joint tissues, as the connective tissues sample harvested from the spine, were immediately fixed in 4 % paraformaldehyde (PFA) in phosphate-buffered saline (PBS, 138mM NaCl, 2.7mM KCl, 4.3mM Na_2HPO_4, 1.5 mMKH_2PO_4, pH 7.4) or immersed in liquid nitrogen, then dissected and processed for histological and immunohistochemical analysis.

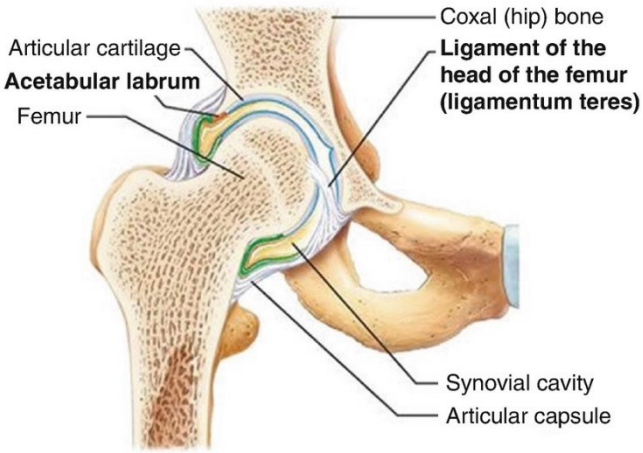

Figure 12. Harvested site for tissue samples from the capsule and the labrum of coxofemoral joint(Murai & Ohseto, 2019).

Patient affected by hip osteoarthritis:

68-year-old man with primary right hip osteoarthritis. Pain had increased over the past five years, associated with a progressive functional limitation. In January 2020, the patient underwent right hip replacement surgery. Specimens were obtained from the labrum and the capsular tissue removed during the necessary surgical steps. In this case is not possible to obtain control tissue, which would require the removal of tissue from the contralateral hip.

Histological and immunofluorescence analyses

Histological and histochemical analyses at light microscopy

For histological analysis at light microscopy, samples were fixed with 4% PFA in PBS overnight at 4°C, embedded in paraffin, and serial-sectioned (5µm) with a Leica JungMulticut 2045 Microtome (Leica, Wien, Austria). After deparaffinization and rehydration through a graded ethanol scale, sections were stained with haematoxylin and eosin (H.E.) (Bio-Optica, Milan, Italy), for a general morphological view, with Masson Trichrome (M.T.) with aniline blue kit(Bio-Optica) to highlight the collagenic component of the tissues and silver impregnation(S.I.) histoenzymatic kit (Bio-Optica) to highlight argyrophilic neurofibrils in the connective tissue.

Samples were observed with a Nikon Eclipse Ni light microscope (Nikon, Tokyo, Japan) equipped with aDS-5M-L1 digital camera system (Nikon).

Ultrastructural analysis at transmission electron microscopy (TEM)

Ultrastructural analysis was performed on tissues harvested from patients affected by CLBP. The samples were fixed for 2 hours in 2% glutaraldehyde in 0.1 M cacodylate buffer, pH 7.4. Specimens were then washed in the same buffer and post-fixed for 1 hour with 1% osmium tetroxide in 0.1 M cacodylate buffer, pH 7.4. After standard ethanol dehydration, specimens were embedded in an Epon-Araldite 812 mixture. Ultrathin sections (80 nm) were obtained with a Reichert UltraCut S ultramicrotome (Leica), stained by uranyl acetate and lead citrate, and observed with a JEOL JEM-1010 EX transmission electron microscope (JEOL, Tokyo, Japan). Data were recorded with a MORADA digital camera system (Olympus, Tokyo, Japan).

Immunofluorescence analysis on connective tissues

For immunofluorescence analysis, samples obtained from spinal tissues were fixed with4% paraformaldehyde for 1 hour (Nakashimo et al., 2010), embedded in paraffin, and serial-sectioned (5µm) with a Leica Jung Multicut 2045 Microtome (Leica). After deparaffinization and rehydration through a graded ethanol scale, sections were immersed in 10mM sodium citrate buffer (pH 6.0) for 10 minutes in a microwave oven for antigen retrieval, and then incubated for 30 minutes with a blocking solution (2% bovine serum albumin - BSA and 0.1% Tween20 in PBS). Sections were then incubated for 1 hour at 37°C(Xiao et al., 2017)with primary antibodies (Alomone Labs, Jerusalem, Israel), all diluted 1:200 in blocking solution. The primary antibodies used are presented in table 1.

After different washes with PBS, the specimens were incubated for1 hour at room temperature with goat anti-rabbit Cy3-conjugatedantibodies (Abcam, Cambridge, UK, excitation 562 nm, emission 576 nm), diluted 1:250 in blocking solution. Nuclei were stained incubating the specimens for 15 minutes with 49.6-diamidino-2-phenylindole (DAPI) 100 ng/ml in PBS (Sigma-Aldrich, Milan, Italy). Slides were mounted with Citifluor

(CitifluorLtd, London, UK) and examined with the Nikon Eclipse Ni fluorescence microscope (Nikon).

Immunofluorescence analysis was also performed on tissue samples obtained from the coxofemoral joint. The procedure was the same as previously described, using only anti-TRPV4 or anti-TRPM8 primary antibodies (Alomone labs).

TRPs		Immunogen peptide	Corresponding amino acid residues
TRPA1	AB_2040232	(C)NSTGIINETSDHSE	747-760 of human TRPA1 (1st extracellular loop);
TRPV1	AB_2313819	(C)EDAEVFKDSMVPGEK	824-838 of rat TRPV1 (Intracellular, C-terminus region)
TRPV2	AB_2040266	(C)KKNPTSKPGKNSASEE	735-750 of rat TRPV2 (Intracellular, C-terminus region)
TRPV4	AB_2040264	CDGHQQGYAPKWRAEDAPL	853-871 of rat TRPV4 (Intracellular, C-terminus region)
TRPM8	AB_2040254	SDVDGTTYDFAHC	917-929 of human TRPM8 (3rd extracellular loop)

Table1. Primary antibodies for immunofluorescence analysis (Alomone labs, Jerusalem, Israel) all diluted 1:200 in blocking solution.

Immunofluorescence and Silver impregnation reaction quantification

In order to standardize the quantification, black staining and fluorescence intensity were assessed on tissue samples from spine using the Image J software package (http://rsbweb.nih.gov/ij/download.html). The percentages of nerve fibers and of fluorescence intensity were assessed by analysing 5 random fields of 45.000 μm^2 for each slide. Graphical representation of quantified molecules was performed with GraphPad Prism version 8.4.2 (GraphPad Software, San Diego, CA, USA)

In addition, the amount of fluorescent signal on samples from the coxofemoral joint was assessed with Image J software package by analysing 5 random fields of 45.000 μm^2 for each slide.

Molecular analyses

RNA extraction and qPCR analysis

Tissues for RNA extraction were weighted and grinded in liquid nitrogen using mortar and pestle.RNA was extracted from tissue using TRIreagent (Sigma-Aldrich), following manufacturer instructions. RNA samples were quantified with a Quantus Fluorometer (Promega, Milan, Italy) and run on an agarose gel or quality control. For real-time quantitative PCR (qPCR), cDNA was obtained from 750 ng of RNA by using the iScriptgDNA Clear cDNA synthesis kit (Bio-Rad, Milan, Italy). Gene expression analysis was performed in triplicate using a CFX96thermal cycler (Bio-Rad) and the iTaq Universal SYBR Green Supermix (Bio-Rad). Primers for the genes under investigation were designed to have at least one of the primers in the pair designed on an exon-exon junction, or to encompass at least one intron. For primer design and thermos-dynamic analysis of their quality, the Primer-Blast tool NCBI (http://www.ncbi.nlm.nih.gov/tools/primer-blast/), the OligoCalc (http://biotools.nubic.northwestern.edu/OligoCalc.html), and the IDT SciTools (http://eu.idtdna.com/pages/scitools) programs were used. Primer sequences are reported in table 2.

Gene	Accession no.		Sequence (5' → 3')	Product length (bp)
TRPA1	NM_007332.3	**Fw**	GACCATGCTTCACAGAGCTTC	108
		Rv	AGTGGAGAGCGTCCTTCAGA	
TRPV1	NM_080705.4	**Fw**	TGAGAGACCTGTGCCGTTTC	106
		Rv	GACGGCAGGGAGTCATTCTT	
TRPV2	NM_016113.5	**Fw**	ATGCTGACCGTTGGCACTAA	80
		Rv	GAAGCCCAGTTCACCTCCTC	
TRPV4	NM_021625.5	**Fw**	TCATGATCGGCTACGCTTCA	80
		Rv	GGTCTGGTCCTCATTGCACA	
TRPM8	NM_024080.5	**Fw**	CAAAAGCCAACGACACCTCAG	94
		Rv	GCAATCTCTTTCAGAAGACCCTT	
B2M	NM_004048.4	**Fw**	AGGCTATCCAGCGTACTCCA	102
		Rv	ATGGATGAAACCCAGACACA	
HPRT1	NM_000194.3	**Fw**	TGCTGAGGATTTGGAAAGGGT	95
		Rv	GGCCTCCCATCTCCTTCATC	
GAPDH	NM_002046.7	**Fw**	GAAGGTGAAGGTCGGAGTC	172
		Rv	GAAGATGGTGATGGGATTTC	

Table2. Sequences of primers used for gene expression analyses in this study.

Relative mRNA quantification was obtained by applying the $2^{\wedge\text{-DDCq}}$ method (Livak & Schmittgen, 2001). Suitability of this normalization method was investigated by evaluating the stability of candidate reference genes across samples, including both pathological and control tissues by the GeNorm algorithm (Fig. 13).

GAPDH (Glyceraldehyde 3-phosphate dehydrogenase) was excluded, whereas beta-2-microglobulin (β-2M) and HPRT1 were both confirmed as suitable reference genes. It was also investigated by checking the efficiency of the assays by constructing calibration curves (Fig. 14) and calculating efficiency as (10–1/slope − 1) * 100.

Efficiency was comprised between 95 and 105% for all assays. Of the two reference genes, β2M had the efficiency most similar to those of the genes of interest; hence, β2M was subsequently used for data normalization. Melting curve analysis was performed to ensure that single amplicons were obtained for each target (Fig. 15).

Graphical representation of quantified molecules was performed with GraphPad Prism version 8.4.2.

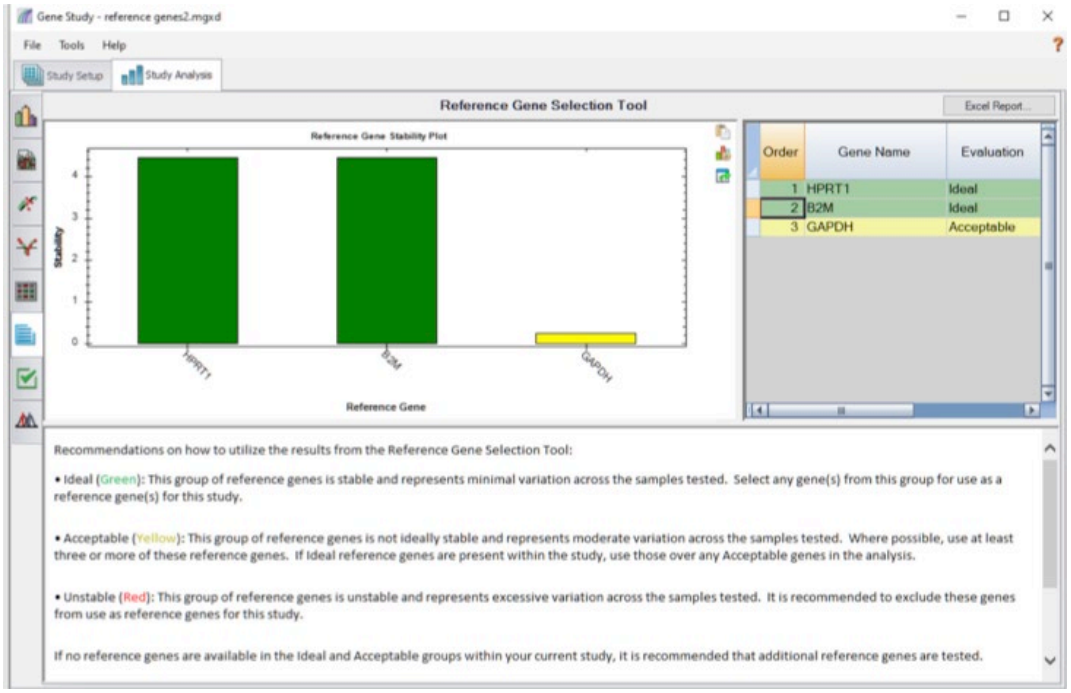

Figure13. Screenshot of the "Reference Gene Selection Tool" from the CFX Maestro software, based on GeNorm, showing the stability of the three reference genes initially tested in this study. Green colored bars indicate ideal reference genes (stable and showing minimal variation across samples); yellow colored bars indicate acceptable reference genes (not ideally stable and showing moderate variation across samples).

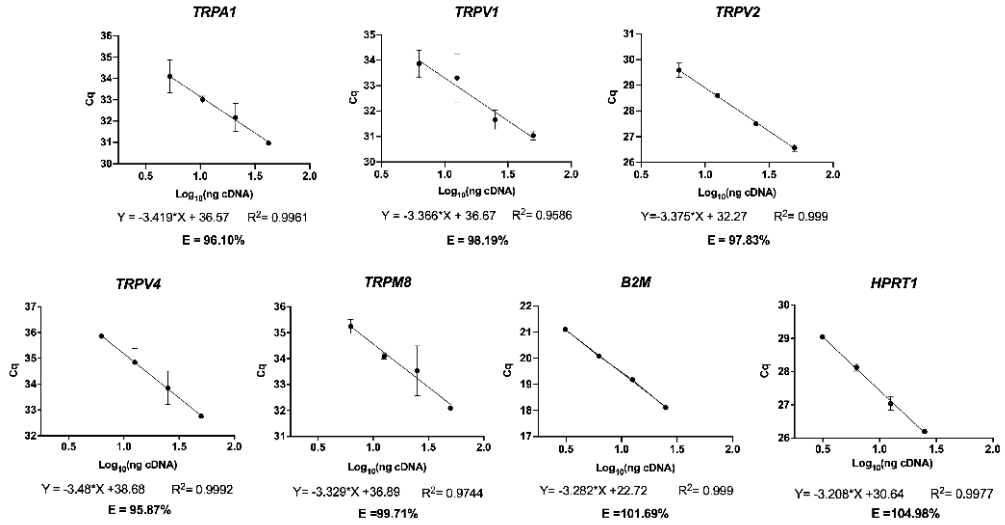

Figure14. Calibration curves for the assays used in this study. All efficiencies (E) were comprised between 95 and 105% and β2M, among the two reference genes analyzed, showed the efficiency most similar to those of the genes under investigation.

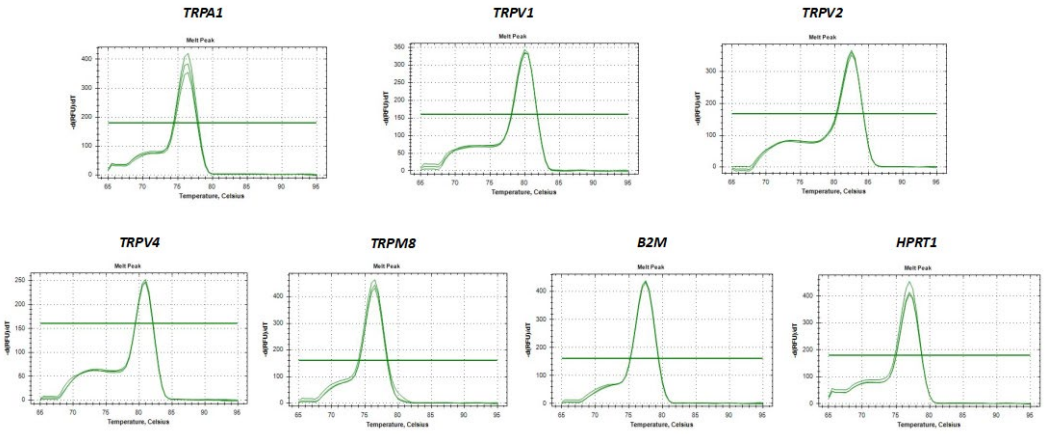

Figure 15.Melting curves of amplicons obtained with the different assays used in this study. The graphs show a single peak, indicating that a single amplification product is obtained.

Electrophysiological analysis in *X. laevis* oocytes

Oocytes collection and preparation

Oocytes were obtained from *X.laevis* adult females (Envigo, San Pietro al Natisone, Italy), which were anesthetized by immersion in a 0.10% (w/v) tricainemethane sulfonate solution (MS222) in tap water adjusted at final pH 7.5 with sodium bicarbonate. After the treatment with an antiseptic agent (0.5% Providone-iodine), a skin incision of 7-8 mm were performed in the lower part of the abdomen, then a second incision of the connective and muscular tissue was necessary. The oocytes were directly extracted from the ovary. After surgical operation, wounds were closed by suturing and animals have been placed in separate tanks for the post-operative course, until the anaesthetic effects were over.

All the employed oocytes were prepared following the procedure previously described (Bossi et al., 2007).

The collected oocyte lobes have been deposited in Petri dishes. Then oocytes have been separated into small groups and treated with 1mg/mL of collagenase (Sigma collagenase Type IA from *Clostridium histolyticum*) in Ca^{2+} free solutionND96 solution (96 mM NaCl; 2 mM KCl; 1 mMMgCl_2; 5 mM Hepes; pH7.6)under stirring for a period of at least 1 hour at 18°C in the dark.

The healthy and full-grown oocytes were selected under stereomicroscope (Wild M3B, Leica Microsystems AG, Wetzlar, Germany), any damaged cells or present residues have been removed. The stage of development was determined analysing appropriate morphological criteria such as size, the clear separation between the animal and vegetative pole and turgidity. Based on these parameters, cells at the V/VI stage of development were selected, isolated and kept at 18°C in NDE solution (ND96 plus 2.5mM pyruvate, 1.8mM $CaCl_2$ and gentamycin sulphate 0.05 mg/mL). This latter solution contains calcium in order to inactivate collagenase effects.

All the procedures were realized in according with the experimental protocol approved locally by the Committee of the “Organismo Preposto al Benessere degli Animali” of the University of Insubria (OPBA -permit. no. 02_15) and the Italian Ministry of Health (authorization number 1011/2015PR – 23 September 2015).

Oocytes transformation

Plasmid preparation

TRPV4 was cloned into the plasmid pXOOM (Fig. 16 A,B) (kindly donated by Professor Nanna MacAulay, Department of Neuroscience and Pharmacology, University of Copenhagen, Copenhagen, Denmark) and TRPM8 was cloned into the plasmid pMO (Fig. 17 A,B)(kindly donated by Melinda Diver, Department of Physiology, University of California,San Francisco, USA). The recombinant plasmids were introduced in *Escherichia*

coli JM109 bacteria strain after heat-shock procedure. Bacteria, kept at -80°C, were incubated with DNA on ice for 20 minutes, subsequently, a thermal shock was performed at 42°C for 2 minutes in order to make membranes temporarily permeable to DNA molecules and then put back on ice again for 2 minutes. At the end of these steps, transformed bacteria were left to grow under stirring for 1 hour at 37 °C in 800 µl of Luria-Bertani (LB) medium. After that, the samples were centrifuged for 10 minutes at 4000 rpm and placed on Petri plates containing selective medium (LB -Agar added with kanamycin 50 mg/mL) and incubated overnight at 37°C. After 24 hours, single colonies were picked up from the plate obtained, and inoculated in liquid selective medium (LB added with kanamycin 50 mg/mL) and incubated overnight at 37 °C under stirring.

The replicated plasmids were extracted from *E. coli* cells using the Wizard®Plus SV Miniprep DNA Purification System Protocol (Promega) following supplier instruction. The extracted plasmid DNAs were then eluted in 50µl of nuclease free water and stored at -20°C.

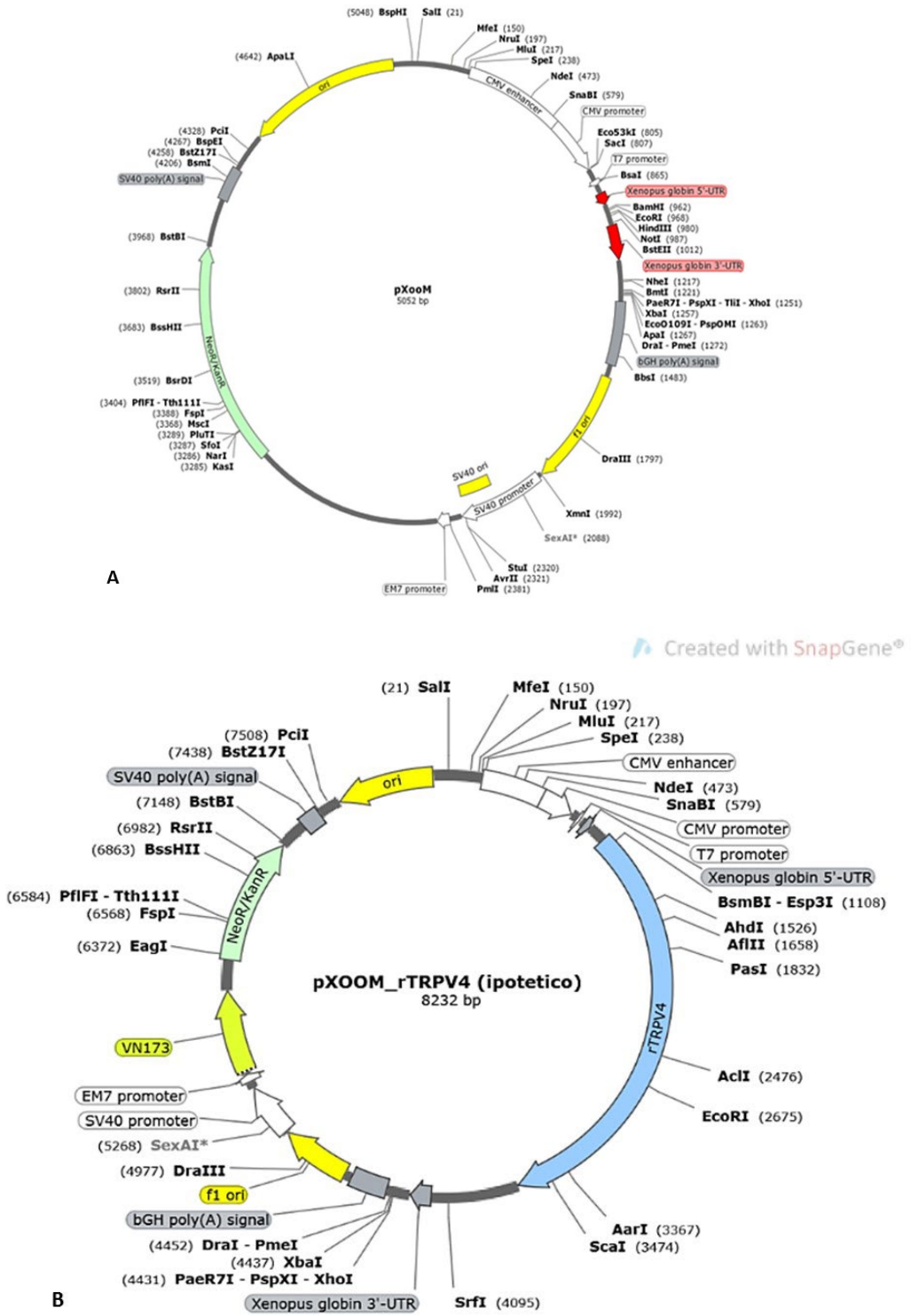

Figure16. Graphic representation of pXOOM plasmid (A, B). pXOOM plasmid structure before (A) and after clonation of TRPV4 in pXOOM plasmid(B).

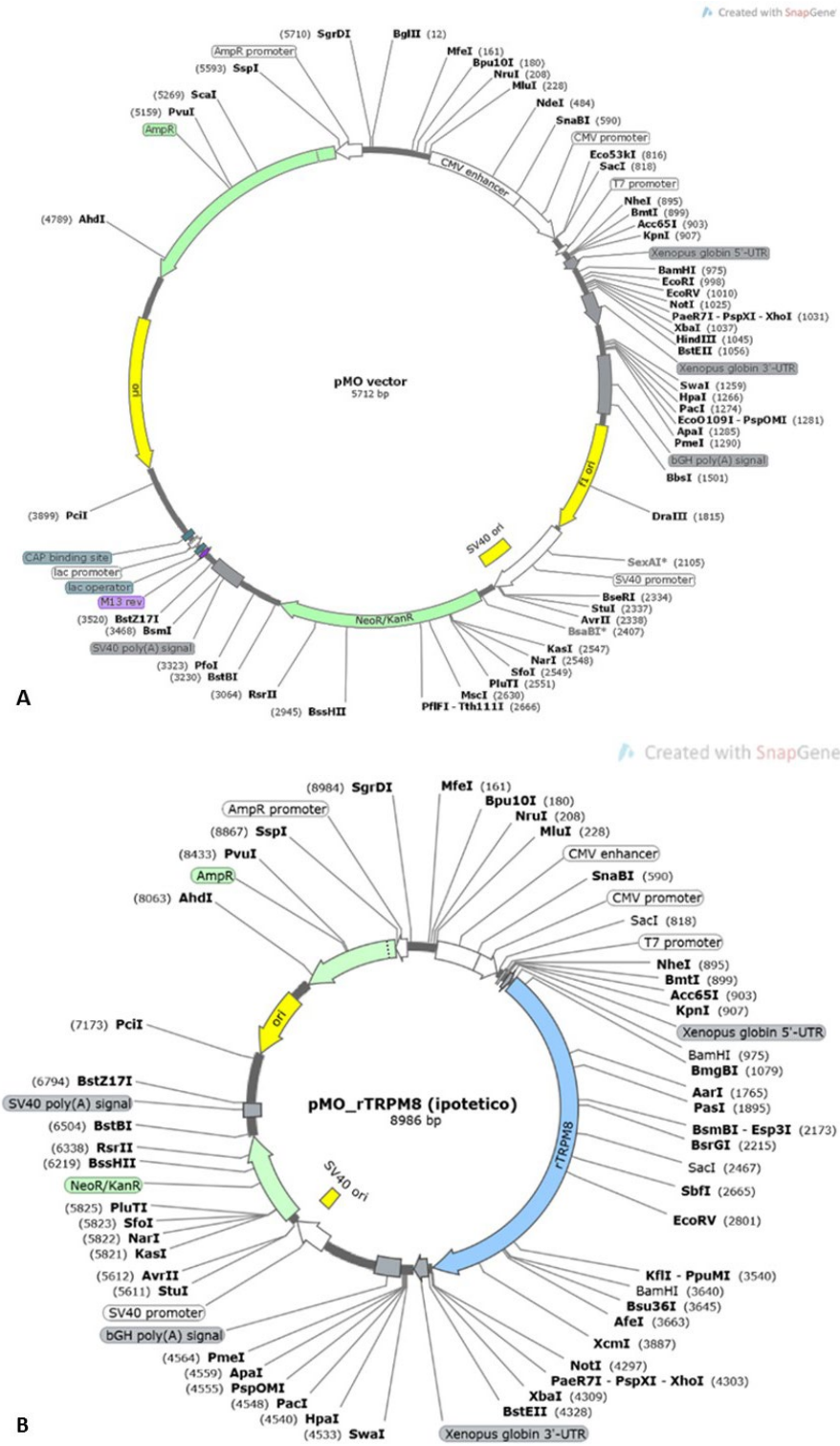

Figure17. Graphic representation of pMO plasmid (A, B). pMO plasmid structure before (A) and after clonation of TRPM8 in pMO plasmid (B).

Plasmid linearization and purification

In order to achieve an efficient *in vitro* transcription, the recombinant plasmid was linearized in 3' direction with respect to the coding region, then purified using the Wizard SV Gel and PCR Clean-Up System (Promega) following supplier instruction, and eluted in 40 µl of nuclease free water.

cRNA in vitro transcription

The linearized DNA plasmids were incubated at 37°C for 3 hours in presence of 200 units of T7 RNA polymerase (Promega). The *in vitro* transcription reaction was composed of 18 µl of 5X Transcription Buffer, 8 µl of100mM Dithiothreitol (DTT), 2µL of40 U/µL RNasin® Ribonuclease Inhibitors (Promega), 13 µL of Ribonucleotide Triphosphates (rNTPs) mix (rATP, rCTP, rUTP 5mM and rGTP 0.5mM), 6.5 µL of10mM Cap Analog, 10 µl of 20 U/µL T7 RNA polymerase (final volume 90 µL). After 10, 20, and 40 minutes from the beginning of the incubation, 1 µL of25mM rGTP was added to the reaction. After 1 hour from the start of the transcription, a mix of 4 µl of 5X Transcription Buffer, 1 µl of 100mM DTT, 1 µL of 40 U/µL RNasin® Ribonuclease Inhibitors, 5 µL of rNTPs mix, 1 µL of20 U/µL T7 RNA polymerase, 1 µL of 25mM GTP, 4 µL of nuclease free water, were added to the sample. At the end of 3 hours, the reaction was stopped by adding 101 µL of nuclease-free and 150 µL of8 mol/L Lithium Chloride (LiCl) and stored at -80 °C overnight. All reagents and enzymes were supplied by Promega. The transcribed cRNA was precipitated and washed with EtOH 70%. The purified cRNA was then resuspended in sterile water to a concentration of 1 µg/µL, visualized by denaturing formaldehyde-agarose gel electrophoresis and quantified by NanoDrop TM 2000 Spectrophotometer (Thermo Fisher Scientific). The cRNA was stored at -80°C, ready for microinjection into *X. laevis* oocytes.

Membrane preparation

Membranes were prepared using tissues from the patient affected by hip osteoarthritis. Teflon glass homogenizer was used to homogenize about 0.5 g of frozen tissue obtain from the capsule or the labrum in 2 ml of glycine buffer (200mM glycine, 150mM NaCl, 50 mM EGTA, 50mM EDTA, 300mM sucrose), associated to 20 µl of protease inhibitors with NaOH (Sigma#P2714), at pH 9. The filtrate was centrifuged for 15 minutes at 8476 g in a Beckman coulter centrifuge (Type 80 Ti rotor). The supernatant was then centrifuged for 2 hours at 939120 g at 4°C.The pellet was washed, resuspended in 5mM glycine, used directly or aliquoted and kept at -80°C for use later.

Injection of heterologous cRNA or membranes

Injection of TRPV4 and/or TRPM8 cRNA and membranes from human coxofemoral capsule expressing TRPV4 and TRPM8, as confirmed by immunofluorescence analysis, were performed.

After 24 hours from the withdrawal, using a manual microinjection system (Drummond Scientific Company nanoject injector, Broomall, PA, USA). The injector requires a tip obtained from a glass capillary pulled with a horizontal puller (Narishige PN-3 Scientific Instrument Glass Micro-Electrode Puller Lab Device) and filled with paraffin, which allowed the injection of the correct amount of cRNA. The oocytes were injected with synthesised cRNA (2ng) of TRPV4 and/or TRPM8 or with membranes (~50 nL). The injection was performed by placing the tip on the line that separates the animal from the vegetative oocyte pole. After injection, the cells were kept in plates containing Kulori solution (90mM NaCl; 1mM KCl; 1mM $CaCl_2$; 1mM $MgCl_2$; 5mM Hepes, pH 7.4) in the presence of Ruthenium Red (1 µM), non-specific channel antagonist, to prevent the oocyte lysis. Finally, oocytes were kept in the same solution at 18°C for 12 to 48 hours, to allow the biosynthetic apparatus of the cell to translate and express proteins in membranes, until TEVC was performed (Fig. 18).

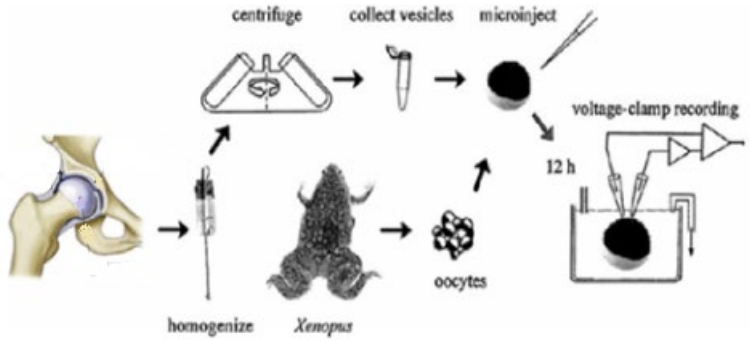

Figure18. Different steps for the injection of human membranes from the coxofemoral joint into X. laevis oocytes. Modified from Miledi et al., 2002.

Different injection procedures were realized in this study:

- injection of TRPV4 cRNA (2 ng/oo);
- injection of TRPM8 cRNA (2 ng/oo);
- co-injection of TRPV4 cRNA(2 ng/oo) and TRPM8 cRNA(2 ng/oo) in the same oocyte;
- injection of membranes from coxofemoral joint.

Immunofluorescence analyses on oocytes

Oocytes microinjected with TRPV4 and/or TRPM8 cRNA or membranes were embedded in Polyfreeze tissue freezing medium (OCT, Tebu-Bio, Le Perray-en-Yvelines, France/Polysciences, Eppelheim, Germany) and immediately frozen in liquid nitrogen. Sample cryosections (7 µm) were obtained with a Leica CM 1850 cryotome on gelatinous

slides and kept at -20 °C. For immunofluorescence analyses, samples have been rehydrated for 5 minutes with PBS and treated with PBS containing 2% BSA for 30 minutes. Subsequently, oocyte slides were incubated for 1 hour at room temperature with the following primary antibodies diluted in BSA blocking solution: rabbit anti-TRPV4 and anti-TRPM8 diluted 1:200 (Alomone Labs). Samples were washed three times for 5 minutes with PBS and incubated with goat Cy3-conjugated secondary antibodies diluted 1:1000 (Abcam). Double-labelling experiments have been performed. Samples were incubated with the same rabbit anti-TRPV4 primary antibody for 1 hour and after PBS washing, the same samples were incubated with goat Cy3-conjugated secondary antibody (Abcam). Following the procedure proposed by Würden & Homberg (1993), since primary antibodies were produced in the same animal, to inhibit a possible unspecific binding, slides were treated with rabbit IgG (Jackson ImmunoResearch Laboratories, West Grove, USA) for two hours (diluted 1:25). Then, slides were incubated with the same rabbit anti-TRPM8 primary antibody for 1 hour and after PBS washing, the same samples were incubated with goat FITC-conjugated secondary antibody (Abcam). According to a previous protocol (Schnell et al., 1999), after immunohistochemistry, sections were incubated with 1mM $CuSO_4$ in 50nM ammonium acetate buffer for 15 minutes at pH 5.0 and washed in PBS. The application of $CuSO_4$ reduced autofluorescence of tissues and at the same time preserves fluorochrome signals. Negative control experiments, in which primary antibodies were omitted and oocyte slides were only treated with secondary antibodies, were performed. Slides were mounted with Citifluor and observed as described before.

Two Electrode Voltage Clamp (TEVC) technique on *X. laevis* oocytes

Two Electrode Voltage Clamp (TEVC) is an electrophysiological technique that allows to control the membrane potential, which is correlated to an electrical imbalance between the extracellular and the intracellular matrix due to a slight excess of cations outside and of anions inside (Wagner et al., 2000). TEVC was employed extensively for studying ion channels and membrane transporters (Hediger et al., 1987; Ikeda & Morizono, 1989; Parent et al., 1992). All the equipments needed for the TEVC recording are placed inside a Faraday cage and are grounded. A stereomicroscope (Wild M3B, Leica Microsystems AG, Wetzlar, Germany) was used to visualize and to place the oocytes in the recording chamber connected to perfusion system. Through the perfusion system, regulated by a computer-controlled electromagnetic valves system, the solution of interest reaches the recording chamber, comes into contact with the oocyte and flows through the action of a vacuum pump, through a suction reservoir connected to the oocyte well. The recording chamber is connected through agar bridges (3% agar in 3 mol/L KCl) to two compartments containing 3 mol/L KCl, which guarantee electrical continuity with the flow. The oocyte, placed in the recording chamber, was impaled by two Ag/AgCl

microelectrodes, formed by a silver wire on which a glass capillary is applied, previously prepared with a horizontal puller and filled with 3 mol/L KCl.
The two microelectrodes are positioned on the electrode holders that were moved using micromanipulators (MM-33, Märtzhäuser Wetzlar GmbH & Co. KG, Wetzlar-Steindorf, Germany).
Before making electrophysiological recordings, it is necessary to check the resistance of the electrodes (<4 MΩ for voltage electrode and <1 MΩ for current one) by slightly breaking the tips of the capillaries at the bottom of the recording chamber.

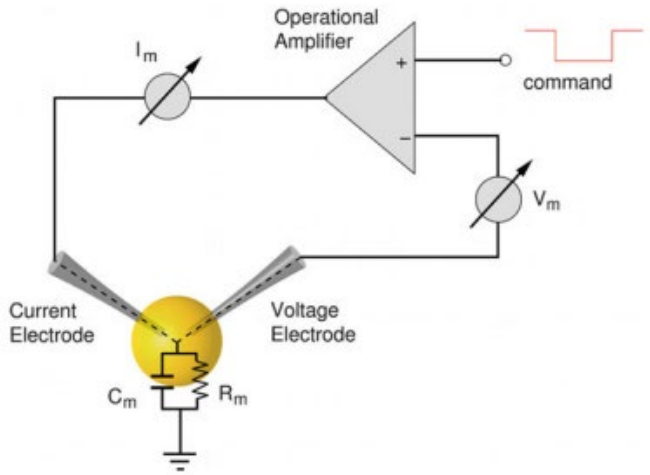

*Figure19. S*chematic system of TEVC (Nowotny & Levi, 2014).

The two reference electrodes are connected to the amplifier, which allows to bring the oocyte to the holding voltage established (-60mV), to evaluate the resistance of the electrodes and the injected current.
The left electrode is responsible for measuring the membrane potential (Vm) which usually is around -30/-35 mV in the oocytes, the right one is responsible for supplying the current. Vm is compared to the control voltage (Vcom), which is defined by the experimenter. The difference between Vm and Vcom is compensated by the injection of a current, through the current electrode, in order to maintain the cell potential at the defined potential Vcom (Fig. 19).
The activation of the channel of interest present on the membrane causes an influx of Ca^{2+}, which induces a variation of the membrane potential. This variation will be quantified through the injection of a current equal and contrary to the flow of Ca^{2+} ions entered the cell, which allows keeping the potential at the set value.
The membrane currents under voltage clamp conditions, controlled by Clampex 10.2 (Molecular Devices, Sunnyvale, CA, USA), were recorded by TEVC (Oocyte Clamp OC-

725C, Warner Instruments, Hamden, CT, USA) that was connected to a computer through an AD/DA (analog-digital, digital-analog) converter (DigiData 1440A, Axon Instr.).
The "membrane test" and the "TAPE" protocols were used.

The "membrane test"

Through the application and removal of a 10mV step with a frequency of 20 Hz, this protocol allows to know the initial parameters of the cell such as membrane capacity (nF), membrane resistance (suitable values between 700 Ω and 1 KΩ), decay constant of the capacitive peak (τ): τ (s) = [Resistance (Ω) x Capacity (F)] / μ), holding current which the system supplies to the cell for keep the holding potential constant and the cell's resting potential. This protocol was used exclusively to assess the viability of the considered oocyte, before being used to perform TEVC experiments.

The "TAPE" protocol

The "TAPE" protocol records a continuous and real-time trace relating to the amount of current that is supplied to maintain the membrane potential at the predetermined value. The oocyte membrane potential was held at -60 mV and current–voltage relationships were constructed by stepping the membrane potential for 2–5 minutes to a desired value before applying agonist or antagonist. In this way, it is possible to analyse the mechanisms that activate the studying protein.

In this study, the oocytes injected with cRNAs and the oocytes transplanted with membranes were analysed by TECV technique in the presence of different agonists and antagonists:

- Kulori solution at >30°C or < 20°C;
- TRPV4 specific agonist GSK1016797A (50 nM);
- TRPV4 specific antagonist HC-067047 (1μM);
- TRPM8 agonist Menthol(50μM);

Solution used, GSK1016797A, HC-067047 and Menthol, were supplied by Sigma-Aldrich.

Statistical Analysis for TEVC

The obtained data were analysed through the Clampfit Analysis Software 10.7 (Molecular Device, USA) and subsequently processed with the Origin8.0 program (OriginLab Corporation, Northampton, MA, USA, https://origin.it.softonic.com).Histograms were obtained with GraphPad Prism version 8.4.2 (GraphPad software).

Results

Morphological analysis of tissue samples from patients with CLBP

Histological and histochemical analyses at light microscopy

Haematoxylin and eosin (Fig. 20 A-N) and Masson Trichrome (Fig. 20A'-N') stainings were performed to evaluate any gross morphological changes in the joint tissues deriving from the pain-affected sites compared to control ones. In all five patients analysed, the control joint level appeared to be composed of compact and well-organized connective tissue, in which numerous cell nuclei were distinguishable (Fig. 20 A, C, F, I, L). As highlighted by the aniline blue component of Masson's Trichrome staining, the main constituent of joint tissue was collagen, that appeared organized in compact bundles (Fig. 20 A',C',F',I',L'). Conversely, the connective tissue samples from pain-affected areas appeared more disorganized. As shown in H.E. (Fig. 20 B, D, E, G, H, J, K, M, N) and M.T. (Fig. 20 B', D', E', G', H', J', K', M', N') stained tissues, numerous empty spaces were visible between the bundles of collagen fibers.

Ultrastructural analysis at transmission electron microscopy (TEM)

Ultrastructural analysis at TEM confirmed the compact and well organized collagenic composition of the control connective tissue (Fig. 20 O). Pathological tissues from different patients presented some areas where collagen fibers were bundled and spatially organized and other areas with connective tissue rarefaction associated to fragmented and disorganized collagen fibers (Fig. 20 P, Q, R).

Silver impregnation

Silver impregnation (S.I.), which selectively distinguishes connective tissue (brown coloured) from argent affine nervous fibers (black coloured), detected only few fibers in control samples (Fig. 21 A, D, H, L, P). Conversely, affected tissues were infiltrated by numerous nerve fibers (Fig. 21 B, E, F, I, J, M, N, Q, R). Furthermore, the amount of black staining, quantified by analysing 5 random fields of 45.000 μm^2 for each slide using Image J software package, significantly increased in pain-affected joint samples compared to control tissue and the differences were graphically represented (Fig. 21 C, G, K, O, S). This finding seemingly supported the hypothesis of a greater infiltration of sensory nerves in the pathological joint tissue.

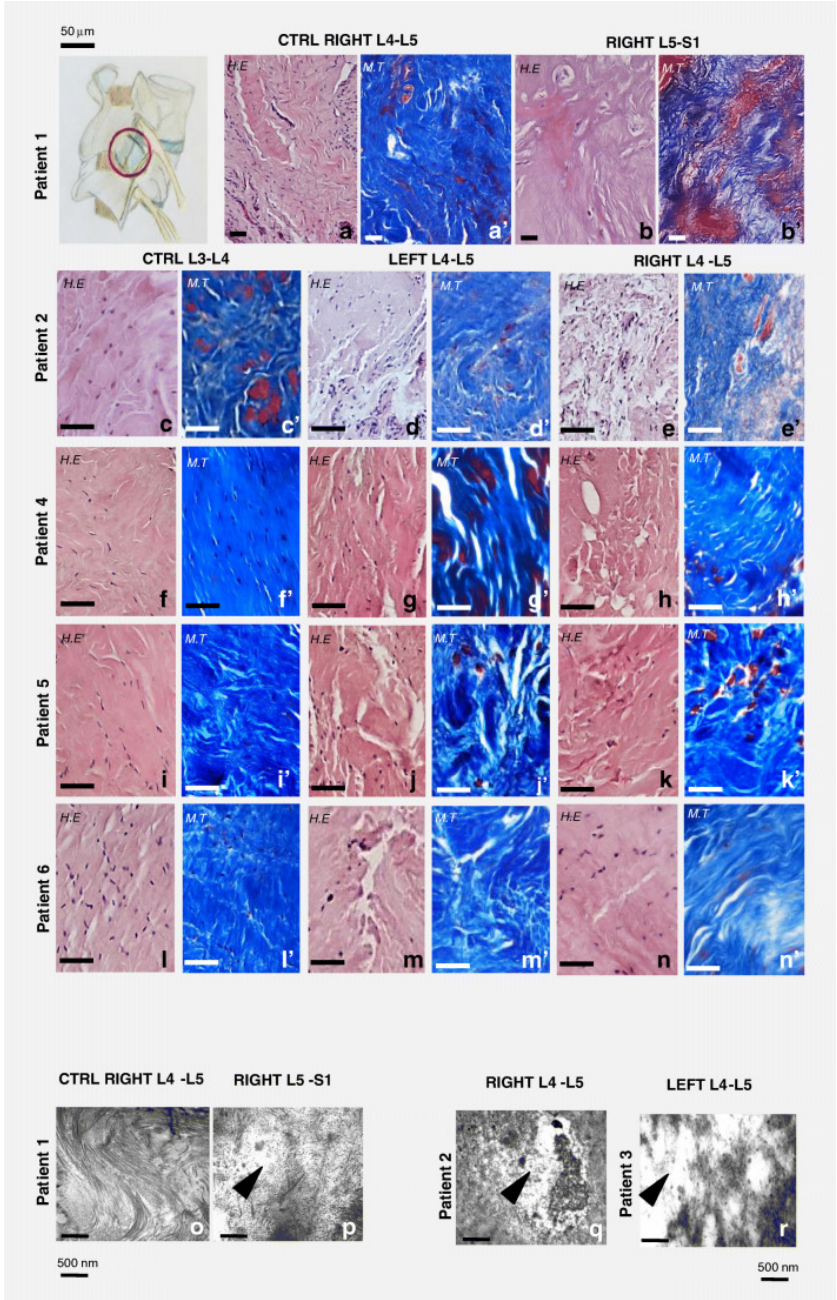

Figure20. Morphological and ultrastructural analyses of control and pathological joint connective tissues. In the top-left drawing, the site from which tissue samples were harvested is shown (encircled). H.E. (staining connective tissue in pink and cells nuclei in violet), M.T. (staining collagen in blue and muscle in red) (A, A'; C, C'; F, F'; I, I'; L, L') and TEM ultrastructural analysis (O) of control connective tissues showed compact and well-organized collagen. A loose and disorganized connective tissue was instead visible in H.E. and M.T. stained pathological tissues (B, B'; D, D'; E, E'; G, G'; H, H'; J, J'; K, K'; M, M'; N-N').Ultrastructural analysis at TEM (P, Q, R) of pathological sections in different patients highlighted that collagen fibers lost the characteristic spatial organization (arrowhead in P, Q, R). Bars in a-n': 50µm; bars in o-r: 500nm.

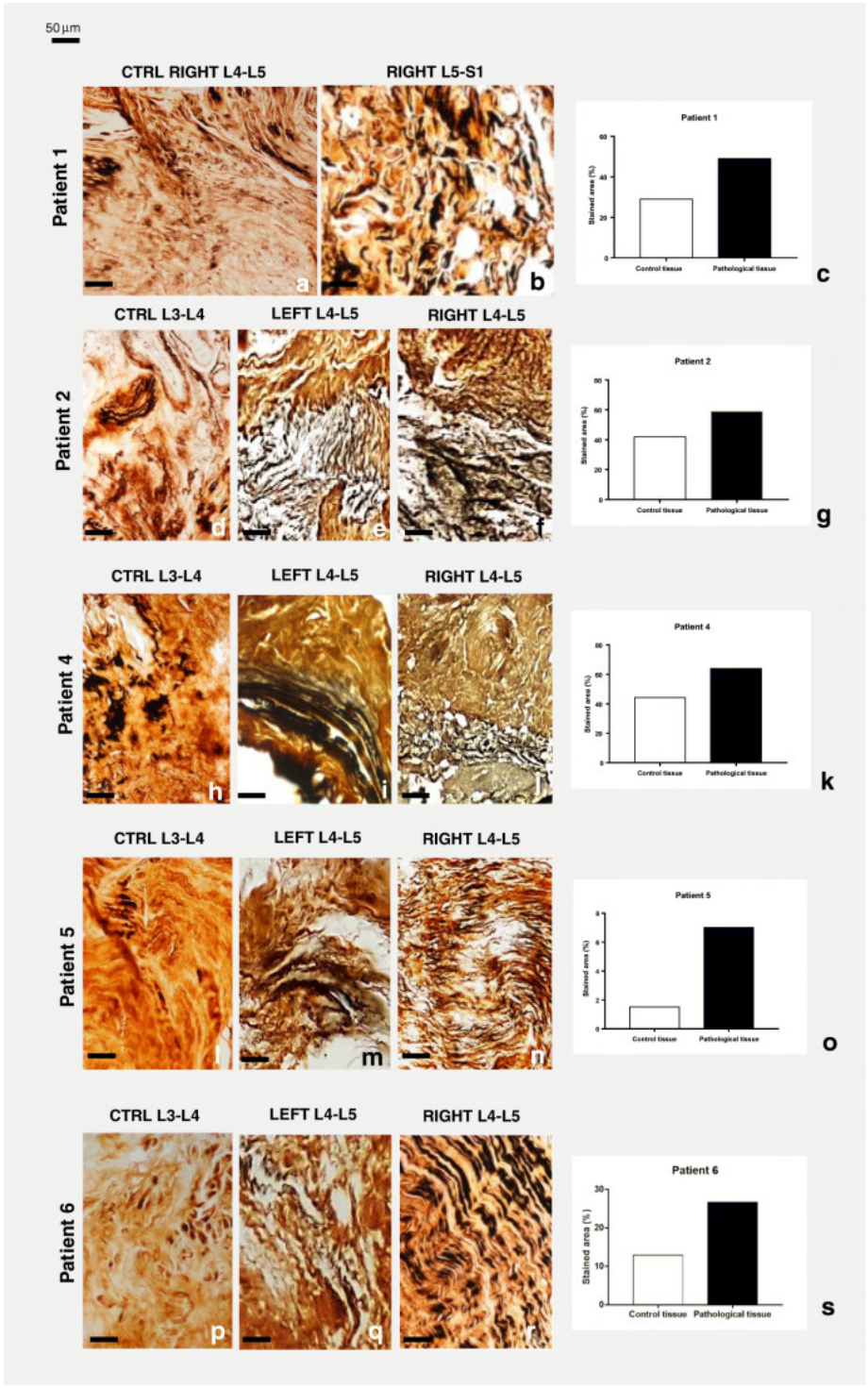

Figure21. Silver Impregnation staining of control and pathological joint connective tissue. Compact and well-organized collagen (in light brown) and few black staining for nervous fibers were observed in control connective tissue (A, D, H, L, P). Numerous black nerve fibers were instead visible in the loose and disorganized pathological connective tissue (B, E, F, I, J, M, N, Q, R). Bars in stained tissues: 50 µm. The graphs (C, G, K, O, S)

show the amount of black staining significantly increased in affected joint samples compared to control tissues, measured by Image J software package.

Immunofluorescence and mRNA expression analyses of tissue samples from patients affected by CLBP

In order to correlate the possible increase of nerve fibers infiltration with an increased pain sensation, we performed immunolocalization of TRPA1, TRPV1, TRPV2, TRPV4, TRPM8, on control and affected tissues of each patient. In addition, transcripts levels of TRP channels (A1, V1, V2, V4 and M8) in almost all tissues deriving from the pain-affected regions were assessed by qPCR.

For patient 1 (Fig. 22), all samples deriving from pathological tissue (Fig. 22 B, E, H, K, N) showed higher expression of all tested TRP receptors, compared to control tissue (Fig. 22 A, D, G, J, M). As very small samples were retrieved from this patient, no molecular analysis was performed. The quantification of immunofluorescence signal of each receptor in pathological and control tissue was measured by Image J software package and graphically represented (Fig. 22 C, F, I, L, O).

For patient 2 (Fig. 23) the immunofluorescence expression of TRPA1 (Fig. 23 A, B, C) and TRPV1 (Fig. 23 E, F, G) was higher in the left side, while TRPV4 (Fig. 23 M, N, O) and TRPM8 (Fig. 23 Q, R, S) were mainly expressed in the right side, as highlighted by the corresponding graphs (Fig. 23 D, H, P, T). In this patient the immunofluorescence expression level of TRPV2 (Fig. 23 I, J, K) was similar in both sides (Fig. 23 L). The gene expression analysis highlighted an increase of TRPV4 and TRPM8 in all pathological samples compared to controls, with the highest expression (6.5-fold) on the right side. TRPA1 transcript showed an increase only in the left side affected tissues (Fig 23.U).

Samples retrieved from patient 3 were very small and were processed only for gene expression analysis (Fig. 24 A). TRPV2, TRPV4 and TRPM8 showed a significant increase in transcript levels in the left side of both affected joint levels (L4-L5 and L5-S1), whereas on the right side only TRPV4 increased in the L4-L5 but not at L5-S1 level. Overall, the highest increase was observed for TRPV4. Modest changes in expression were observed for TRPA1 and TRPV1.

For patient 4 (Fig. 25), an increase in the immunofluorescence of all receptors was observed in the pathological tissues; the increase was particularly evident for TRPV4 (Fig. 25 M, N, O), TRPM8 (Fig. 25 Q, R, S) and TRPV2 (Fig. 25 I, J, K). A graphical representation of immunofluorescence quantification for all TRP channels by Image J software package is shown (Fig. 25 D, H, L, P, T). The increase in TRPV4 and TRPM8 protein levels correlated with an increase in transcript (Fig. 25 U).

For patient 5 (Fig. 26), all pathological samples (Fig. 26 B, C, F, G, J, K, N, O, R, S) showed a general increase in all receptors compared to control tissues (Fig. 26 A, E, I, M, Q). A graphical representation of TRP channels expression is shown (Fig. 26 D, H, L, P, T). At the

transcript level, TRPM8 showed the highest and most consistent increase. TRPV4 transcript increased at the L4-L5 level bilaterally, whereas a less consistently increased of TRPA1 was observed. TRPV1 and TRPV2 were unmodified or even decreased (Fig. 26 U). TRPA1, TRPV4 and TRPM8 transcript levels correlated with protein levels.

Patient 6 (Fig. 27) showed a different pattern of receptor expression compared to previous patients. TRPA1 (Fig. 27 A, B, C) and TRPV1 (Fig. 27 E, F, G) expressed levels of proteins similar to other patients (Fig. 27 D, H). TRPV4 (Fig. 27 M, N, O) and TRPM8 (Fig. 27 Q, R, S) were almost absent in control tissue and poorly expressed in the pathological samples (Fig. 27 P, T). TRPV2 (Fig. 27 I, J, K) was almost equally expressed in both sides (Fig. 27 L).At the transcript level, this patient was the only one without increased TRPV4 levels (Fig. 27 U). A reduction or no changes were observed also for TRPV1 and TRPM8. TRPA1 and TRPV2 showed just a modest increase (less than 5-fold) in transcript levels in pathological compared to control tissues and compared to previously described samples.

No signal was detected in negative control experiments where the primary antibodies were omitted, and samples were incubated only with secondary antibodies (Fig. 28).

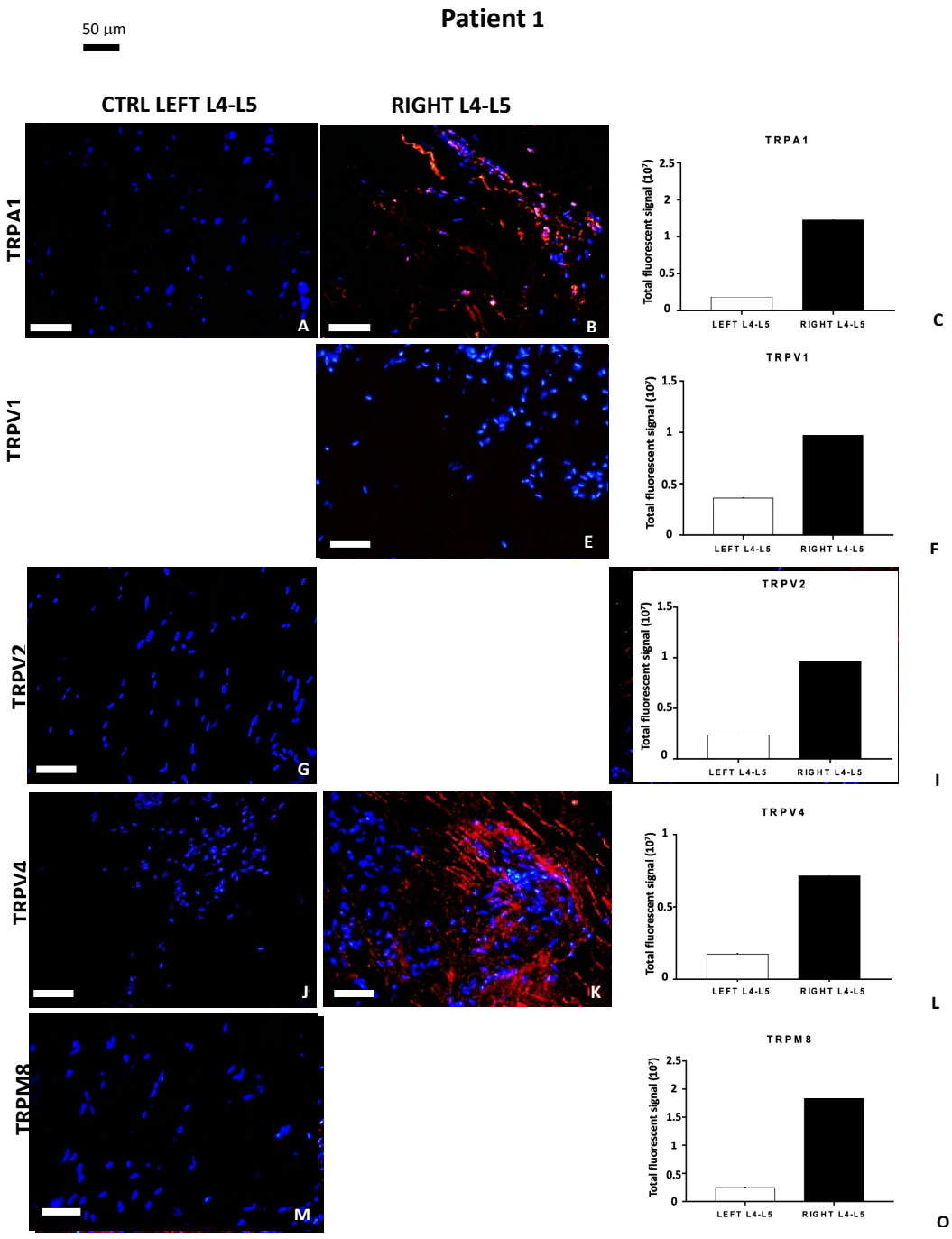

Figure22. Expression of TRP channels proteins in patient 1. Immunolocalization in control (A, D, G, J, M) and pathological (B, E, H, K, N) joint tissues from patient 1. Receptors stained in red, nuclei counterstained in blue (DAPI). Bars: 50 µm. The graphs (C, F, I, L, O) show the amount of immunofluorescence in control and pathological tissues for each TRP channel analyzed, measured by Image J software package, increased in affected joint samples compared to control tissues. See text for details.

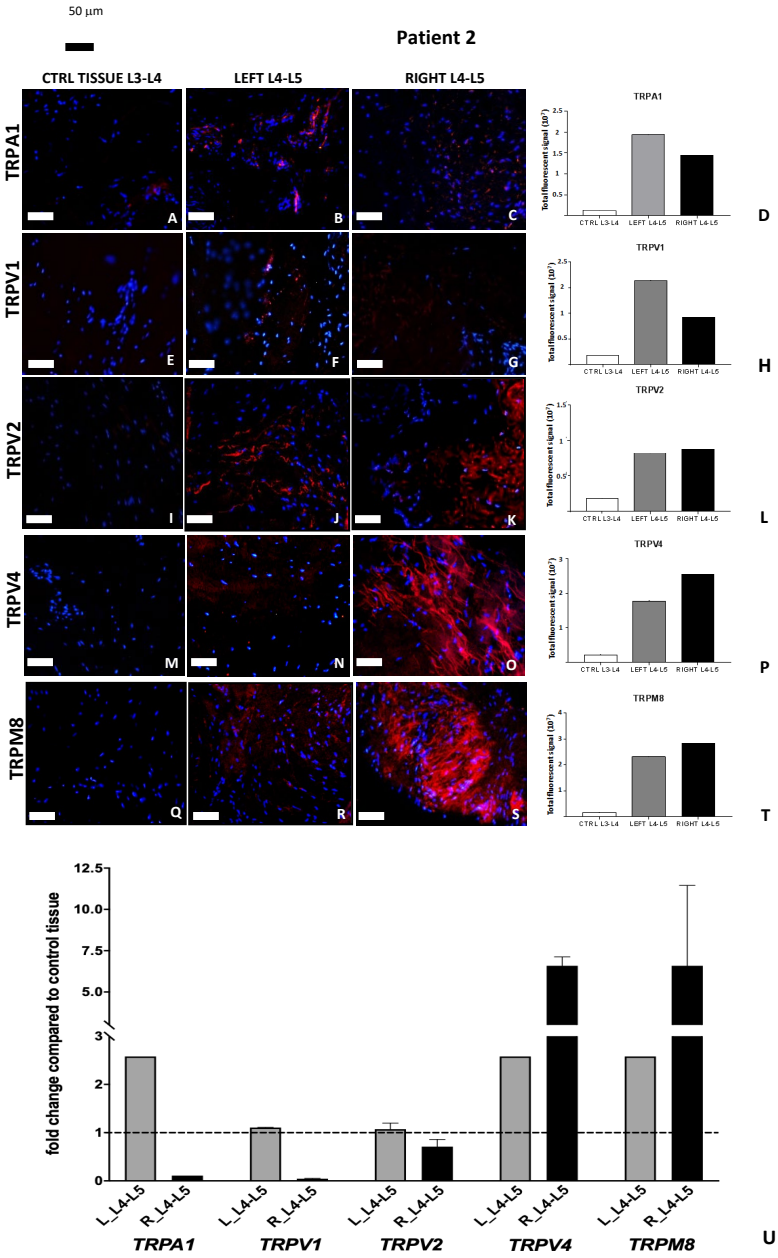

Figure23. Expression of TRP channels proteins and transcripts in patient 2. Immunolocalization of TRPs in control (A, E, I, M, Q) and pathological (B, C, F, G, J, K, N, O, R, S) joint tissues from patient 2. Receptors stained in red, nuclei counterstained in blue (DAPI). Bars: 50 µm. The graphs (D, H, L, P, T) show the amount of immunofluorescence in control and pathological tissues for each TRP channel analyzed, measured by Image J software package, increased in affected joint samples compared to control tissues. Expression of TRP channels' transcripts in different samples from patient 2 (U). The fold change in expression in pathological samples compared to control tissue (dotted line) is reported. Left-hand side samples: grey bars; right-hand side samples: black bars. See text for details.

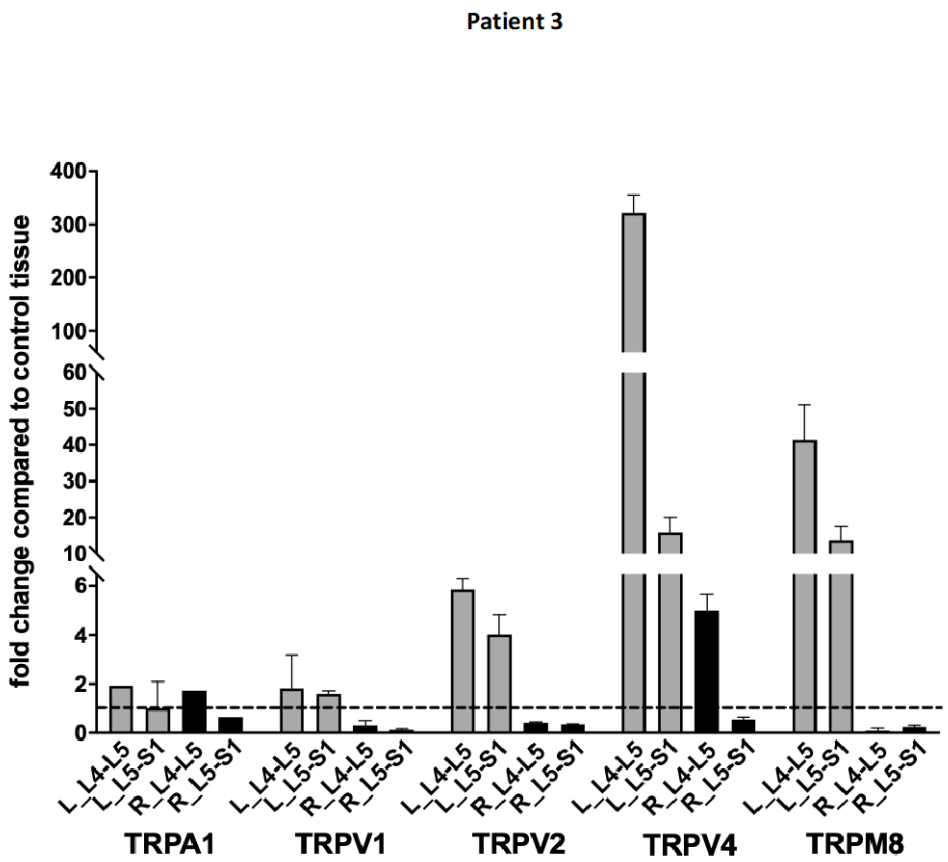

Figure24. TRP transcripts levels in patient 3. Expression of TRP channels' transcript in different samples from patient 3. The fold change in expression in pathological samples compared to control tissue (dotted line) is reported. Left-hand side samples: grey bars; right-hand side samples: black bars. See text for details.

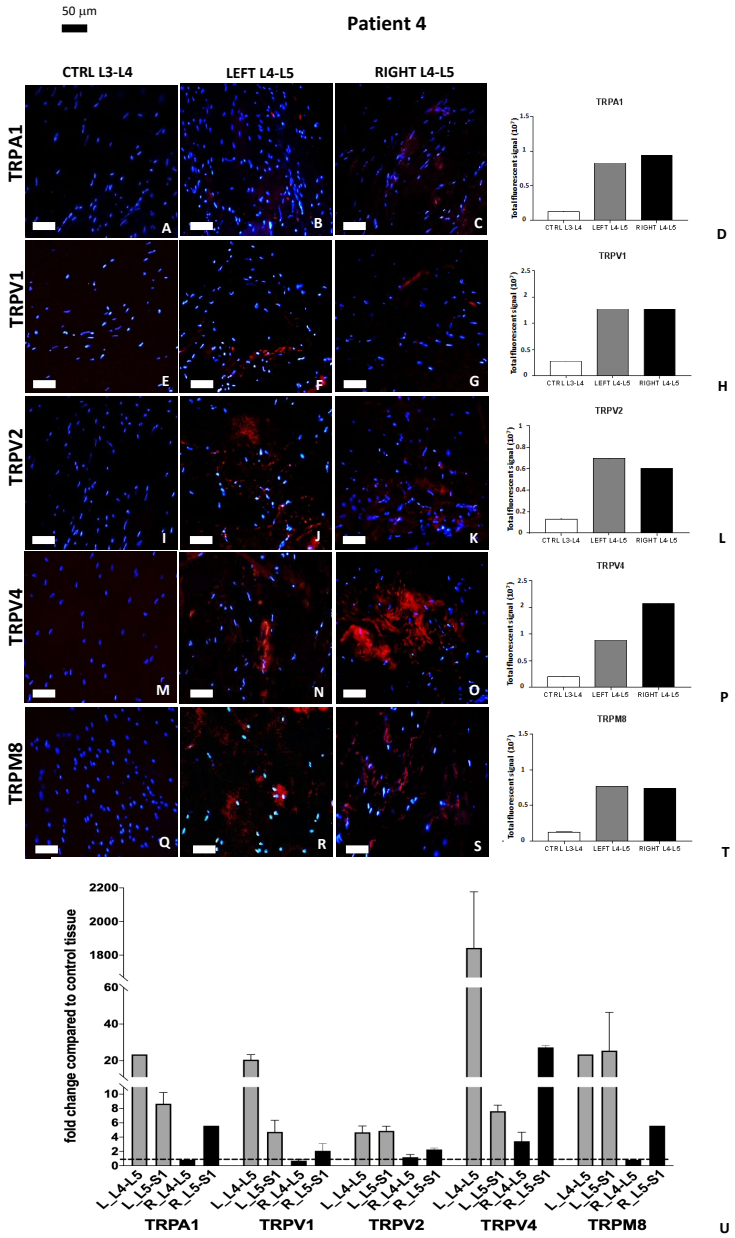

Figure25. Expression of TRP channels proteins and transcripts in patient 4. Immunolocalization of TRPs in control (A, E, I, M, Q) and pathological (B, C, F, G, J, K, N, O, R, S) joint tissues from patient 4. Receptors stained in red, nuclei counterstained in blue (DAPI). Bars: 50 µm. The graphs (D, H, L, P, T) show the amount of immunofluorescence in control and pathological tissues for each TRP channel analyzed, measured by Image J software package, increased in affected joint samples compared to control tissues. Expression of TRP receptors' transcript in different samples from patient 4 (U). The fold change in expression in pathologic samples compared to control tissue (dotted line) is reported. Left-hand side samples: grey bars; right-hand side samples: black bars. See text for details.

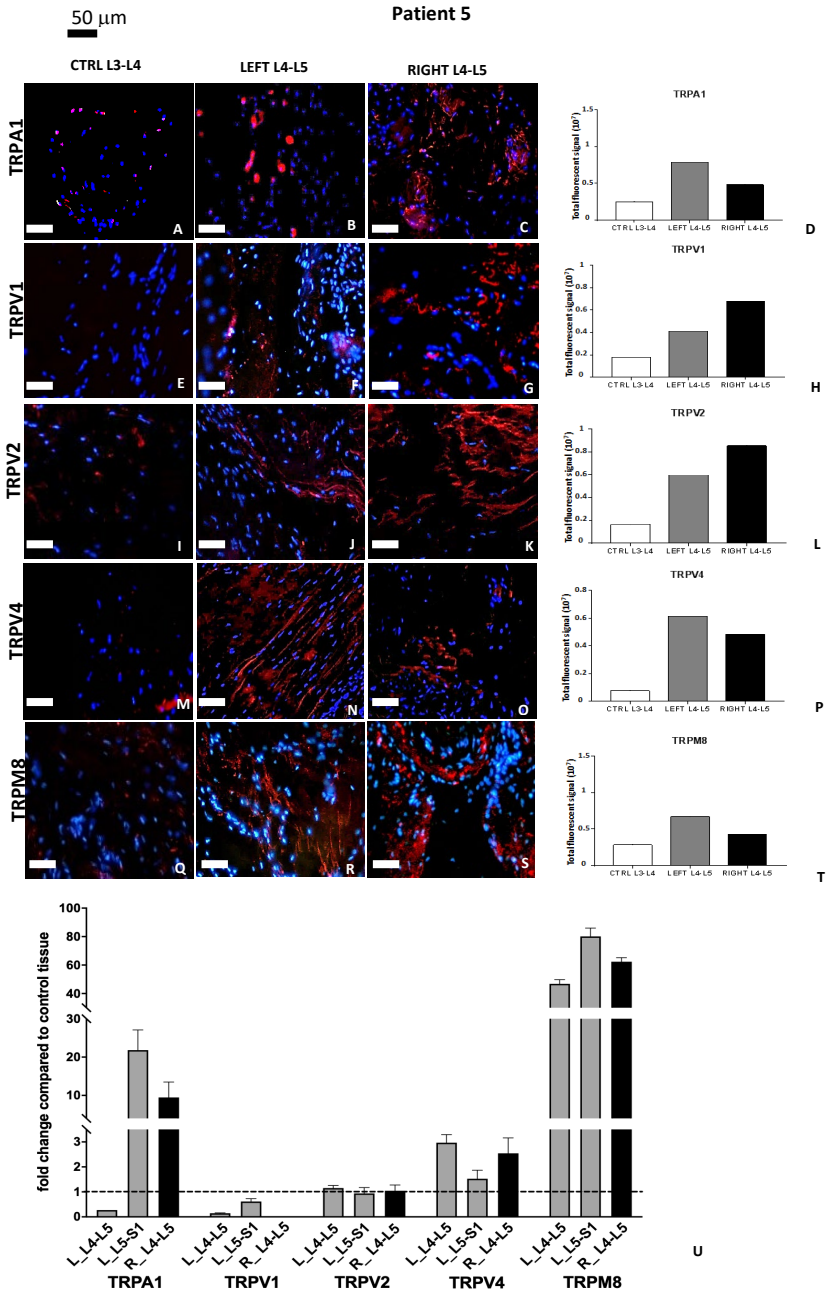

Figure26. Expression of TRP channels proteins and transcripts in patient 5. Immunolocalization of TRPs in control (A, E, I, M, Q) and pathological (B, C, F, G, J, K, N, O, R, S) joint tissues from patient 5. Receptors stained in red, nuclei counterstained in blue (DAPI). Bars: 50 µm. The graphs (D, H, L, P, T) show the amount of immunofluorescence in control and pathological tissues for each TRP channel analyzed, measured by Image J software package, increased in affected joint samples compared to control tissues. Expression of TRP receptors' transcript in different samples from patient 5 (U). The fold change in expression in pathologic samples compared to control tissue (dotted line) is reported. Left-hand side samples: grey bars; right-hand side samples: black bars. See text for details.

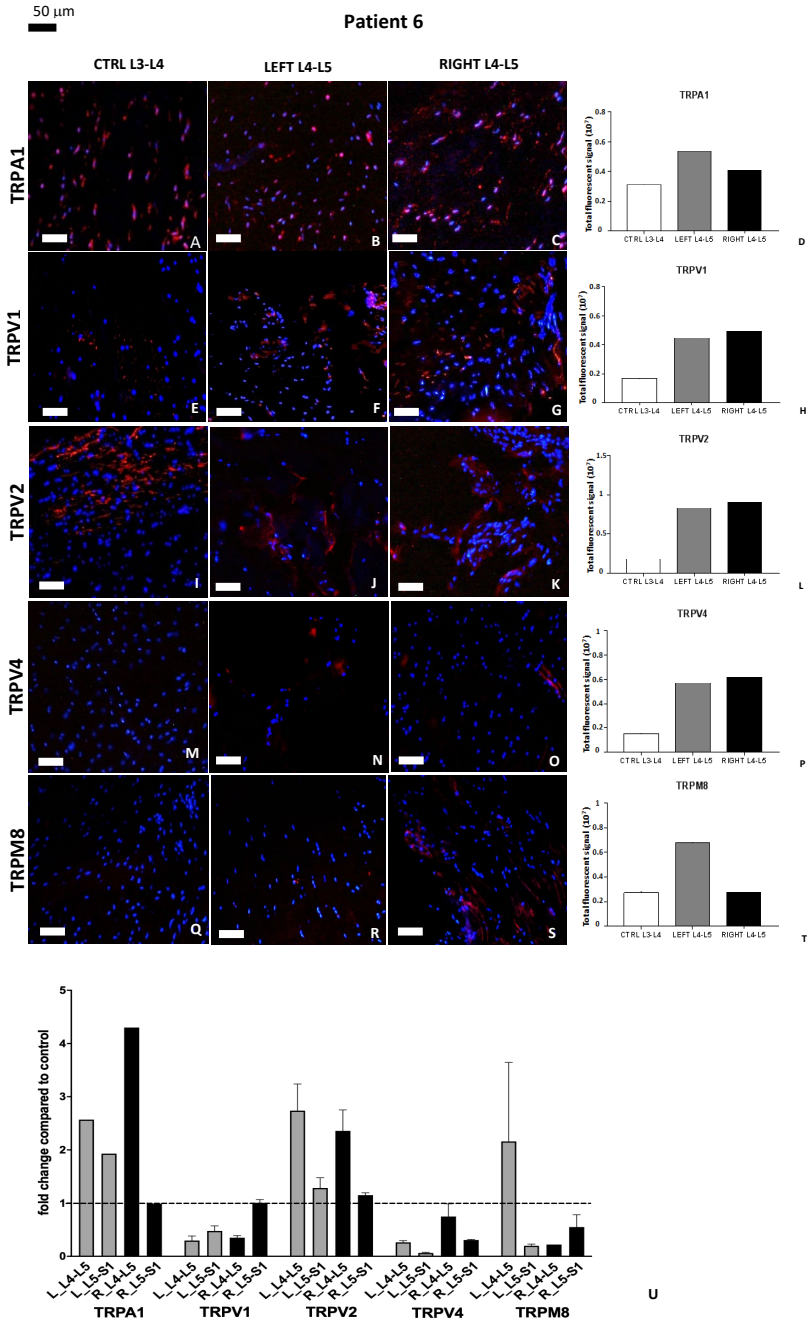

Figure 27. Expression of TRP proteins and transcripts in patient 6.Immunolocalization of TRP in control (A, E, I, M, Q) and pathological (B, C, F, G, J, K, N, O, R, S) joint tissues from patient 6. Receptors stained in red, nuclei counterstained in blue (DAPI). Bars: 50 µm. The graphs (D, H, L, P, T) show the amount of immunofluorescence in control and pathological tissues for each TRP channel analyzed, measured by Image J software package. Expression of TRP receptors' transcript in different samples from patient 6 (U). Fold change in expression of these receptors in pathologic samples compared to control tissue (dotted line) is reported. Left-hand side samples: grey bars; right-hand side samples: black bars. See text for details.

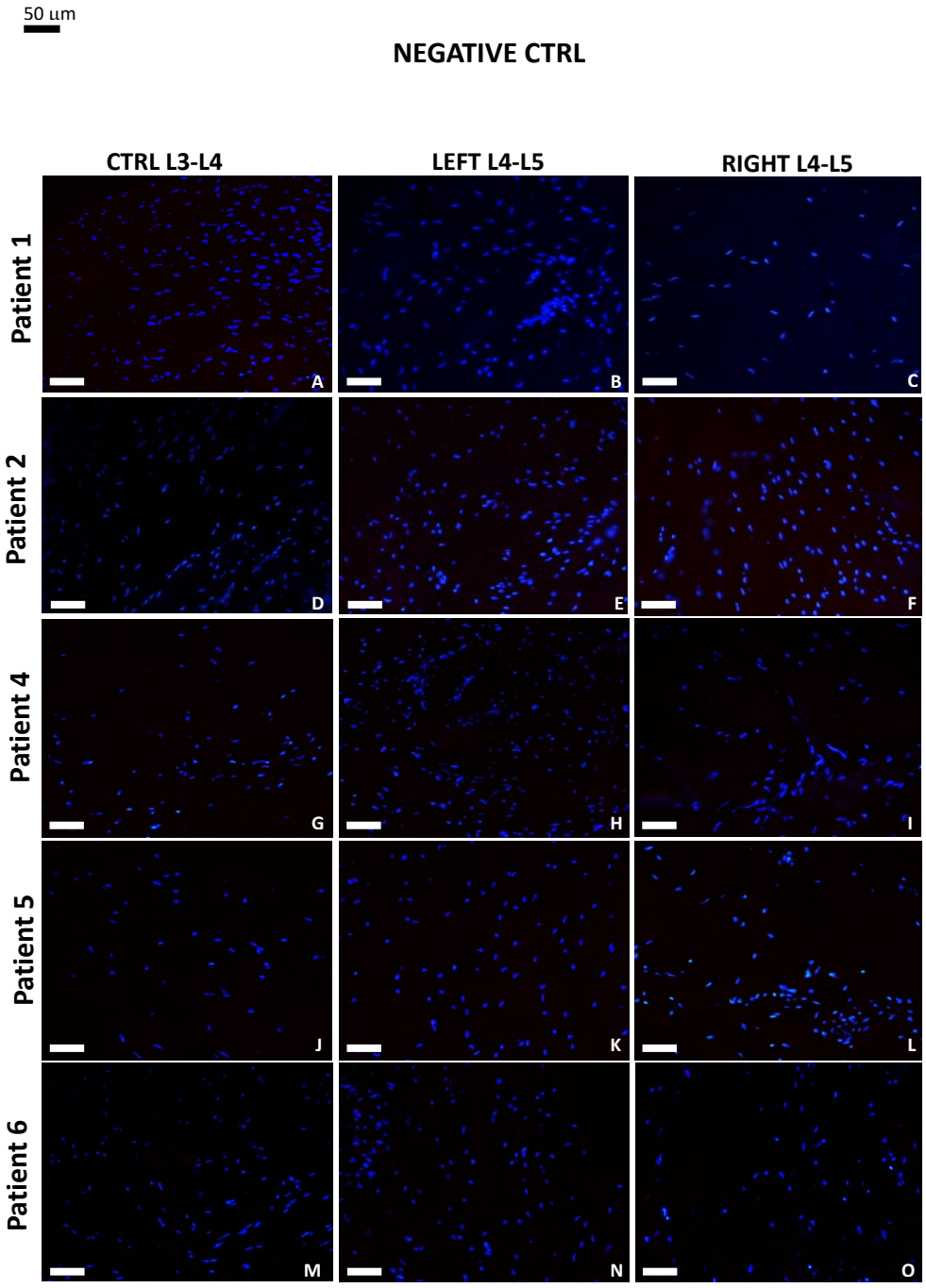

Figure 28.Negative control of immunofluorescence experiments. Sections from control and pathological tissues, retrieved from patient 1 (A-C), patient 2 (D-F), patient 4 (G-I), patient 5 (J-L), patient 6 (M-O) were incubated only with the secondary antibodies, while primary antibodies against TRPA1, TRPV1, TRPV2, TRPV4, TRPM8 were omitted. No red signal is detectable in any of the examined tissues. Nuclei counterstained with DAPI (blue). Bars: 50 µm.

Morphological analysis on tissue samples from patient affected by hip osteoarthritis

Histological and histochemical analyses at light microscopy

Haematoxylin and Eosin (Fig. 29 A-D) and Masson Trichrome (Fig. 29 E-H) stains were performed to evaluate the morphological aspects of samples harvested from the coxofemoral joint. The tissue samples from the capsule (Fig. 29 A, B, E, F) and from the labrum (Fig. 29 C, D, G, H) appear disorganized with empty spaces between the bundles of collagen fibers, which form the main component. Some blood vessels are visible in all the slides analyzed. The morphological appearance of these specimens is similar to that found in pathological tissue samples collected from patients affected by CLBP.

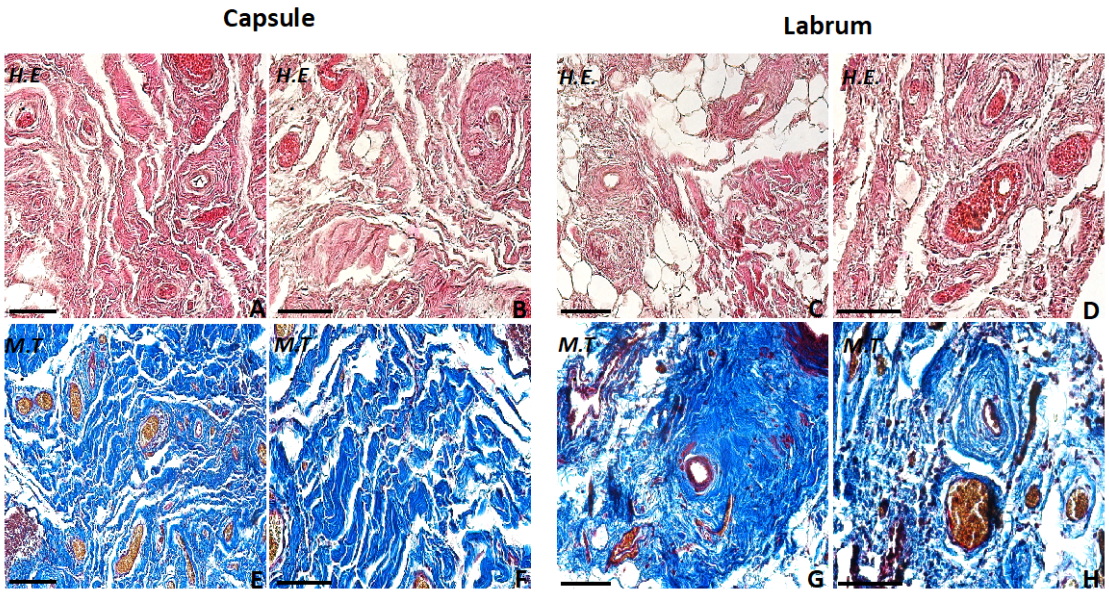

Figure29. Haematoxylin and Eosin (A-D) and Masson Trichrome (E-H) stains were performed in samples from the coxofemoral joints. The morphological aspect of the capsule (A, B, E, F) and of the labrum (C, D, G, H) appear lax and disorganized. Bars: 100 µm.

Silver impregnation

Silver impregnation (S.I.), which selectively distinguishes connective tissue (brown colored) from argent affine nervous fibers (black colored), were performed also on tissues harvested from the capsule (Fig. 30 A,B) and the labrum (Fig. 30 C,D) of the coxofemoral joint of the considered patient. Tissues sample were infiltrated by numerous nerve fibers. This finding seemingly supported the hypothesis of a greater infiltration of sensory nerves in the pathological joint tissue.

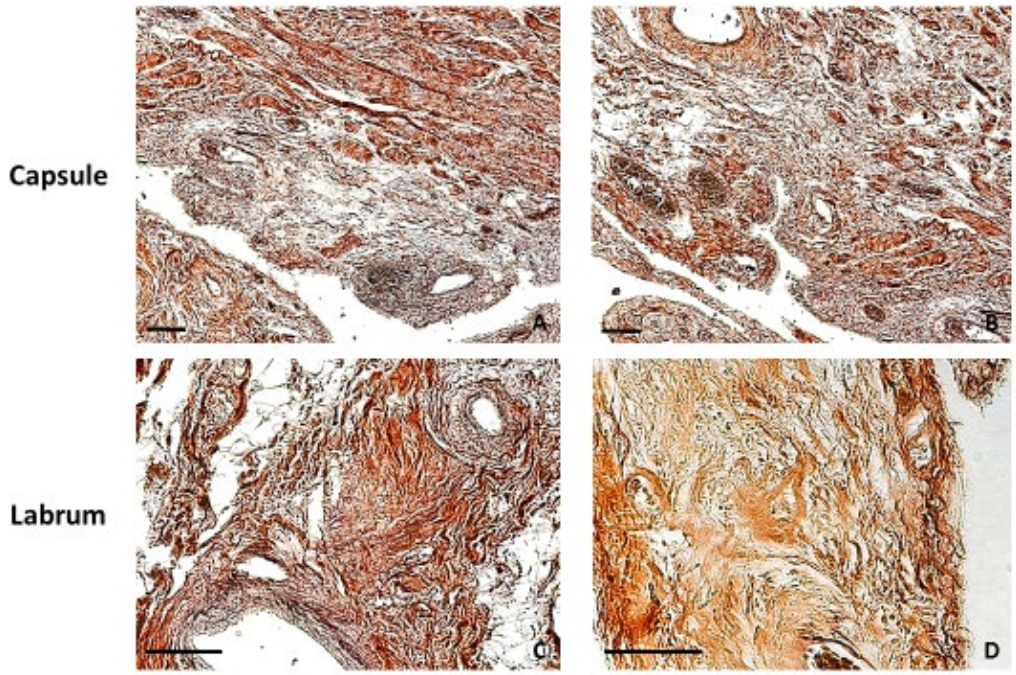

Figure30. Silver impregnation staining of pathological coxofemoral connective tissues. Numerous black nerve fibers were visible in disorganized pathological connective tissue from the capsule (A, B) and the labrum (C, D). Bars in A, B, C stained tissues: 100 µm. Bar in D stained tissue: 50 µm.

Immunofluorescence analyses on tissue samples from patient affected by hip osteoarthritis

Immunolocalization of TRPV4 and TRPM8, on tissues harvested from the capsule (Fig. 31 A-C) and the labrum (Fig. 31 D-F) of the coxofemoral joint of the considered patient were performed. The images obtained at the immunofluorescence analyses confirmed the presence of TRPV4 and TRPM8 on tissues from pathological coxofemoral joint. The amount of fluorescent signal resulted higher in the capsule compared to labrum, both for TRPV4 and TRPM8 (Fig. 31 G, H). No signal was detected in negative control experiments (Fig. 31 C, F).

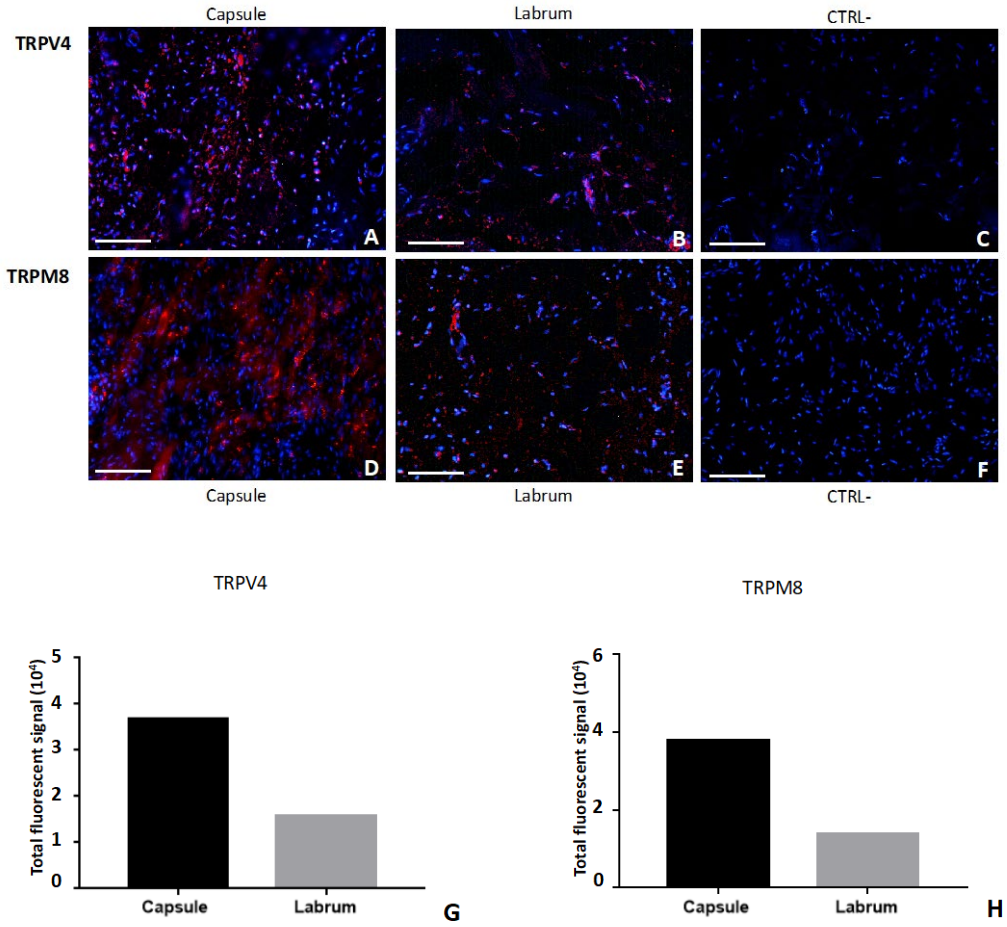

Figure31. Expression of TRPV4 and TRPM8 proteins in patient affected by hip osteoarthritis (A-H). Immunolocalization in tissues from capsule (A, D) and labrum (B, E) and respective negative controls (C, F). Receptors stained in red, nuclei counterstained in blue (DAPI). Bars: 50 µm. The graphs (G, H) show the amount of fluorescent signal, which results higher in the capsule compared to labrum. Measurements were obtained with Image J software package.

Immunofluorescence analyses on *X. laevis* oocytes

Immunofluorescence analyses were performed on oocytes after injection of TRPV4 cRNA (Fig. 32 A, B), after injection of TRPM8 cRNA (Fig. 32 C, D) and after co-injection of TRPV4 and TRPM8 cRNAs (Fig. 32 E, F). The obtained images showed the respective presence of TRPV4 (Fig. 32 A) and TRPM8 channels (Fig. 32 B) on the oocyte membrane after the expression of the relative cRNA microinjected. In oocytes co-injected with TRPV4 and TRPM8 cRNAs (Fig. 32 E), double-labelling experiments showed the simultaneous presence of both channels. Based on the different secondary antibody used, TRPV4 is highlighted in red and TRPM8 in green (Fig. 32 E). Negative control experiments were performed, in which primary antibodies were omitted and oocytes slides were only treated with secondary antibodies (Fig. 32 B, D, F).No signal was detected in negative control experiments.

Moreover, oocytes microinjected with membranes from coxofemoral tissue showed TRP channels on their surface at the immunofluorescence analyses, confirming the presence of these channels on the plasmatic membrane (Fig. 33 A-D). The amount of fluorescent signal was higher for TRPV4 (Fig. 33 A) then for TRPM8 (Fig. 33 B). No signal was detected in negative control experiments (Fig. 33 B, D).

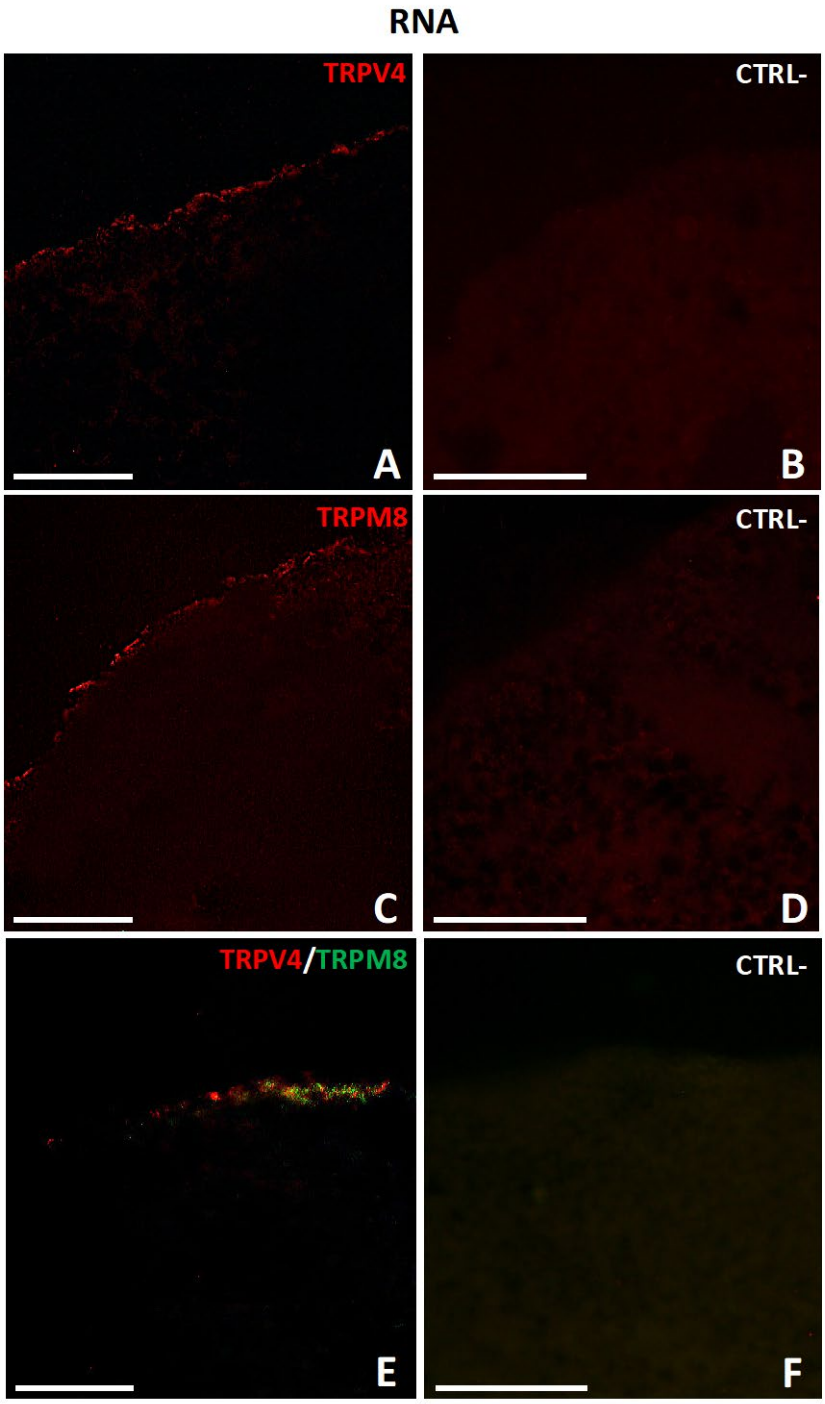

Figure32. Expression of TRPV4 and TRPM8 proteins in microinjected oocytes (A-F). Immunolocalization of TRPV4 protein in oocytes injected with TRPV4 cRNA (A), immunolocalization of TRPM8 protein in oocytes injected with TRPM8 cRNA (C), double-labelling experiments in oocytes co-injected with TRPV4 and TRPM8 cRNAs (E). No signal was detected in negative control experiments (B, D, F), in which primary antibodies were omitted. Bars: 50 µm.

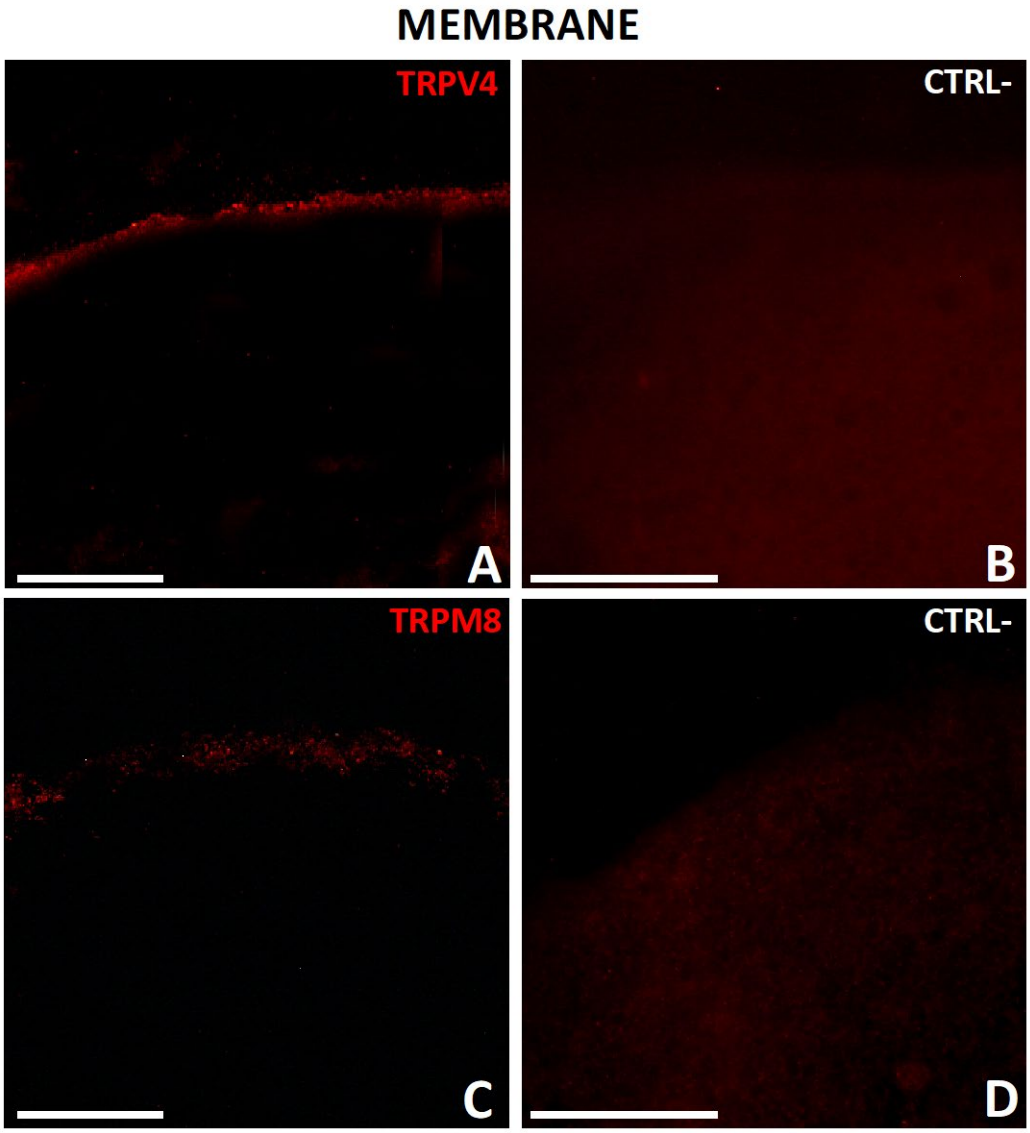

Figure33. Expression of TRPV4 and TRPM8 proteins in oocytes microinjected with membranes from coxofemoral tissues (A, D). Immunolocalization of TRPV4 proteins (A) and of TRPM8 proteins (C), and respective negative controls (B, D). Receptors stained in red. No signal was detected in negative control experiments (B, D), in which primary antibodies were omitted. Bars: 50 µm.

Electrophysiological analyses

X. laevis oocytes injected with TRPV4 cRNA (2ng/oo)

To characterize the functionality of TRPV4 channels, we tested *X. laevis* oocytes injected with TRPV4 cRNA at the TEVC, using different agonist and antagonist substances (Fig.34 A, B).

First, experiments concerning to temperature-mediated activation were conducted. TRPV4-injected oocytes were tested after heating Kulori solution at >30°C, determining a mean inward current of -141.49± 30.9nA (n= 7; at least two batches; Fig.34 A). Instead, the application of Kulori solution at temperature lower than 20°C closed channels giving rise to a small outward current of about 36,67 ±21,75 nA (n= 3; at least two batches; Fig.34 A).

These oocytes have also been tested with the application of menthol to check any possible activation of TRPV4 channels and to compare the responses obtained with those recorded with oocytes injected with TRPM8 cRNA. In TRPV4-injected oocytes the application of menthol (50µM) generated a mean outward current of 34,23±2,99 nA (n= 3; at least two batches; Fig.34 A).

Further analyses allowed to evaluate the behaviour of these oocytes in the presence of GSK1016790A, a synthetic TRPV4-agonist.The use of GSK1016790A generated an average inward current of -1093.39 ± 382.17 nA (n= 11; at least two batches; Fig.34 A). The effects of GSK1016790A were abolished if the oocytes were pre-incubated for 1 minute with HC-067047, the specific TRPV4 antagonist (data not shown).

The amplitude and direction of the currents generated in the oocytes injected with TRPV4 cRNA, after the application of different substances, was graphically represented (Fig. 34 B).

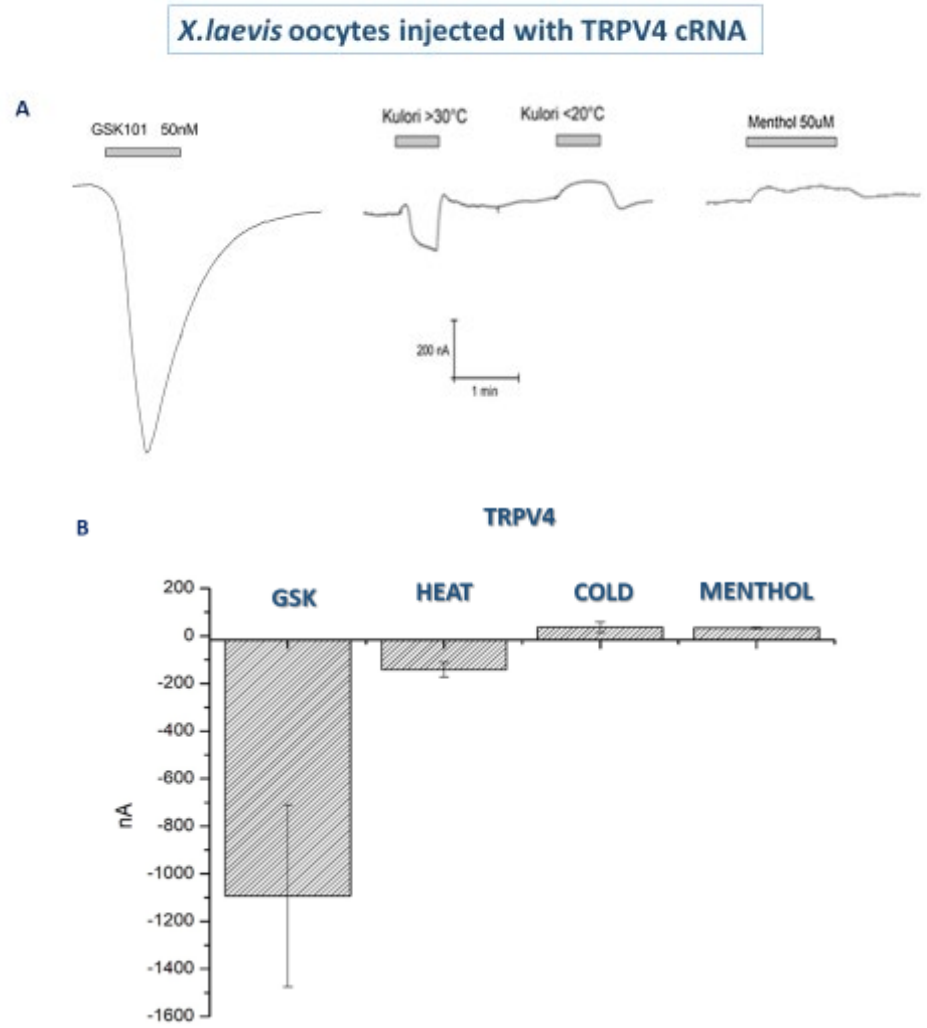

Figure34. Graphic representation of the currents generated in oocytes injected with TRPV4 cRNA, recorded by TEVC following the administration of different solutions (A, B). The bars indicate the application times of the various solutions. Histograms were obtained with GraphPad Prism version 8.4.2(B).

X. laevis oocytes injected with TRPM8 cRNA (2ng/oo)

Using the same agonist and antagonist substances applied on TRPV4-injected oocytes, *X. laevis* oocytes injected with TRPM8cRNA were tested at the TEVC (Fig.35 A, B). These experiments were conducted to confirm the functionality of TRPM8 channels expressed on *X. laevis* oocyte membranes, and to highlight any difference in the responses compared to TRPV4-injected ones.

At first, the application of heated Kulori solution at >30°C on TRPM8-injected oocytes generated a mean outward current of 30.77 ± 5.57nA (n= 9; at least two batches; Fig.35 A). Instead, the use of Kulori solution at a cold temperature (<20°C), evoked a mean inward current of -144.77 ± 68.47nA (n= 9; at least two batches; Fig.35 A).

The application of menthol (50µM) determined the opening of the TRPM8 channels, evoking a mean inward current of -1945.6 ± 483.44nA (n= 3; at least two batches; Fig.35 A).

The use of GSK1016790A on TRPM8 cRNA oocytes generated a small average inward current of 9.3 ± 0.1nA (n= 2; at least two batches; Fig.35 A), confirming that the TRPV4 agonist has no effect on TRPM8 channels.

The amplitude and direction of the currents generated in the oocytes injected with TRPM8 cRNA, after the application of different substances, was graphically represented (Fig.35 B).

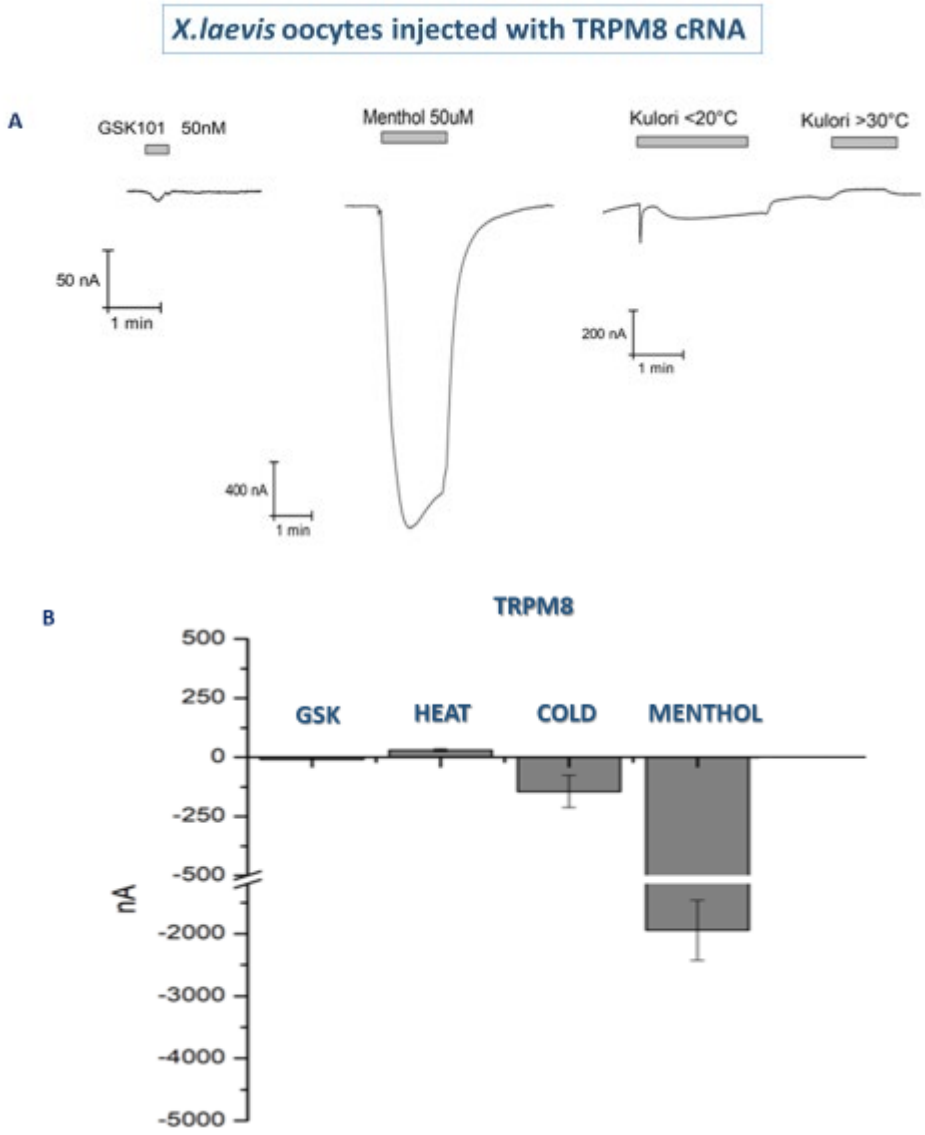

Figure35.Graphic representation of the currents generated in oocytes injected with TRPM8 cRNA, recorded by TEVC following the administration of different solutions (A, B). The bars indicate the application times of the various solutions. Histograms were obtained with GraphPad Prism version 8.4.2(B).

X. laevis oocytes injected with TRPV4 cRNA (2ng/oo) and TRPM8 cRNA (2ng/oo)

After co-injection with TRPV4 and TRPM8 cRNAs, *X. laevis* oocytes were tested at the TEVC, applying the substances, used in single-injected oocytes (Fig. 36 A, B).
The use of warm Kulori solution (>30°C), generated a mean inward current of -189.7 ± 146.40 nA (n= 3; at least two batches; Fig. 36 A). Instead, the application of cold Kulori solution (<20°C) evoked a mean inward current of -24.53 ± 4.10 nA (n= 3; at least two batches; Fig. 36 A).
After that, the application of menthol was tested. The menthol (50µM) determined the opening of the channels, evoking a mean inward current of -2091.7 ± 920.20 nA (n= 3; at least two batches; Fig. 36 A).
Lastly, with administration of GSK1016790A was recorded an average inward current of -1313.18 ± 404.15 nA (n= 4; at least two batches; Fig. 36 A).
The amplitude and direction of the currents generated in the oocytes injected with TRPV4 and TRPM8 cRNAs, after the application of different substances, was graphically represented (Fig. 36 B).

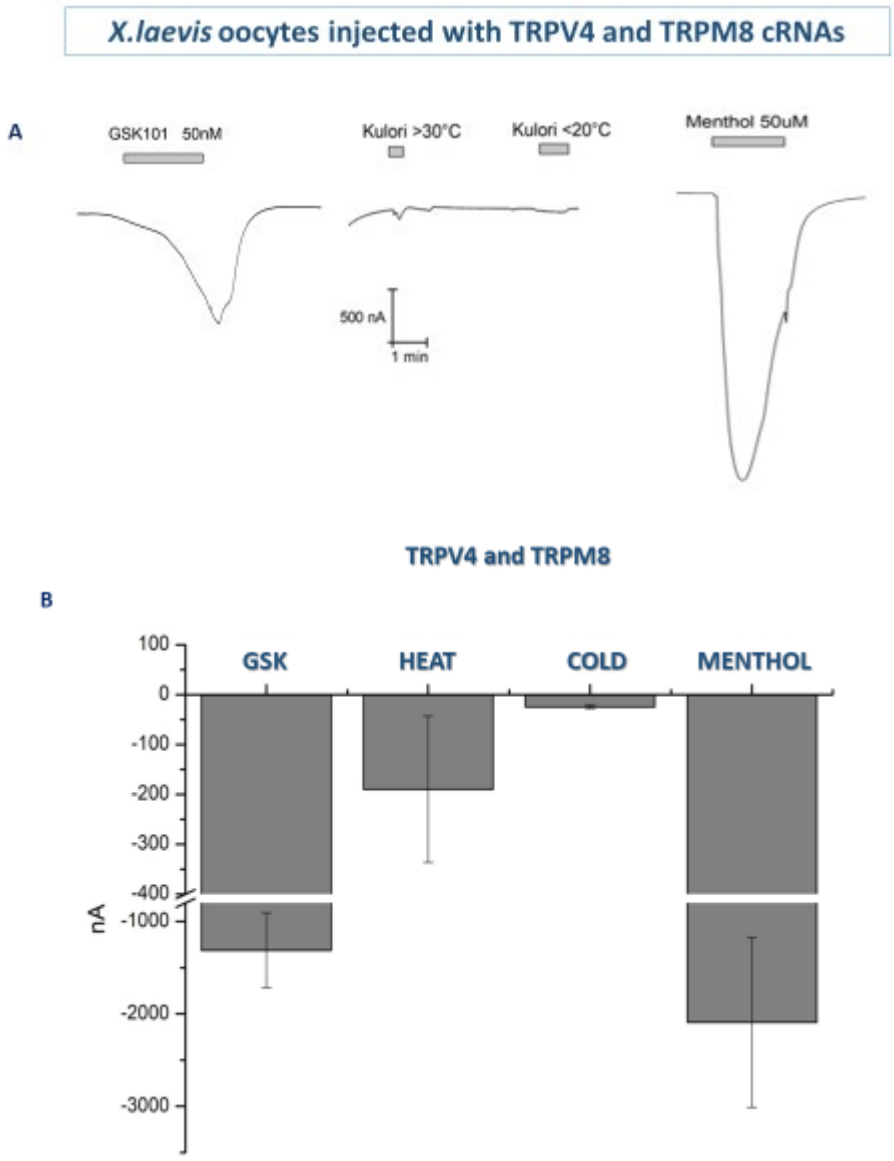

Figure36. Graphic representation of the currents generated in oocytes injected with TRPV4 and TRPM8 cRNA, recorded by TEVC following the administration of different solutions (A, B). The bars indicate the application times of the various solutions. Histograms were obtained with GraphPad Prism version 8.4.2. (B).

X. laevis oocytes injected with membranes.

X. laevis oocytes injected with membranes from the coxofemoral joint were also tested at the TEVC. Different measurements were recorded for the capsule and the labrum (Fig. 37 A-D).

After stimulation with heated Kulori solution (>30°C) a mean inward current of -4.33 ±1.19nA (n= 7; At least two batches; Fig. 37 A) was recorded in oocytes injected with membranes from the capsule, and an average inward current of -3.93 ±0.63nA (n= 6; at least two batches; Fig. 37 B) in those injected with membranes obtained from the labrum.

Otherwise, the administration of cold Kulorisolution (<20°C), evoked a mean inward current of -0.9± 0.31nA (n= 5; at least two batches; Fig. 37 A) if applied on membranes from the capsule, instead a mean outward current of 2.75 ± 0.69nA was recorded using membrane obtained from the labrum (n= 4; at least two batches; Fig. 37 B).

The application of menthol (50µM) in oocytes injected with capsular membranes determined a small deflection of the trace of -1.33 ±0.27nA (n= 4; at least two batches; Fig. 37 A). Instead, in oocytes injected with membranes from the labrum any noticeable current was recorded (n= 4; at least two batches; Fig. 37 B).

A different response was obtain using GSK1016790A, which caused an average inward current of -39.53 ±19.25nA (n= 7; at least two batches; Fig. 37 A) in oocytes injected with capsular membranes, and a mean inward current of -2.88 ± 1.34nA (n= 4; at least two batches; Fig. 37 B) in those injected with membranes from the labrum.

The amplitude and direction of the currents generated in the oocytes injected with membranes from the capsule (Fig. 37 C) and the labrum (Fig. 37 D), after the application of different substances, was graphically represented.

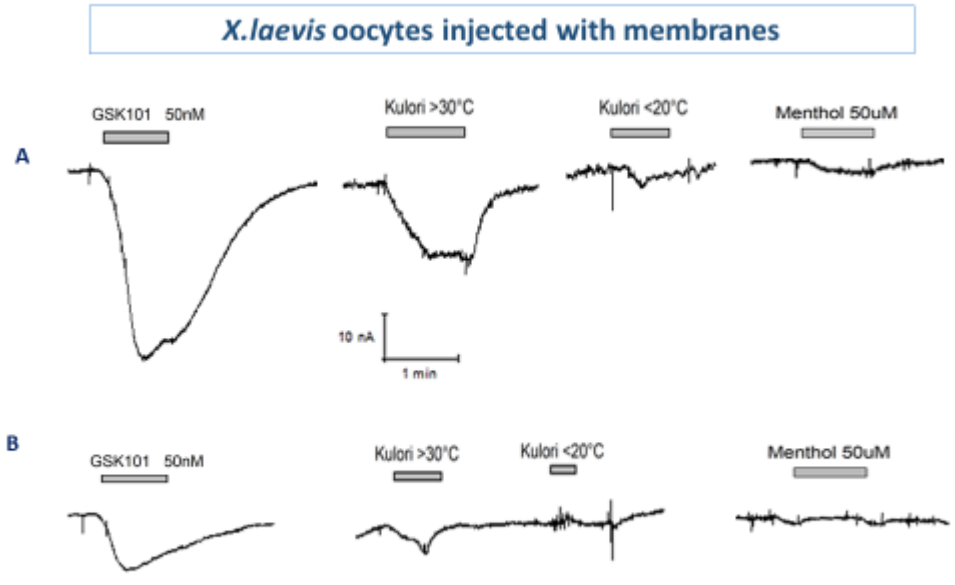
X.laevis oocytes injected with membranes
A
GSK101 50nM
Kulori >30°C
Kulori <20°C
Menthol 50uM
10 nA
1 min
B
GSK101 50nM
Kulori >30°C
Kulori <20°C
Menthol 50uM

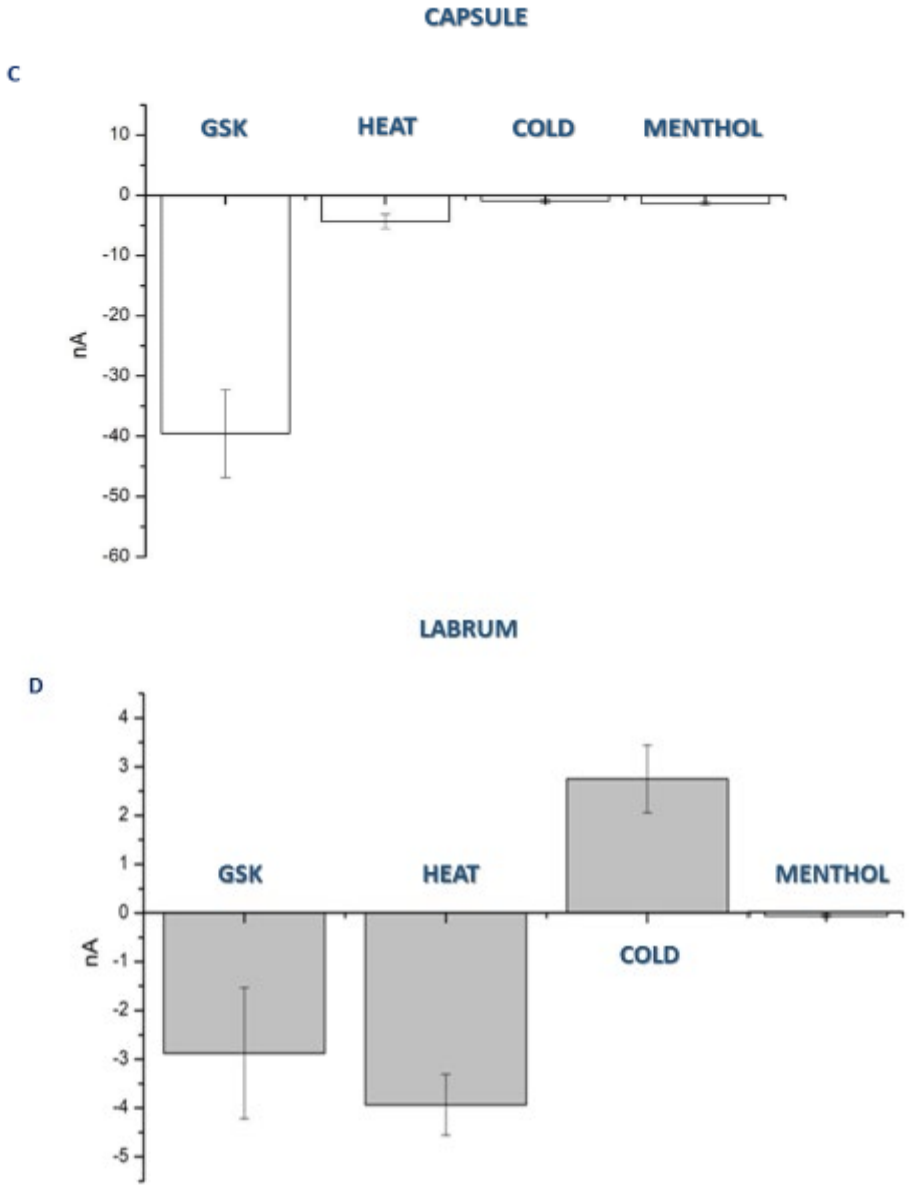

Figure37.Graphic representation of the currents generated in oocytes injected with membranes from coxofemoral joint, recorded by TEVC following the administration of different solutions (A-D).Currents recorded in oocytes injected with membranes obtained from the capsule (A, C), currents recorded in oocytes injected with membranes obtained from the labrum (B, D). The bars indicate the application times of the various solutions. Histograms were obtained with GraphPad Prism version 8.4.2. (C, D).

X. laevis oocytes not injected were tested at the TEVC and used as negative controls.
The use of Kulori solution at different temperature did not generate any meaningful currents, at >30°C the mean current was 0.29 ±0.39nA (n= 7; at least two batches) and at <20°C was 0.43 ± 0.46nA (n= 7; at least two batches).
The application of menthol was not associated to detectable current.
The administration of GSK1016790A, instead, generated an average inward current of -5.92 ±1.51 nA (n= 4; at least two batches).
The results obtained from the different experiments were graphically represented together (Fig. 40), to show more clearly the effects caused by the substances tested on the diverse experimental groups of oocytes. As expected, the values of the recorded currents were much higher in oocytes injected with cRNAs (Fig. 40 A) than in those injected with membranes (Fig 40. B), due to different quantity of channels present in the two experimental conditions. In the oocytes injected with membranes, after the administration of heated Kulori solution, a similar inward current was evident for both the capsule and the labrum. The response to menthol administration of membranes-injected oocytes was almost absent. The administration of GSK1016790A determined a greater activation in oocytes injected with membranes obtained from the capsule than in the labrum (Fig. 40 B), which can be correlated to the presence of higher quantity of TRPV4.

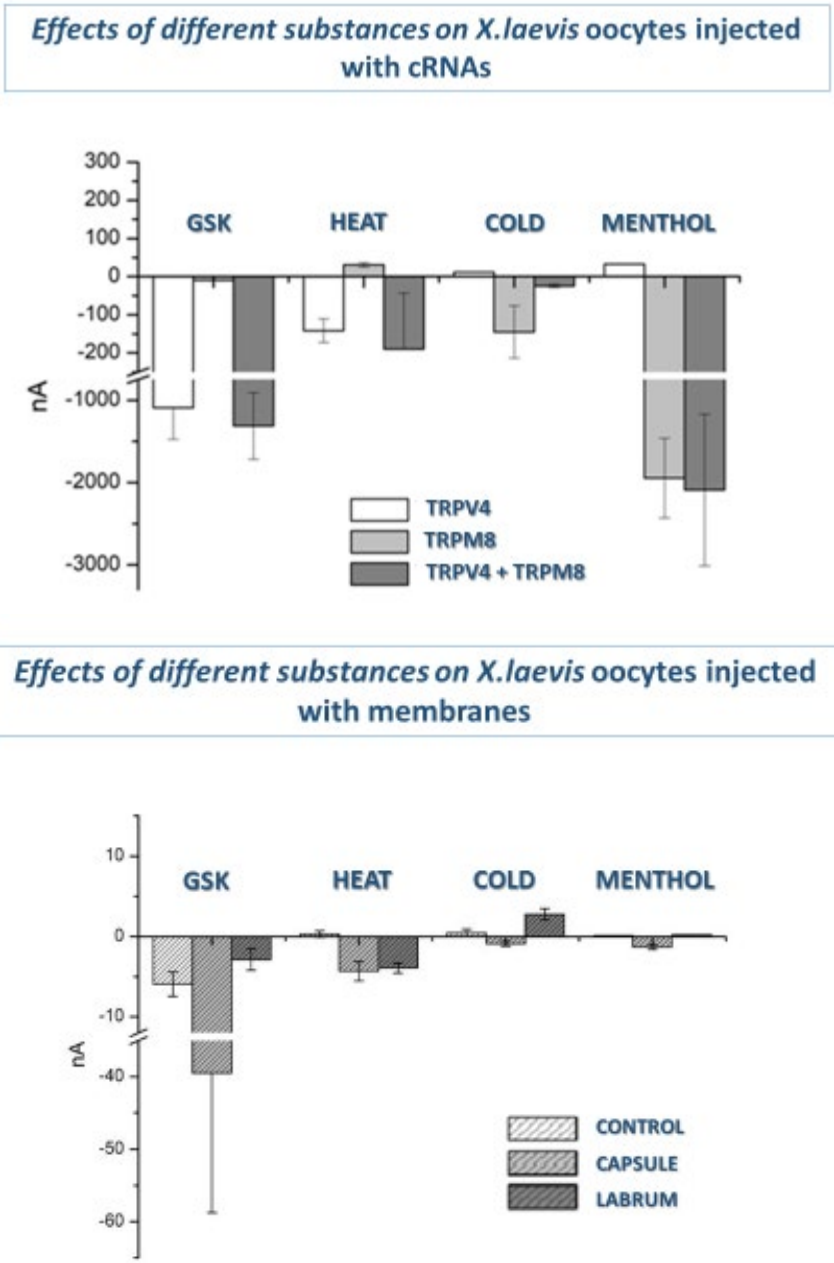

Figure38.The graph shows the amplitude and direction of the currents depending on the different substances used in different sets of X.laevis oocytes (A, B). Oocytes injected with TRPV4 and/or TRPM8 cRNA (A) and X.laevis oocytes injected with membranes (B). Histograms were obtained with GraphPad Prism version 8.4.2.

Discussion

Degeneration of the intervertebral disc is one of the leading causes of chronic low back pain (CLBP), which not only affects the patients' quality of life, but also constitutes a high financial burden on the society (Surace et al., 2012). With the aging population, the occurrence and costs of CLBP are predicted to grow. Hence, it is crucial to gain a better insight into the molecular processes of development of chronic pain, along with a potential research of new and targeted treatment strategies.

TRP channels have emerged as potential contributors to disc pathologies, as they are regulated by a diverse range of stimuli, including mechanical and osmotic stress, and furthermore modulate inflammatory responses. Applied mechanical stimuli can also change channels' molecular distribution, altering their membrane trafficking and spatial/temporal distribution, which in turn can influence activity threshold levels (Sadowska et al., 2019). TRP channels are Ca^{2+}-permeable cation channels, thus an increase of their intracellular concentration might promote pain perception, suggesting an involvement in cell signaling beyond the generation of electrical activity (Bourinet et al., 2014).

Under pathological conditions, TRP channels are sensitized, and their activation threshold reduced, perception of painful (hyperalgesia) and non-painful (allodynia) stimuli is enhanced (Levine & Alessandri-Haber, 2007; Dai, 2016).

In this work, evidence of morphological alterations of the pathological connective tissues harvested from patients affected by CLBP is provided. The samples from areas affected by chronic pain are characterized by degraded extracellular matrix, resulting in an increased tissue weakening which manifests with clefts. These anatomic changes are also related to altered tissue osmolarity that, associated to repetitive mechanical loadings, can contribute to tissue inflammation by modulating pro-inflammatory mediators (Sadowska et al., 2019). The inflammation could increase TRP channels expression in sensory neurons and can influence TRPs gene regulation through neurotrophic factors, such as nerve growth factor (NGF).In addition to mechanical force, hydrostatic, compressive, osmotic and tensile-hear stresses can also influence joint tissue homeostasis(McNulty et al., 2015).

At the silver impregnation experiments, a significantly greater infiltration of nervous fibers was observed in all pathological tissues from patients affected by CLBP. Notably, sprouting of nerve fibers was described as a landmark for articular hypersensitivity and subsequent allodynia (Ghilardi et al., 2012). Supporting this hypothesis, the presence of NGF and its receptor TrkA (Tyrosine kinase receptor A) in the periarticular and articular tissues of degenerative lumbar facet joints was previously described (Surace et al., 2009; Suzuki et al., 2013).

Immunofluorescence analyses highlighted a significant increase in the levels of TRP channels in the pathological tissues. These observations suggest that the augment in TRP channels could be related to the higher infiltration by nervous fibers in pathological samples, evidenced by the silver impregnation experiments performed. Previous studies have already identified these channels on axons in peripheral tissues (Fernández-Montoya et al., 2017). The TRP channels increase could also be related to enhanced stimulation (Coggeshall & Carlton, 1998; M. G. Salter & Fern, 2005; Woolf, 2010; Ferrari et al., 2014; Li et al., 2019). Indeed, the activation and/or sensitization of TRP channels in sensory nerves during inflammation are considered to be the main mechanism underlying neuropathic and inflammatory pain (Livak& Schmittgen, 2001; Nilius, 2007; Levine & Alessandri-Haber, 2007; Dai, 2016).

Between TRP channels there are some candidates mainly involved in CLBP: TRPV4 and TRPM8.Increased TRPV4 expression in pathological samples was the most consistent finding in this study, regardless of the location and number of affected sites in each patient. TRPV4 act as a sensor for mechanical or osmotic signals and is present in nervous and musculoskeletal tissues including cartilage, bone and synovium. This channel has been shown to have altered expression in pathological conditions, such as degenerated intervertebral disk, and to play a role in pain perception in CLBP (McNulty et al., 2015). In intervertebral disk and cartilage, TRPV4 regulates the metabolic response to load through changes in the local osmotic environment, and influences the expression of proinflammatory cytokines (O'Conor et al., 2014; Walter et al., 2016). Moreover, TRPV4 was proven to be a key component in promoting cartilage matrix synthesis in mice (O'Conor et al., 2014), in regulating bone formation and resorption (Suzuki et al., 2013) in the osteoblastic differentiation (Valdes et al., 2011) but above all in the transduction of mechanical signals (O'Conor et al., 2014). Calcium signalling and regulation, significant for bone homeostasis, are proven to be affected by mechanical stimuli. When mechanical stimuli are applied Ca^{2+} oscillations are induced in osteoblasts expressing TRPV4 (Lieben & Carmeliet, 2012), thus TRPV4 acts as a mechanical sensor, and induces bone loss under non-loading condition(McNulty et al., 2015).

TRPV4 has also been associated to musculoskeletal diseases, skeletal dysplasias and arthropathies. Several amino-acid substitutions have been identified in TRPV4 and related to musculoskeletal disorders (Lamandé et al., 2011; McEntagart, 2012; Nilius & Voets, 2013). Moreover, the activation, regulation and expression of TRPV4 vary according to different pathological conditions, such as those provided by the mechanical loading of the cartilage (Rock et al., 2008; O'Conor et al., 2014;McNulty et al., 2015). The loss of TRPV4 in adult mice was proven to alleviate age-related, degenerative changes in cartilage (O'Conor et al., 2014). Conversely, other studies previously stated that reduced TRPV4 function could result in degenerative changes in hyaline cartilage, while overactive TRPV4 was associated with alterations in growth plate cartilage (McNulty et al., 2015).

Interestingly, the increased expression of TRPV4 was also observed in human primary synovial cells isolated from subjects with inflammatory arthropathies (Kochukov et al., 2009). Therefore, TRPV4 could represent an attractive therapeutic target to modulate the effects of joint diseases, in conditions of chronic pain.

The second receptor most consistently overexpressed in pathological tissues compared to control ones was TRPM8. TRPM8, a cold temperature sensor, is expressed on both Aδ and C fibers and has a role in detection of mechanical, thermal and chemical stimuli (Dai, 2016; Sihong Wang et al., 2018; Liu et al., 2020). TRPM8 is overexpressed in painful condition and has a role in amplifying pain sensation after injury, especially in model of neuropathic pain. To date its role is not completely understood, some data show that TRPM8 is active in reducing pain, others seem to confirm that it increases pain after injury (Marwaha et al., 2016; Jankowski et al., 2017; Weyer & Lehto, 2017). In a chronic constriction injury model, the expression of TRPM8 is increased in sensory neurons and is associated with mechanical allodynia, cold and thermal hyperalgesia (Frederick et al., 2007; Marwaha et al., 2016; Liu et al., 2020). In addition to nerve injury, inflammation also causes increasedTRPM8 expression, enhancing cold sensitivity (Liu et al., 2020).This model can be compared to the condition of lumbar spinal stenosis, which causes compression of nerve roots, causing CLBP (Surace et al., 2012).

Modulation of TRPM8 channels is a good target for treatment of neuropathic pain and associated cold allodynia (Liu et al., 2020). Detection of TRM8 antagonists may be useful in pain-treatment (Koh et al., 2016; Weyer & Lehto, 2017). A pharmacological blockade of TRPM8 signalling results in a reduction of cold hypersensitivity induced by nerve injuries (Knowlton et al., 2011; Xiao et al., 2017). Down-regulation of TRPM8 protein or ablation of TRPM8-expressing neurons also attenuated cold hyperalgesia.

All patients affected by CLBP included in this study, except one, showed the same pattern of TRP channels expression. The exception was represented by patient 6, in whom the expression of TRPV4 and TRPM8 channels was similar to control tissue and TRPA1, TRPV1 and TRPV2 were also expressed, albeit to a lesser extent, in the tissue used as control, probably due to an initial degree of osteoarthritis. This pattern of receptors expression compared to the other patients is particularly interesting and could be related to the different clinical history. More specifically, this patient underwent previous surgery at the same level with the implant of an interspinous process device which is known to prevent mechanical loading of the posterior joints by blocking extension (Surace et al., 2012). This finding suggests that overexpression of TRPV4 and TRPM8 could be mainly due to mechanical stimuli (Valdes et al., 2011).

Our data demonstrate an overexpression of TRP channels, in particular TRPV4 and TRPM8, associated to a proliferation of nerve fibers in pathological connective tissues. These results suggest the involvement of TRP channels in sensory nerve function in

contest of chronic pain. Targeting TRPV4 and TRPM8 function may provide a direct therapeutic approach for the treatment of arthropathies and related pain symptoms.

In the second phase of the study, specimens of coxofemoral joint, affected by osteoarthritis, were analyzed. The main characteristics of osteoarthritis are progressive degenerative and inflammatory changes such as cartilage destruction, pathologic bone remodeling, and synovial inflammation that lead to pain and loss of joint function. Pain is the leading cause of sufferings in patients with osteoarthritis, even more important than reduced joint mobility. Since cartilage lacks direct innervation, pain in joint disease is related to inflammatory signalling, rather than the result of pathological damage to the joint surface (McNulty et al., 2015). However, the etiopathogenesis of osteoarthritis is poorly understood even though mechanical factors are known to play a critical role in its onset and progression (Guilak, 2011;Barbour et al., 2015; McNulty et al., 2015). Therefore, the mechanisms by which cells perceive and respond to mechanical signals may provide new targets for the development of disease-modifying osteoarthritis drugs (McNulty et al., 2015). Consequently, we have analysed tissues samples derived from the capsule and the labrum of coxofemoral joint affected by osteoarthritis, to understand if the morphological changes and the expression pattern of TRPV4 and TRPM8, obtained in spinal samples of chronic pain conditions, are maintained in different tissues. However, in this case we have no unaffected tissue that could be used as a control, because it would require the removal of tissue from the contralateral hip, causing damage to the patient.

At morphological analyses, the tissue samples from the capsule and labrum appear disorganized with empty spaces between the bundles of collagen fibers, similar to the morphological appearance of pathological tissue samples collected from patients affected by CLBP. In healthy samples, instead, it was confirmed that collagen fibers have a compact and well-organised distribution.

Osteoarthritis involves the release of pro-inflammatory cytokines (Gawri et al., 2014; Walter et al., 2016), which contributes to matrix breakdown and pain (Goldring & Otero, 2011). With progressive joint degeneration, the damaged extracellular matrix is increased and causes alterations in tissue osmolarity and in the biologic response to mechanical loads, proceeding towards a more catabolic response (Salter et al., 2002; Sowa & Agarwal, 2008; Torzilli et al., 2010; Walter et al., 2016). As degeneration progresses, changes in osmotically regulated mechanical transduction can occur, based on how cells perceive and respond to their mechanical environment (Walter et al., 2016).

Numerous blood vessels are also present in coxofemoral samples. In normal conditions the labrum is not vascularized in the internal part and has few blood vessels only in the most peripheral part, entering from the joint capsule (Berendes et al., 2018). In previous studies, close proximity of blood vessels to free nerve endings was noted suggesting a possible relationship (Tomlinson et al., 2020). Changes in tissue homeostasis, related to

changes in vascular permeability due to inflammation, could have an osmotic and mechanical effect on free nerve endings.

Even at the silver impregnation analyses, the same characteristics found in samples harvested from spinal tissues are maintained in the in coxofemoral samples. Tissues sample from the capsule and the labrum were infiltrated by numerous nerve fibers, compared to healthy tissues where free nerve endings can be found unevenly distributed (Berendes et al., 2018). This finding apparently supported the hypothesis of a greater infiltration of sensory nerves in the pathological joint tissues. Free nerve endings in the labrum are responsible for detection and transmission of pain sense to cerebral cortex (Kapetanakis et al., 2017) and those presented in the capsule have also a role in mechano-sensitivity (Tomlinson et al., 2020). An altered density of innervation has been noticed in painful patients indicating potentially greater nociceptive functioning. However, destructive changes in capsular mechano-receptors has been found in association with the progression of osteoarthritis (Tomlinson et al., 2020) and this could be related to pain reduction associated with a loss of motion in the more advanced stages. Differences in free nerve endings could be also related to age, sex, disease progression and individual variation, so further studies will be necessary considering demographic and anthropometric data.

Immunofluorescence analyses on coxofemoral tissues confirm the presence of TRPV4 and TRPM8 channels, with a higher amount of fluorescent signal in the capsule than in the labrum. The number of TRP channels expressed on the plasma membrane could be a critical determinant of channel function.

The presence of TRPV4 may be related to its role in hip proprioception and nociception. The labrum also has a function in preserving the cartilage health by reducing mechanical stresses on it and labral lesions are associated with hip degeneration (Berendes et al., 2018).

The confirmed presence of these channels on coxofemoral tissues at the immunofluorescence analyses allows us to use these tissues to prepare membranes to be injected into *X. laevis* oocytes for receptor characterization.

Using heterologous expression techniques in *X. laevis* oocytes and TEVC technique is possible to study TRPV4 and TRPM8 functionality, through the analysis of the ionic currents evoked by the activation of these receptors, considering them alone or together, under controlled conditions. We study the behaviour of TRPV4 and/or TRPM8 after cRNAs or membranes injection into *X. laevis* oocytes, with application of different stimuli. Identifying the molecules that regulates the activity of these channels could provide more effective treatments for inflammatory or neuropathic pain (Liu et al., 2020).

Immunofluorescence analyses performed on oocytes injected with cRNAs, confirmed the ability of the microinjected oocyte to synthesize heterologous proteins and express them on its plasma membrane in a very high amount. Double-labelling experiments on oocytes

co-injected with TRPV4 and TRPM8 cRNAs, confirmed the simultaneous presence of both channels. The distribution of the considered channels on the injected-oocyte was uniform, as can be deduced from a rather linear fluorescence signal.

Also, oocytes microinjected with membranes from coxofemoral tissues showed TRP channels on their surface at the immunofluorescence analyses. The amount of fluorescent signal was higher for TRPV4 than for TRPM8. This difference could be related to an increased TRPV4-expression compared to TRPM8 in the pathological tissues of the patient affected by hip osteoarthritis.

X. laevis oocytes injected with TRPV4 cRNA were tested at TEVC after application of the same solution at different temperature. The administration of Kulori solution at temperatures higher than 30°C determined the opening of the TRPV4 channels, evoking moderate inward currents. The obtained response confirms the activation of TRPV4with warmth. Instead, reducing the temperature of Kulori solution small outward currents were obtained. The perfusion with menthol on these oocytes seems to have only a mild inhibitory effect, generating small outward currents. Application of TRPV4 activator GSK1016790A (50 nM) resulted in a significantly greater Ca^{2+} flux in cells. The currents generated after the application of GSK1016790A, were completely abolished if the oocytes were pre-incubating with HC-067047 for 1 minute, indicating a specific action of the agonist on TRPV4 channels. *In vivo* the activation of TRPV4 channels could be related to an increased in tissues temperature, which is one of the main characteristics of inflammatory condition (Poudel et al., 2020), and to a reduced osmolarity due to a greater degradation of extracellular matrix in pathological tissues (Walter et al., 2016).

X. laevis oocytes injected with TRPM8 cRNA were also studied at TEVC. The application of Kulori solution at <20°C confirmed the role of TRPM8 as a cold sensor, instead the use of the same solution heated to more than 30°C, generates slight outward currents. Temperature variations drive transitions between resting and active states in this channel, as confirmed by the literature (Raddatz et al., 2014). Applying menthol (50μM), the opening of the TRPM8 channels was determined, with a high Ca^{2+} influx in the oocytes. The use ofTRPV4 agonist on oocytes injected with TRPM8 cRNA did not generate significant currents, demonstrating GSK1016790A specificity only forTRPV4 channels.

Then *X. laevis* oocytes injected with TRPV4 and TRPM8 cRNAs were tested. The results achieved in the co-injected oocytes were compared to those obtained in oocytes with a single type of expressed channel. Kulori solution at different temperatures evokes a Ca^{2+} influx, higher with the warm solution than with the cold one. Furthermore, the currents recorded by applying heated Kulori increased compared to oocytes with TRPV4 expression alone. Instead, after stimulation with cold Kulori solution the currents were reduced compared to TRPM8-oocytes. These results hint a possible functional relation between the two channels, suggesting that TRPV4 played a predominant role. Menthol in co-injected oocytes caused the opening of the TRPM8 channels, evoking larger inward

currents than those obtained in oocytes with only one expressed channel. However, the result obtained with the application of this substance could be influenced by the interference with other channel proteins endogenously present in the oocytes (Gentry et al., 2010). Stimulation of co-injected oocytes with GSK1016790A generates higher conductance. This current is higher than that recorded in TRPV4-oocytes.

We then investigated the channels expressed on membranes from the coxofemoral tissues with the same protocols. As expected, the values of the recorded currents are much higher in oocytes injected with cRNAs than in those injected with the membranes. Application of heated Kulori solution in oocytes injected with membranes, both from the capsule and the labrum, generates inward currents. Instead, cold Kulori solution evokes slight inward currents using capsular membranes and a small outward current when applied to oocytes injected with membranes from the labrum. Perfusion with menthol on oocytes injected with membranes from the capsule evokes slight inward currents, whereas currents were not recorded using membranes from the labrum. These last experiments suggest that TRPM8 channels on the membranes do not function, although their presence has been confirmed by immunofluorescence analyses both in oocytes and in specimen from the original tissue. Using GSK1016790A on oocytes injected with capsular membranes, high inward currents were recorded. Slight inward currents were recorded in oocytes injected with membranes from the labrum.

Reduced TRPV4 function is known to cause arthritic changes in the articular cartilage (McNulty, 2015). Indeed, TRPV4-deficient mice developed osteoarthritis at a younger age and to a more severe extent than their wild-type controls (Clark et al., 2010). Moreover, an activated TRPV4 channel was found in patients with osteoporosis or excessive bone resorption, and blocking it may be a valuable tool for increasing bone mass in patients with osteoporosis or excessive bone resorption (Dai, 2016).

TRPM8 function appears to be abolished in pathological coxofemoral tissues. These changes could be correlated to a mutation or peculiar inactivate state.

The main finding of this study is the applicability of the membrane transplantation from specimens of pathological tissues in oocytes of *X.laevis.* This method allows studying the mechanisms of activation and modulation of the native channels of any single patient, defining the biophysical and pharmacological specific properties of the expressed and known involved proteins. Moreover, this method if compared to RNA injection allows to maintain the native structure in the lipid environment of the considered channels. In this way the behavior of the channels after membranes injections reflects more faithfully the properties of the receptors in their native cells (Miledi et al., 2002).

As future prospects, the molecular analysis of the channels in tissues collected from patients with osteoarthrtritis will let to identify possible mutations to understand the dis-functionality and consequently the possible alteration of pain sensation.

Conclusions

Different types of receptors and of voltage- and ligand-gated ion channels are involved in the detection and processing of painful stimuli at several anatomical sites, such as intervertebral disks, joints and nerve roots.

Our data demonstrate an overexpression of TRP channels, in particular TRPV4 and TRM8, associated with an increase in nervous fibers, in pathological connective tissues. These results suggest the involvement of TRP channels in sensory nerve function in the context of chronic pain, underlining the potential importance of these channels as targets for the next generation of pain therapies.

The main limitations of this study are the small number of patients included and the absence of non-pathological tissues from the coxofemoral joint that could be used as negative controls.

However, the *X.laevis* oocyte model offers a valid tool for the study of TRP channels in sample from pathological tissues. Different drugs can be tested to inhibit or activate specific TRP channels, which could represent possible new therapeutic targets for next generation of chronic pain therapies. Treatments focused on TRPV4 or TRPM8 should specifically target the pathological joint tissue, due to the presence of these channels in a variety of tissues and their involvement in numerous pathophysiological processes, which could be related to several side effects. In orthopaedic diseases, direct agonists or antagonists could be intra-articular administered to prevent systemic side effects.

The future propose would be to create, by identifying specific mutations or functional alteration, a personalized pain therapy that targets altered channels without generalized systemic effects.

References

Albrecht, D. S., Ahmed, S. U., Kettner, N. W., Borra, R. J. H., Cohen-Adad, J., Deng, H., Houle, T. T., Opalacz, A., Roth, S. A., Melo, M. F. V., Chen, L., Mao, J., Hooker, J. M., Loggia, M. L., & Zhang, Y. (2018). Neuroinflammation of the spinal cord and nerve roots in chronic radicular pain patients. *Pain*, *159*(5), 968–977. https://doi.org/10.1097/j.pain.0000000000001171

Asgar, J., Zhang, Y., Saloman, J. L., Wang, S., Chung, M. K., & Ro, J. Y. (2015). The role of TRPA1 in muscle pain and mechanical hypersensitivity under inflammatory conditions in rats. *Neuroscience*, *310*, 206–215. https://doi.org/10.1016/j.neuroscience.2015.09.042

Auer-Grumbach, M., Olschewski, A., Papi, L., Kremer, H., McEntagart, M. E., Uhrig, S., Fischer, C., Fröhlich, E., Bálint, Z., Tang, B., Strohmaier, H., Lochmüller, H., Schlotter-Weigel, B., Senderek, J., Krebs, A., Dick, K. J., Petty, R., Longman, C., Anderson, N. E., … Guelly, C. (2010). Alterations in the ankyrin domain of TRPV4 cause congenital distal SMA, scapuloperoneal SMA and HMSN2C. *Nature Genetics*, *42*(2), 160–164. https://doi.org/10.1038/ng.508

Barbour, K. E., Lui, L. Y., Nevitt, M. C., Murphy, L. B., Helmick, C. G., Theis, K. A., Hochberg, M. C., Lane, N. E., Hootman, J. M., & Cauley, J. A. (2015). Hip osteoarthritis and the risk of all-cause and disease-specific mortality in older women: A population-based cohort study. *Arthritis and Rheumatology*, *67*(7), 1798–1805. https://doi.org/10.1002/art.39113

Basbaum, A. I., Bautista, D. M., Scherrer, G., & Julius, D. (2009). Cellular and Molecular Mechanisms of Pain. *Cell*, *139*(2), 267–284. https://doi.org/10.1016/j.cell.2009.09.028

Belmonte, C., Brock, J. A., & Viana, F. (2009). Converting cold into pain. *Experimental Brain Research*, *196*(1), 13–30. https://doi.org/10.1007/s00221-009-1797-2

Berendes, T., Geurkink, T., Willemsen, K., Weinans, H., Castelein, R., Nelissen, R., & Van der Wal, B. (2018). Labral (Pathologic) Similarities for the Human Shoulder and Hip Joint. *Journal of Orthopedics*, *1*(101), 1–7.

Bossi, E., Fabbrini, M., & Ceriotti, A. (2007). Exogenous Protein Expression in Xenopus Oocytes. In *In: Grandi G. (eds) In Vitro Transcription and Translation Protocols.* (Vol. 375, Issue Methods in Molecular Biology™, pp. 107–131). https://doi.org/https://doi.org/10.1007/978-1-

Bourinet, E., Altier, C., Hildebrand, M. E., Trang, T., Salter, M. W., & Zamponi, G. W. (2014). Calcium-permeable ion channels in pain signaling. *Physiological Reviews*, *94*(1), 81–140. https://doi.org/10.1152/physrev.00023.2013

Brederson, J. D., Kym, P. R., & Szallasi, A. (2013). Targeting TRP channels for pain relief. *European Journal of Pharmacology*, *716*(1–3), 61–76. https://doi.org/10.1016/j.ejphar.2013.03.003

Camacho, N., Krakow, D., Johnykutty, S., Katzman, P. J., Pepkowitz, S., Vriens, J., Nilius, B., Boyce, B. F., & Cohn, D. H. (2010). Dominant TRPV4 mutations in nonlethal and lethal metatropic dysplasia. *American Journal of Medical Genetics, Part A*, *152*(5), 1169–1177. https://doi.org/10.1002/ajmg.a.33392

Cao, E., Liao, M., Cheng, Y., & Julius, D. (2013). TRPV1 structures in distinct conformations reveal activation mechanisms. *Nature*, *504*(7478), 113–118. https://doi.org/10.1038/nature12823

Caspani, O., Zurborg, S., Labuz, D., & Heppenstall, P. A. (2009). The contribution of TRPM8 and TRPA1 channels to cold allodynia and neuropathic pain. *PLoS ONE*, *4*(10).

https://doi.org/10.1371/journal.pone.0007383

Caterina, M. J., & Julius, D. (2001). The vanilloid receptor: A molecular gateway to the pain pathway. *Annual Review of Neuroscience*, *24*, 487–517. https://doi.org/10.1146/annurev.neuro.24.1.487

Caterina, Michael J. (2014). TRP channel cannabinoid receptors in skin sensation, homeostasis, and inflammation. *ACS Chemical Neuroscience*, *5*(11), 1107–1116. https://doi.org/10.1021/cn5000919

Chung, M. K., Lee, H., Mizuno, A., Suzuki, M., & Caterina, M. J. (2004). 2-Aminoethoxydiphenyl borate activates and sensitizes the heat-gated ion channel TRPV3. *Journal of Neuroscience*, *24*(22), 5177–5182. https://doi.org/10.1523/JNEUROSCI.0934-04.2004

Clark, A. L., Votta, B. J., Kumar, S., Liedtke, W., & Guilak, F. (2010). Chondroprotective role of the osmotically sensitive ion channel transient receptor potential vanilloid 4: Age- and sex-dependent progression of osteoarthritis in Trpv4-deficient mice. *Arthritis and Rheumatism*, *62*(10), 2973–2983. https://doi.org/10.1002/art.27624

Coggeshall, R. E., & Carlton, S. M. (1998). Ultrastructural analysis of NMDA, AMPA, and kainate receptors on unmyelinated and myelinated axons in the periphery. *Journal of Comparative Neurology*, *391*(1), 78–86. https://doi.org/10.1002/(SICI)1096-9861(19980202)391:1<78::AID-CNE7>3.0.CO;2-O

Corey, D. P., Garcia-Añoveros, J., Holt, J. R., Kwan, K. Y., Lin, S. Y., Vollrath, M. A., Amalfitano, A., Cheung, E. L. M., Derfler, B. H., Duggan, A., Géléoc, G. S. G., Gray, P. A., Hoffman, M. P., Rehm, H. L., Tamasauskas, D., & Zhang, D. S. (2004). TRPA1 is a candidate for the mechanosensitive transduction channel of vertebrate hair cells. *Nature*, *432*(7018), 723–730. https://doi.org/10.1038/nature03066

Dai, Y. (2016). TRPs and pain. *Seminars in Immunopathology*, *38*(3), 277–291. https://doi.org/10.1007/s00281-015-0526-0

de Petrocellis, L., Orlando, P., Moriello, A. S., Aviello, G., Stott, C., Izzo, A. A., & di Marzo, V. (2012). Cannabinoid actions at TRPV channels: Effects on TRPV3 and TRPV4 and their potential relevance to gastrointestinal inflammation. *Acta Physiologica*, *204*(2), 255–266. https://doi.org/10.1111/j.1748-1716.2011.02338.x

Eitner, A., Hofmann, G. O., & Schaible, H. G. (2017). Mechanisms of osteoarthritic pain. Studies in humans and experimental models. *Frontiers in Molecular Neuroscience*, *10*(November), 1–22. https://doi.org/10.3389/fnmol.2017.00349

Erler, I., Al-Ansary, D. M. M., Wissenbach, U., Wagner, T. F. J., Flockerzi, V., & Niemeyer, B. A. (2006). Trafficking and assembly of the cold-sensitive TRPM8 channel. *Journal of Biological Chemistry*, *281*(50), 38396–38404. https://doi.org/10.1074/jbc.M607756200

Everaerts, W., Nilius, B., & Owsianik, G. (2010). The vanilloid transient receptor potential channel TRPV4: From structure to disease. *Progress in Biophysics and Molecular Biology*, *103*(1), 2–17. https://doi.org/10.1016/j.pbiomolbio.2009.10.002

Fernández-Montoya, J., Avendaño, C., & Negredo, P. (2017). The Glutamatergic System in Primary Somatosensory Neurons and Its Involvement in Sensory Input-Dependent Plasticity. *International Journal of Molecular Sciences*, *19*(1), 69. https://doi.org/10.3390/ijms19010069

Ferrari, L. F., Bogen, O., & Levine, J. D. (2014). Second messengers mediating the expression of neuroplasticity in a model of chronic pain in the rat. *Journal of Pain*, *15*(3), 312–320. https://doi.org/10.1016/j.jpain.2013.12.005

Frederick, J., Buck, M. E., Matson, D. J., & Cortright, D. N. (2007). Increased TRPA1, TRPM8, and TRPV2 expression in dorsal root ganglia by nerve injury. *Biochemical and Biophysical*

Research Communications, *358*(4), 1058–1064. https://doi.org/10.1016/j.bbrc.2007.05.029

Gawri, R., Rosenzweig, D. H., Krock, E., Ouellet, J. A., Stone, L. S., Quinn, T. M., & Haglund, L. (2014). High mechanical strain of primary intervertebral disc cells promotes secretion of inflammatory factors associated with disc degeneration and pain. *Arthritis Research and Therapy*, *16*(1), 1–14. https://doi.org/10.1186/ar4449

Gellhorn, A. C., Katz, J. N., & Suri, P. (2013). Osteoarthritis of the spine: the facet joints. *Nat Rev Rheumatol.*, *9*(4), 216–224. https://doi.org/10.1038/nrrheum.2012.199. Osteoarthritis

Gentry, C., Stoakley, N., Andersson, D. A., & Bevan, S. (2010). The roles of iPLA2, TRPM8 and TRPA1 in chemically induced cold hypersensitivity. *Molecular Pain*, *6*, 1–11. https://doi.org/10.1186/1744-8069-6-4

Ghilardi, J. R., Freeman, K. T., Jimenez-Andrade, J. M., Coughlin, K. A., Kaczmarska, M. J., Castaneda-Corral, G., Bloom, A. P., Kuskowski, M. A., & Mantyh, P. W. (2012). Neuroplasticity of sensory and sympathetic nerve fibers in a mouse model of a painful arthritic joint. *Arthritis and Rheumatism*, *64*(7), 2223–2232. https://doi.org/10.1002/art.34385

Goldring, M. B., & Otero, M. (2011). Inflammation in osteoarthritis. *Current Opinion in Rheumatology*, *23*(5), 471–478. https://doi.org/10.1097/BOR.0b013e328349c2b1

Guilak, F. (2011). Biomechanical factors in osteoarthritis. *Best Practice and Research: Clinical Rheumatology*, *25*(6), 815–823. https://doi.org/10.1016/j.berh.2011.11.013

Hediger, M. A., Coady, M. J., Ikeda, T. S., & Wright, E. M. (1987). Expression cloning and cDNA sequencing of the Na+ /glucose co-transporter. *Nature*, *330*, 379–381.

Hinman, A., Chuang, H. H., Bautista, D. M., & Julius, D. (2006). TRP channel activation by reversible covalent modification. *Proceedings of the National Academy of Sciences of the United States of America*, *103*(51), 19564–19568. https://doi.org/10.1073/pnas.0609598103

Hu, F., Zhu, W., & Wang, L. (2013). MicroRNA-203 up-regulates nitric oxide expression in temporomandibular joint chondrocytes via targeting TRPV4. *Archives of Oral Biology*, *58*(2), 192–199. https://doi.org/10.1016/j.archoralbio.2012.08.013

Iannotti, F. A., Hill, C. L., Leo, A., Alhusaini, A., Soubrane, C., Mazzarella, E., Russo, E., Whalley, B. J., Di Marzo, V., & Stephens, G. J. (2014). Nonpsychotropic plant cannabinoids, Cannabidivarin (CBDV) and Cannabidiol (CBD), activate and desensitize Transient Receptor Potential Vanilloid 1 (TRPV1) channels in vitro: Potential for the treatment of neuronal hyperexcitability. *ACS Chemical Neuroscience*, *5*(11), 1131–1141. https://doi.org/10.1021/cn5000524

Ikeda, K., & Morizono, T. (1989). Electrochemical profile for calcium ions in the stria vascularis: Cellular model of calcium transport mechanism. *Hearing Research*, *40*(1–2), 111–116. https://doi.org/10.1016/0378-5955(89)90104-4

Itoh, Y., Hatano, N., Hayashi, H., Onozaki, K., Miyazawa, K., & Muraki, K. (2009). An environmental sensor, TRPV4 is a novel regulator of intracellular Ca2+ in human synoviocytes. *American Journal of Physiology - Cell Physiology*, *297*(5), 1082–1090. https://doi.org/10.1152/ajpcell.00204.2009

Jankowski, M. P., Rau, K. K., & Koerber, H. R. (2017). Cutaneous TRPM8-expressing sensory afferents are a small population of neurons with unique firing properties. *Physiological Reports*, *5*(7), 1–11. https://doi.org/10.14814/phy2.13234

Jardín, I., López, J. J., Diez, R., Sánchez-Collado, J., Cantonero, C., Albarrán, L., Woodard, G. E., Redondo, P. C., Salido, G. M., Smani, T., & Rosado, J. A. (2017). TRPs in pain sensation. *Frontiers in Physiology*, *8*(JUN), 1–10. https://doi.org/10.3389/fphys.2017.00392

Ji, R. R., Nackley, A., Huh, Y., Terrando, N., & Maixner, W. (2018). Neuroinflammation and

central sensitization in chronic and widespread pain. *Anesthesiology*, *129*(2), 343–366. https://doi.org/10.1097/ALN.0000000000002130

Jin, M., Wu, Z., Chen, L., Jaimes, J., Collins, D., Walters, E. T., & O'Neil, R. G. (2011). Determinants of TRPV4 activity following selective activation by small molecule agonist GSK1016790A. *PLoS ONE*, *6*(2). https://doi.org/10.1371/journal.pone.0016713

Kameda, T., Zvick, J., Vuk, M., Sadowska, A., Tam, W. K., Leung, V. Y., Bölcskei, K., Helyes, Z., Applegate, L. A., Hausmann, O. N., Klasen, J., Krupkova, O., & Wuertz-Kozak, K. (2019). Expression and activity of TRPA1 and TRPV1 in the intervertebral disc: Association with inflammation and matrix remodeling. *International Journal of Molecular Sciences*, *20*(7). https://doi.org/10.3390/ijms20071767

Kapetanakis, D. S., Mangina, E., & Finn, D. P. (2017). Input variable selection for thermal load predictive models of commercial buildings. *Energy and Buildings*, *137*, 13–26. https://doi.org/10.1016/j.enbuild.2016.12.016

Kato, K., & Morita, I. (2011). Acidosis environment promotes osteoclast formation by acting on the last phase of preosteoclast differentiation: A study to elucidate the action points of acidosis and search for putative target molecules. *European Journal of Pharmacology*, *663*(1–3), 27–39. https://doi.org/10.1016/j.ejphar.2011.04.062

Kelly, S., Chapman, R. J., Woodhams, S., Sagar, D. R., Turner, J., Burston, J. J., Bullock, C., Paton, K., Huang, J., Wong, A., McWilliams, D. F., Okine, B. N., Barrett, D. A., Hathway, G. J., Walsh, D. A., & Chapman, V. (2015). Increased function of pronociceptive TRPV1 at the level of the joint in a rat model of osteoarthritis pain. *Annals of the Rheumatic Diseases*, *74*(1), 252–259. https://doi.org/10.1136/annrheumdis-2013-203413

Kim, S., Chen, J., Cheng, T., Gindulyte, A., He, J., He, S., Li, Q., Shoemaker, B. A., Thiessen, P. A., Yu, B., Zaslavsky, L., Zhang, J., & Bolton, E. E. (2021). PubChem in 2021: new data content and improved web interfaces. *Nucleic Acids Research*, *49*(D1), D1388–D1395. https://doi.org/10.1093/nar/gkaa971

Knowlton, W. M., Daniels, R. L., Palkar, R., McCoy, D. D., & McKemy, D. D. (2011). Pharmacological blockade of TRPM8 ion channels alters cold and cold pain responses in mice. *PLoS ONE*, *6*(9). https://doi.org/10.1371/journal.pone.0025894

Kochukov, M. Y., McNearney, T. A., Yin, H., Zhang, L., Ma, F., Ponomareva, L., Abshire, S., & Westlund, K. N. (2009). Tumor necrosis factor-alpha (TNF-α) enhances functional thermal and chemical responses of TRP cation channels in human synoviocytes. *Molecular Pain*, *5*, 1–16. https://doi.org/10.1186/1744-8069-5-49

Koh, W. U., Choi, S. S., Kim, J. H., Yoon, H. J., Ahn, H. S., Lee, S. K., Leem, J. G., Song, J. G., & Shin, J. W. (2016). The preventive effect of resiniferatoxin on the development of cold hypersensitivity induced by spinal nerve ligation: Involvement of TRPM8. *BMC Neuroscience*, *17*(1), 1–9. https://doi.org/10.1186/s12868-016-0273-8

Krakow, D., Lachman, R. S., & Rimoin, D. L. (2009). Guidelines for the prenatal diagnosis of fetal skeletal dysplasias. *Genetics in Medicine*, *11*(2), 127–133. https://doi.org/10.1097/GIM.0b013e3181971ccb

Lamandé, S. R., Yuan, Y., Gresshoff, I. L., Rowley, L., Belluoccio, D., Kaluarachchi, K., Little, C. B., Botzenhart, E., Zerres, K., Amor, D. J., Cole, W. G., Savarirayan, R., McIntyre, P., & Bateman, J. F. (2011). Mutations in TRPV4 cause an inherited arthropathy of hands and feet. *Nature Genetics*, *43*(11), 1142–1146. https://doi.org/10.1038/ng.945

Landouré, G., Zdebik, A. A., Martinez, T. L., Burnett, B. G., Stanescu, H. C., Inada, H., Shi, Y., Taye, A. A., Kong, L., Munns, C. H., Choo, S. S., Phelps, C. B., Paudel, R., Houlden, H., Ludlow, C. L., Caterina, M. J., Gaudet, R., Kleta, R., Fischbeck, K. H., & Sumner, C. J.

(2010). Mutations in TRPV4 cause Charcot-Marie-Tooth disease type 2C. *Nature Genetics*, *42*(2), 170–174. https://doi.org/10.1038/ng.512

Latorre, Ramón, Brauchi, S., Madrid, R., & Orio, P. (2011). A cool channel in cold transduction. *Physiology*, *26*(4), 273–285. https://doi.org/10.1152/physiol.00004.2011

Latorre, Ramon, Zaelzer, C., & Brauchi, S. (2009). Structure-functional intimacies of transient receptor potential channels. *Quarterly Reviews of Biophysics*, *42*(3), 201–246. https://doi.org/10.1017/S0033583509990072

Lepage, P., & Boulay, G. (2007). Molecular determinants of TRP channel assembly. *Biochem Soc Trans*, *1 february*(35 (1)), 81–83. https://doi.org/https://doi.org/10.1042/BST0350081

Levine, J. D., & Alessandri-Haber, N. (2007). TRP channels: Targets for the relief of pain. *Biochimica et Biophysica Acta - Molecular Basis of Disease*, *1772*(8), 989–1003. https://doi.org/10.1016/j.bbadis.2007.01.008

Li, X. H., Miao, H. H., & Zhuo, M. (2019). NMDA Receptor Dependent Long-term Potentiation in Chronic Pain. *Neurochemical Research*, *44*(3), 531–538. https://doi.org/10.1007/s11064-018-2614-8

Lieben, L., & Carmeliet, G. (2012). The involvement ofTRP channels in bone homeostasis. *Frontiers in Endocrinology*, *3*(AUG), 1–9. https://doi.org/10.3389/fendo.2012.00099

Lippoldt, E. K., Elmes, R. R., McCoy, D. D., Knowlton, W. M., & McKemy, D. D. (2013). Artemin, a glial cell line-derived neurotrophic factor family member, induces TRPM8-dependent cold pain. *Journal of Neuroscience*, *33*(30), 12543–12552. https://doi.org/10.1523/JNEUROSCI.5765-12.2013

Liu, Y., Mikrani, R., He, Y., Faran Ashraf Baig, M. M., Abbas, M., Naveed, M., Tang, M., Zhang, Q., Li, C., & Zhou, X. (2020). TRPM8 channels: A review of distribution and clinical role. *European Journal of Pharmacology*, *882*(January), 173312. https://doi.org/10.1016/j.ejphar.2020.173312

Livak, K. J., & Schmittgen, T. D. (2001). Analysis of relative gene expression data using real-time quantitative PCR and the 2-ΔΔCT method. *Methods*, *25*(4), 402–408. https://doi.org/10.1006/meth.2001.1262

Macpherson, L. J., Xiao, B., Kwan, K. Y., Petrus, M. J., Dubin, A. E., Hwang, S. W., Cravatt, B., Corey, D. P., & Patapoutian, A. (2007). An ion channel essential for sensing chemical damage. *Journal of Neuroscience*, *27*(42), 11412–11415. https://doi.org/10.1523/JNEUROSCI.3600-07.2007

Marwaha, L., Bansal, Y., Singh, R., Saroj, P., Bhandari, R., & Kuhad, A. (2016). TRP channels: potential drug target for neuropathic pain. *Inflammopharmacology*, *24*(6), 305–317. https://doi.org/10.1007/s10787-016-0288-x

Masuyama, R., Vriens, J., Voets, T., Karashima, Y., Owsianik, G., Vennekens, R., Lieben, L., Torrekens, S., Moermans, K., Vanden Bosch, A., Bouillon, R., Nilius, B., & Carmeliet, G. (2008). TRPV4-Mediated Calcium Influx Regulates Terminal Differentiation of Osteoclasts. *Cell Metabolism*, *8*(3), 257–265. https://doi.org/10.1016/j.cmet.2008.08.002

McEntagart, M. (2012). TRPV4 axonal neuropathy spectrum disorder. *Journal of Clinical Neuroscience*, *19*(7), 927–933. https://doi.org/10.1016/j.jocn.2011.12.003

McNulty, A. L., Leddy, H. A., Liedtke, W., & Guilak, F. (2015). TRPV4 as a therapeutic target for joint diseases. *Naunyn-Schmiedeberg's Archives of Pharmacology*, *388*(4), 437–450. https://doi.org/10.1007/s00210-014-1078-x

Miledi, R., Eusebi, F., Martínez-Torres, A., Palma, E., & Trettel, F. (2002). Expression of functional neurotransmitter receptors in Xenopus oocytes after injection of human brain membranes.

Proceedings of the National Academy of Sciences of the United States of America, *99*(20), 13238–13242. https://doi.org/10.1073/pnas.192445299

Muller, C., Morales, P., & Reggio, P. H. (2019). Cannabinoid ligands targeting TRP channels. *Frontiers in Molecular Neuroscience*, *11*(January), 1–15. https://doi.org/10.3389/fnmol.2018.00487

Murai, K., & Ohseto, K. (2019). Intra-articular Injection of the Hip Joint. In *Ohseto K., Uchino H., Iida H. (eds) Nerve Blockade and Interventional Therapy.* (pp. 201–203). Springer, Tokyo. https://doi.org/https://doi.org/10.1007/978-4-431-54660-3_50

Nakashimo, Y., Takumida, M., Fukuiri, T., Anniko, M., & Hirakawa, K. (2010). Expression of transient receptor potential channel vanilloid (TRPV) 14, melastin (TRPM) 5 and 8, and ankyrin (TRPA1) in the normal and methimazole-treated mouse olfactory epithelium. *Acta Oto-Laryngologica*, *130*(11), 1278–1286. https://doi.org/10.3109/00016489.2010.489573

Nilius, B. (2007). TRP channels in disease. *Biochimica et Biophysica Acta - Molecular Basis of Disease*, *1772*(8), 805–812. https://doi.org/10.1016/j.bbadis.2007.02.002

Nilius, B., Mahieu, F., Prenen, J., Janssens, A., Owsianik, G., Vennekens, R., & Voets, T. (2006). The Ca2+-activated cation channel TRPM4 is regulated by phosphatidylinositol 4,5-biphosphate. *EMBO Journal*, *25*(3), 467–478. https://doi.org/10.1038/sj.emboj.7600963

Nilius, B., & Owsianik, G. (2011). The transient receptor potential family of ion channels. *Genome Biology*, *12*(3). https://doi.org/10.1186/gb-2011-12-3-218

Nilius, B., & Voets, T. (2013). The puzzle of TRPV4 channelopathies. *EMBO Reports*, *14*(2), 152–163. https://doi.org/10.1038/embor.2012.219

Nowotny, T., & Levi, R. (2014). Voltage-Clamp Technique. In *Jaeger D., Jung R. (eds) Encyclopedia of Computational Neuroscience*. Springer, New York, NY. https://doi.org/10.1007/978-1-4614-7320-6

O'Conor, C. J., Leddy, H. A., Benefield, H. C., Liedtke, W. B., & Guilak, F. (2014). TRPV4-mediated mechanotransduction regulates the metabolic response of chondrocytes to dynamic loading. *Proceedings of the National Academy of Sciences of the United States of America*, *111*(4), 1316–1321. https://doi.org/10.1073/pnas.1319569111

Parent, L., Supplisson, S., Loo, D. D. F., & Wright, E. M. (1992). Electrogenic Properties of the Cloned Na+/Glucose Cotransporter: II. A Transport Model under Nonrapid Equilibrium Conditions. *New York*, *125*, 63–79.

Patapoutian, A., Peier, A. M., Story, G. M., & Viswanath, V. (2003). Thermotrp channels and beyond: Mechanisms of temperature sensation. *Nature Reviews Neuroscience*, *4*(7), 529–539. https://doi.org/10.1038/nrn1141

Paulsen, C. E., Armache, J. P., Gao, Y., Cheng, Y., & Julius, D. (2015). Structure of the TRPA1 ion channel suggests regulatory mechanisms. *Nature*, *520*(7548), 511–517. https://doi.org/10.1038/nature14367

Peier, A. M., Moqrich, A., Hergarden, A. C., Reeve, A. J., Andersson, D. A., Story, G. M., Earley, T. J., Dragoni, I., McIntyre, P., Bevan, S., & Patapoutian, A. (2002). A TRP channel that senses cold stimuli and menthol. *Cell*, *108*(5), 705–715. https://doi.org/10.1016/S0092-8674(02)00652-9

Pérez De Vega, M. J., Gómez-Monterrey, I., Ferrer-Montiel, A., & González-Muñiz, R. (2016). Transient Receptor Potential Melastatin 8 Channel (TRPM8) Modulation: Cool Entryway for Treating Pain and Cancer. *Journal of Medicinal Chemistry*, *59*(22), 10006–10029. https://doi.org/10.1021/acs.jmedchem.6b00305

Phelps, C. B., & Gaudet, R. (2007). The role of the N terminus and transmembrane domain of

TRPM8 in channel localization and tetramerization. *Journal of Biological Chemistry*, *282*(50), 36474–36480. https://doi.org/10.1074/jbc.M707205200

Poudel, P., Goyal, A., Bansal, P., & Lappin, S. L. (2020). *Inflammatory Arthritis.* StatPearls Publishing. https://www.ncbi.nlm.nih.gov/books/NBK507704/

Raddatz, N., Castillo, J. P., Gonzalez, C., Alvarez, O., & Latorre, R. (2014). Temperature and voltage coupling to channel opening in transient receptor potential melastatin 8 (TRPM8). *Journal of Biological Chemistry*, *289*(51), 35438–35454. https://doi.org/10.1074/jbc.M114.612713

Rock, M. J., Prenen, J., Funari, V. A., Funari, T. L., Merriman, B., Nelson, S. F., Lachman, R. S., Wilcox, W. R., Reyno, S., Quadrelli, R., Vaglio, A., Owsianik, G., Janssens, A., Voets, T., Ikegawa, S., Nagai, T., Rimoin, D. L., Nilius, B., & Cohn, D. H. (2008). Gain-of-function mutations in TRPV4 cause autosomal dominant brachyolmia. *Nature Genetics*, *40*(8), 999–1003. https://doi.org/10.1038/ng.166

Ryckmans, T., Aubdool, A. A., Bodkin, J. V., Cox, P., Brain, S. D., Dupont, T., Fairman, E., Hashizume, Y., Ishii, N., Kato, T., Kitching, L., Newman, J., Omoto, K., Rawson, D., & Strover, J. (2011). Design and pharmacological evaluation of PF-4840154, a non-electrophilic reference agonist of the TrpA1 channel. *Bioorganic and Medicinal Chemistry Letters*, *21*(16), 4857–4859. https://doi.org/10.1016/j.bmcl.2011.06.035

Sadowska, A., Hitzl, W., Karol, A., Jaszczuk, P., Cherif, H., Haglund, L., Hausmann, O. N., & Wuertz-Kozak, K. (2019). Differential regulation of TRP channel gene and protein expression by intervertebral disc degeneration and back pain. *Scientific Reports*, *9*(1), 1–16. https://doi.org/10.1038/s41598-019-55212-9

Sałat, K., & Filipek, B. (2015). Antinociceptive activity of transient receptor potential channel TRPV1, TRPA1, and TRPM8 antagonists in neurogenic and neuropathic pain models in mice. *Journal of Zhejiang University: Science B*, *16*(3), 167–178. https://doi.org/10.1631/jzus.B1400189

Salter, D., Millward-Sadler, S. ., Nuki, G., & Wright, M. (2002). Differential responses of chondrocytes from normal and osteoarthritic human articular cartilage to mechanical stimulation. *Biorheology*, *39*(1–2), 97–108.

Salter, M. G., & Fern, R. (2005). NMDA receptors are expressed in developing oligodendrocyte processes and mediate injury. *Nature*, *438*(7071), 1167–1171. https://doi.org/10.1038/nature04301

Schindl, R., & Romanin, C. (2007). Assembly domains in TRP channels. *Biochem Soc Trans*, *1 February*(3(1)), 84–85. https://doi.org/https://doi.org/10.1042/BST0350084

Schnell, S. A., Staines, W. A., & Wessendorf, M. W. (1999). Reduction of lipofuscin-like autofluorescence in fluorescently labeled tissue. *Journal of Histochemistry and Cytochemistry*, *47*(6), 719–730. https://doi.org/10.1177/002215549904700601

Sherkheli, M. A., Vogt-eisele, A. K., Bura, D., & Márques, L. R. B. (2010). Characterization of Selective TRPM8 Ligands and their Structure. *J Pharm Pharmaceut Sci*, *13*(2), 242–253.

Sowa, G., & Agarwal, S. (2008). Cyclic tensile stress exerts a protective effect on intervertebral disc cells. *American Journal of Physical Medicine and Rehabilitation*, *87*(7), 537–544. https://doi.org/10.1097/PHM.0b013e31816197ee

Story, G. M., Peier, A. M., Reeve, A. J., Eid, S. R., Mosbacher, J., Hricik, T. R., Earley, T. J., Hergarden, A. C., Andersson, D. A., Hwang, S. W., McIntyre, P., Jegla, T., Bevan, S., & Patapoutian, A. (2003). ANKTM1, a TRP-like channel expressed in nociceptive neurons, is activated by cold temperatures. *Cell*, *112*(6), 819–829. https://doi.org/10.1016/S0092-

8674(03)00158-2

Surace, M. F., Fagetti, A., Fozzato, S., & Cherubino, P. (2012). Lumbar spinal stenosis treatment with aperius perclid interspinous system. *European Spine Journal*, *21*(SUPPL. 1). https://doi.org/10.1007/s00586-012-2222-2

Surace, M. F., Prestamburgo, D., Campagnolo, M., Fagetti, A., & Murena, L. (2009). Presence of NGF and its receptor TrkA in degenerative lumbar facet joint specimens. *European Spine Journal*, *18*(SUPPL. 1), 123–126. https://doi.org/10.1007/s00586-009-0994-9

Suzuki, T., Notomi, T., Miyajima, D., Mizoguchi, F., Hayata, T., Nakamoto, T., Hanyu, R., Kamolratanakul, P., Mizuno, A., Suzuki, M., Ezura, Y., Izumi, Y., & Noda, M. (2013). Osteoblastic differentiation enhances expression of TRPV4 that is required for calcium oscillation induced by mechanical force. *Bone*, *54*(1), 172–178. https://doi.org/10.1016/j.bone.2013.01.001

Talavera, K., Gees, M., Karashima, Y., Meseguer, V. M., Vanoirbeek, J. A. J., Damann, N., Everaerts, W., Benoit, M., Janssens, A., Vennekens, R., Viana, F., Nemery, B., Nilius, B., & Voets, T. (2009). Nicotine activates the chemosensory cation channel TRPA1. *Nature Neuroscience*, *12*(10), 1293–1299. https://doi.org/10.1038/nn.2379

Tékus, V., Bölcskei, K., Kis-Varga, Á., Dézsi, L., Szentirmay, É., Visegrády, A., Horváth, C., Szolcsányi, J., & Petho, G. (2010). Effect of transient receptor potential vanilloid 1 (TRPV1) receptor antagonist compounds SB705498, BCTC and AMG9810 in rat models of thermal hyperalgesia measured with an increasing-temperature water bath. *European Journal of Pharmacology*, *641*(2–3), 135–141. https://doi.org/10.1016/j.ejphar.2010.05.052

Tomlinson, J., Zwirner, J., Ondruschka, B., Prietzel, T., & Hammer, N. (2020). Innervation of the hip joint capsular complex: A systematic review of histological and immunohistochemical studies and their clinical implications for contemporary treatment strategies in total hip arthroplasty. *PLoS ONE*, *15*(2), 1–27. https://doi.org/10.1371/journal.pone.0229128

Torzilli, P. A., Bhargava, M., Park, S., & Chen, C. T. C. (2010). Mechanical load inhibits IL-1 induced matrix degradation in articular cartilage. *Osteoarthritis and Cartilage*, *18*(1), 97–105. https://doi.org/10.1016/j.joca.2009.07.012

Valdes, A. M., De Wilde, G., Doherty, S. A., Lories, R. J., Vaughn, F. L., Laslett, L. L., Maciewicz, R. A., Soni, A., Hart, D. J., Zhang, W., Muir, K. R., Dennison, E. M., Wheeler, M., Leaverton, P., Cooper, C., Spector, T. D., Cicuttini, F. M., Chapman, V., Jones, G., … Doherty, M. (2011). The Ile585Val TRPV1 variant is involved in risk of painful knee osteoarthritis. *Annals of the Rheumatic Diseases*, *70*(9), 1556–1561. https://doi.org/10.1136/ard.2010.148122

Vay, L., Gu, C., & McNaughton, P. A. (2012). The thermo-TRP ion channel family: Properties and therapeutic implications. *British Journal of Pharmacology*, *165*(4), 787–801. https://doi.org/10.1111/j.1476-5381.2011.01601.x

Vincent, F., Acevedo, A., Nguyen, M. T., Dourado, M., DeFalco, J., Gustafson, A., Spiro, P., Emerling, D. E., Kelly, M. G., & Duncton, M. A. J. (2009). Identification and characterization of novel TRPV4 modulators. *Biochemical and Biophysical Research Communications*, *389*(3), 490–494. https://doi.org/10.1016/j.bbrc.2009.09.007

Vlaeyen, J. W. S., Maher, C. G., Wiech, K., Van Zundert, J., Beraldo Meloto, Carolina Diatchenko, L., Battié, M. C., Goossens, M., Koes, B., & Linton, S. J. (2018). Low Back Pain. *Nature Reviews Disease Primers Volume*, *4*. https://doi.org/https://doi.org/10.1038/s41572-018-0052-1

Vriens, J., Watanabe, H., Janssens, A., Droogmans, G., Voets, T., & Nilius, B. (2004). Cell swelling, heat, and chemical agonists use distinct pathways for the activation of the cation

channel TRPV4. *Proceedings of the National Academy of Sciences of the United States of America*, *101*(1), 396–401. https://doi.org/10.1073/pnas.0303329101

Wagner, C., Friedrich, B., Setiawan, I., Lang, F., & Bröer, S. (2000). The use of Xenopus laevis oocytes for the functional characterization of heterologously expressed membrane proteins. *Cell Physiol Biochem*, *10*(1–2), 1–12. https://doi.org/10.1159/000016341.

Walter, B. A., Purmessur, D., Moon, A., Occhiogrosso, J., Laudier, D. M., Hecht, A. C., & Iatridis, J. C. (2016). REDUCED TISSUE OSMOLARITY INCREASES TRPV4 EXPRESSION AND PRO-INFLAMMATORY CYTOKINES IN INTERVERTEBRAL DISC CELLS. *Eur Cell Mater*, *32*, 123–136. https://doi.org/https://doi.org/10.22203/ecm.v032a08

Wang, Sheng, Brigoli, B., Lim, J., Karley, A., & Chung, M. K. (2018). Roles of TRPV1 and TRPA1 in Spontaneous Pain from Inflamed Masseter Muscle. *Neuroscience*, *384*, 290–299. https://doi.org/10.1016/j.neuroscience.2018.05.048

Wang, Sihong, Xu, J., Wang, W., Wang, G. J. N., Rastak, R., Molina-Lopez, F., Chung, J. W., Niu, S., Feig, V. R., Lopez, J., Lei, T., Kwon, S. K., Kim, Y., Foudeh, A. M., Ehrlich, A., Gasperini, A., Yun, Y., Murmann, B., Tok, J. B. H., & Bao, Z. (2018). Skin electronics from scalable fabrication of an intrinsically stretchable transistor array. *Nature*, *555*(7694), 83–88. https://doi.org/10.1038/nature25494

Weyer, A. D., & Lehto, S. G. (2017). Development of TRPM8 antagonists to treat chronic pain and migraine. *Pharmaceuticals*, *10*(2), 1–9. https://doi.org/10.3390/ph10020037

Woolf, C. J. (2010). What is this thing called pain? *Journal of Clinical Investigation*, *120*(11), 3742–3744. https://doi.org/10.1172/JCI45178

Wurden, S., & Homberg, U. (1993). A simple method for immunofluorescent double staining with primary antisera from the same species. *Journal of Histochemistry and Cytochemistry*, *41*(4), 627–630. https://doi.org/10.1177/41.4.8450202

Xiao, X., Feng, Y. P., Du, B., Sun, H. R., Ding, Y. Q., & Qi, J. G. (2017). Antibody incubation at 37°c improves fluorescent immunolabeling in free-floating thick tissue sections. *BioTechniques*, *62*(3), 115–122. https://doi.org/10.2144/000114524

Yee, N. S. (2015). Roles of TRPM8 ion channels in cancer: Proliferation, survival, and invasion. *Cancers*, *7*(4), 2134–2146. https://doi.org/10.3390/cancers7040882

Yekkirala, A. S. (2013). Two to tango: GPCR oligomers and GPCR-TRP channel interactions in nociception. *Life Sciences*, *92*(8–9), 438–445. https://doi.org/10.1016/j.lfs.2012.06.021